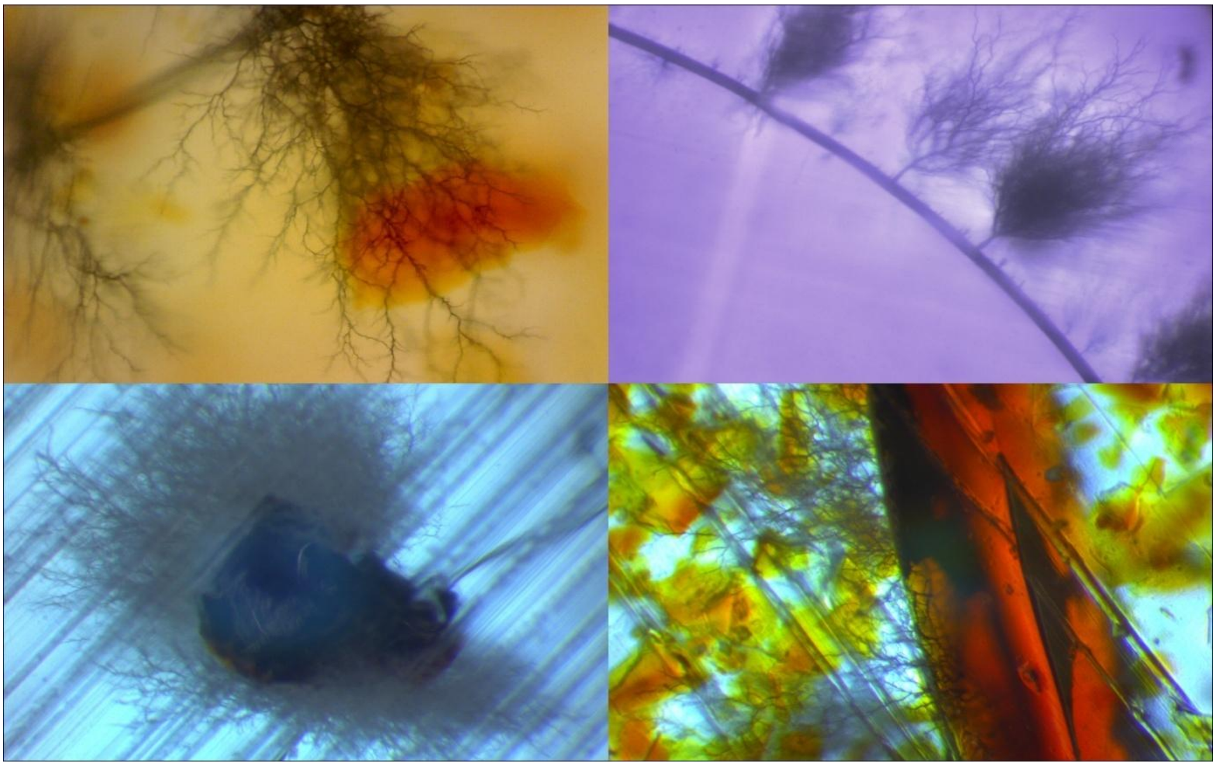

Organic Contaminants in Crosslinked Polyethylene for Demanding High Voltage Applications

Diploma Work in the Master programme of Electric Power Engineering

ESPEN H. DOEDENS

Department of Materials and Manufacturing Technology
Division of High Voltage Engineering
CHALMERS UNIVERSITY OF TECHNOLOGY
Gothenburg, Sweden, 2012
Report No. 83/2012

Organic Contaminants in Crosslinked Polyethylene for Demanding High Voltage Applications

by

ESPEN H. DOEDENS

Diploma work No. 83/2012
at the Department of Materials and Manufacturing Technology
CHALMERS UNIVERSITY OF TECHNOLOGY
Gothenburg, Sweden

Diploma work in the Master programme of Electric Power Engineering

Performed at: Chalmers University of Technology
SE-412 96 Gothenburg, Sweden

Supervisors: Dr. Susanne Nilsson
R&D Department, Submarine High Voltage Cables
Nexans AS NO-1751 Halden, Norway

Anette Johansson
Department of Materials and Manufacturing Technology
Chalmers University of Technology, SE-412 96 Gothenburg, Sweden

Markus Jarvid
Department of Chemical and Biological Engineering
Chalmers University of Technology, SE-412 96 Gothenburg, Sweden

Examiner: Prof. Stanislaw Gubanski
Department of Materials and Manufacturing Technology
Chalmers University of Technology, SE-412 96 Gothenburg, Sweden

Organic Contaminants in Crosslinked Polyethylene for Demanding High Voltage Applications

ESPEN H. DOEDENS

Diploma work no. 83/2012
Department of Materials and Manufacturing Technology
Chalmers University of Technology
SE-412 96 Gothenburg
Sweden
Telephone + 46 (0)31-772 1000

Cover:
Top left: Electrical Trees in XLPE sample with organic contaminants, Appendix III picture 57.
Top right: Electrical Trees and water trees in XLPE sample, page 36
Bottom left: Electrical Tree in aged XLPE sample, initiated around organic contaminant, page 36
Bottom right: Electrical Trees in XLPE sample, propagated along organic contaminant, page 41

Chalmers reproservice
Gothenburg, Sweden 2012

Summary

Oxidation or chemical aging of polyethylene may occur before, during or even after the extrusion process used to produce crosslinked polyethylene (XLPE), creating oxidized particles referred to as organic contaminants. XLPE is a common insulating material used for e.g. high voltage cables. Not much work is published on the effect of organic contaminants on electrical degradation such as electrical treeing and water treeing. This work aims to examine the effects of organic contaminants with different degrees of oxidation on in particular electrical treeing. These contaminants were introduced in XLPE samples made for electrical treeing measurements. Instead of using a commonly used needle-needle or needle-plane configuration, a wire-plane configuration was used for all test samples. The electrical tree initiation and propagation was examined with a method developed at Chalmers University of Technology. As found in the literature, the organic contaminants are known to have increasing conductivity and permittivity depending on the degree of oxidation. These properties could create local field enhancements in the material. Also the morphology of the material might be affected when contaminants are inserted. A combination of these factors might influence the electrical performance of the insulation. As this was the first time organic contaminants were introduced into the wire-plane test method, a wide variety of tests were performed such as wet and dry aging, AC tests and DC tests. From these tests a number of observations were made, giving support to a set of possible conclusions for these topics.

Keywords: Organic contaminants, XLPE, HVAC, HVDC, Electrical degradation, Electrical treeing, Water treeing, Insulation material.

Acknowledgements

Chalmers University is greatly acknowledged for all support and contribution to this thesis work.

To Nexans Norway AS, I am grateful for supporting this thesis work.

I would like to commence with acknowledging Dr. Susanne Nilsson from Nexans AS for supervising throughout the entire project. Besides supervising I would also like to thank her for the interesting discussions, tips and the study visit to Trondheim University. Also Jerker Kjellqvist and the other members of the organic contaminant project group: “Organic Contaminations in Polymer Submarine HV XLPE Cable Insulations for Demanding Applications.” from Dow Chemical Company (Dow), and Sintef are acknowledged for contributing to the project and the interesting discussions on the study visit. Also Mattias Andersson, fellow master thesis student is acknowledged for all help with the electrical experiments. Next I would like to thank my other three supervisors Anette B. Johansson, dr. Xiangrong Chen and Markus Jarvid at Chalmers University for all the support, insights and learning opportunities they provided. Gratitude also goes to prof. Stanislaw Gubanski for being a good examiner throughout the thesis. I would like to thank Yuriy Serdyuk for assistance and valuable tips for the finite element method calculations of the electric fields in the project. A big thank you is also aimed towards Xiangdong Xu for the assistance with the conductivity measurements. Staffan Josefsson is also acknowledged all help with the electrical aging test setup at Nexans. Ida Anna Budalen from Nexans is acknowledged as well for performing the HPLC-measurements. I would also like to thank everybody from the Division of High Voltage Engineering and Polymer Technology and from Nexans for helping out and allowing me to have access to all valuable equipment. Last of all I would like to thank my girlfriend Louise Béwe for her patience and love through all the late evenings and extra weekends I worked on this thesis.

Espen Doedens

Göteborg 13/6 2012 Sweden

Table of Contents

1 Introduction

This master thesis project has been performed at Chalmers in cooperation with Nexans Norway AS. The impact of organic contaminants on electrical treeing and water treeing is investigated. Both optical and statistic observations have been made with the aid of different microscopes, voltage measurements and a high resolution camera. The provided reference material, in this case polyethylene pellets, was supplied by Nexans AS and manufactured by Dow Chemical Company. Organic contaminant grains were obtained from Sintef Energi AS in Trondheim, while organic contaminant powder was manufactured from the supplied pellets. The rest of the used materials and equipment was supplied by Chalmers.

1.1 Background

When determining the quality of high voltage cables, the electric lifetime of the cable is an extremely important measure. A prolonged lifetime is closely related to sustainable development, which is a key subject to engineers around the world. As often occurring in high voltage engineering, the insulation thickness of a high voltage cable is a trade-off between reliability and costs. A thicker insulation might be a more reliable option with a longer lifetime, since a lower electric field is present in the material. A reduction of the insulation thickness will reduce the material costs drastically. The craving for long lifetime at low costs is a driving factor for improvement of high voltage cables, and in particular for improvement of the cable insulation. For crosslinked polyethylene (XLPE) insulations different aging and degrading phenomena are present, which will limit the electrical lifetime of the insulation. Two types of electrical degradation are electrical treeing and water treeing. These types of degradation are often initiated at points with high divergent electrical fields, caused by imperfections or impurities in the material. From these points tree like structures are then created over long time (hence the name treeing), increasing the probability for a breakdown in the material. Organic contaminants present in XLPE, in this case chemically aged XLPE, are also known to initiate electrical treeing and water treeing. This makes further knowledge on these contaminants and their impact on treeing a key issue for further improvements. It can also be noted that very little is known within this subject.

1.2 Purpose

The main purpose of this master’s thesis is to create a model of different contaminants and their impact on treeing and electrical breakdown strength in:

1) XLPE.
2) Water-saturated XLPE.

The study uses a wire-plane configuration. The electrical field distribution in the configuration is further investigated. Different degree of oxidation of the contaminants is included in the study, as well as different distributions such as a homogenous distribution throughout the entire sample or insertion of small grains of the contaminant in the vicinity of the wire.

1.3 Scope

The main priority of this thesis was to investigate the influence of organic contaminants on electrical treeing and water treeing degradation. A series of reference tests were performed in order to characterize the supplied material. Also a test method for aging of the samples over a longer time was developed. The initial ramping speed of the applied voltage was set to 250 V/s, since this was the lowest ramping speed the generator could provide. Tests on inserted grains where performed with water saturated XLPE, in order to study possible water tree development in the samples. Also, tests with homogenously distributed contaminants where performed with normal XLPE, to discover if an earlier treeing initiation was present in the samples. All contaminants where characterized with IR-scans. Also the gel content was measured, to investigate if the samples were fully crosslinked. All AC voltages in the thesis had a frequency of 50 Hz. At last, DC tests were performed on samples with homogenously distributed contaminants, to reveal the impact on DC breakdown strength.

1.4 Method

For an evaluation of the electric field, the configuration was simulated in COMSOL multiphysics [1]. The used samples were created at the Division of Polymer Technology of Chalmers, using the provided polyethylene and other materials. Electrical tree growth tests were performed at a high voltage laboratory at the Division of High Voltage Engineering, also at Chalmers. The test setup for these tests was already in place due to other ongoing research on electrical treeing. The water tree growth tests were performed at Nexans AS. Here the test setup was constructed with assistance from Susanne Nilsson and Staffan Josefsson.

2 Literature review

In this chapter, different subjects of importance are elucidated further. At first typical high voltage cables and their characteristics are described. Then the processes behind electrical treeing are explained. Most of the theory on breakdown and aging was found in Dissado's and Fothergill's book: Electrical degradation and breakdown in polymers [2]. Also the organic contaminants used are described. At last the function of the wire plan test method is described.

2.1 High voltage cables

A typical high voltage cable contains of several layers with various functions. The simplest version is shown in figure 1, although often even more layers are present [3]. The different layers, as presented in figure 1, are: (2) Conductor, (3) Inner Semiconducting Layer, (4) Cable Insulation, (5) Outer Semiconducting Layer, (6) Ground layer and (7) Outer shell.

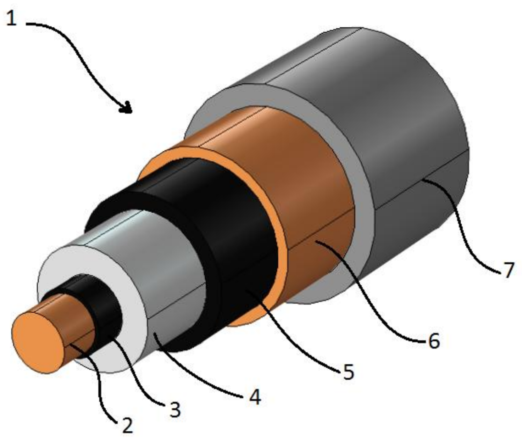

Figure 1.Schematic of a typical high voltage cable

For underground cables, the conductor is made of copper or aluminum for obtaining good conduction as well as good mechanical properties. For obtaining a smooth surface around the conductor, a semiconducting layer is present. This is to avoid local field enhancement due to defects. A local field higher than 100kV/mm is said to be able to inject a high amount of electrons into the insulation system [4]. The insulation layer has to withstand the high divergent field between the conductor and the grounding layer (further described in 2.1.1). The outer semiconducting layer is yet again present to smooth out local field enhancing defects. Connected to this layer is the grounding layer, which typically is made of small copper wires for underground cables or a lead barrier for submarine cables. Outer protective layers are often made of polymers such as PVC or polyethylene, providing good mechanical resistance at low cost. The protective layers and grounding layer often also contain the mentioned lead shield barrier and additional swelling tapes, functioning as a water sealing. The water sealing is to avoid water penetration in the high voltage cable.

For medium voltage submarine cables, with rated voltages up to 36 kV, it is normal to exclude water sealing of the cables in order to reduce the weight and cost of the cables. Also for dynamic cables for e.g. offshore wind farms, the lead barrier normally is excluded, as lead is not fatigue resistant. The result is that water penetrates into the cable, saturating the polymeric insulation of the cable. When water is present in the polymeric matrix particular water trees can grow. Water trees are further described in chapter 2.3.

2.1.1 Cable insulation materials

Conventional high voltage AC cables commonly used paper insulations with oil, or mass impregnated paper as insulation layer. The oil-paper consists of thin paper strips impregnated with dielectric oil, lapped around the inner conductor [3]. In particular mass impregnated cables are still manufactured today, due to the ability for quick voltage reversals (in DC) and high reliability [5]. These properties make them suitable for High Voltage DC (HVDC) cables. Nowadays, for many high voltage cables, in particular AC cables the insulation material used is instead crosslinked polyethylene (XLPE). This material is used due to less complicated manufacturing by extrusion. It also has good insulation properties such as low dielectric losses, which is referred to as tan(δ), and good mechanical strength. But for HVDC these extruded cables do not have the same reliability, nor the same voltage reversal capability as the conventional oil-paper insulated cables. XLPE has the ability to trap charges for a longer time than the oil-paper insulation, with the possibility for creating a homocharged field enhancement directly after the reversal. Also the long term reliability has been reduced due to the aging of the material.

Early XLPE AC cables had a tendency to break down prematurely due to imperfections and moisture within the cable, creating different trees in the insulation. By increasing the cleanliness and the prevention of contaminants in the manufacturing process this degradation mechanism has been greatly reduced [6].

2.1.2 Crosslinked polyethylene (XLPE)

XLPE is created by cross-linking of the polymer chains in polyethylene. By chemically binding the polymer chains, the high temperature performance is improved [7]. As high voltage cables generally are desired to withstand as high currents as possible, the limiting factor involved is the temperature in the cable core created by joule heating. If the temperature in polyethylene is increased above the melt temperature (T_m), the material will melt [7]. For XLPE the material will never melt, only soften slightly, since the introduced crosslinks retain the dimensional stability. There are several different ways to crosslink polyethylene. The pellets provided in this thesis contained peroxide crosslinking agents. Peroxide crosslinking creates links between the polymer chains, as seen in figure 2.

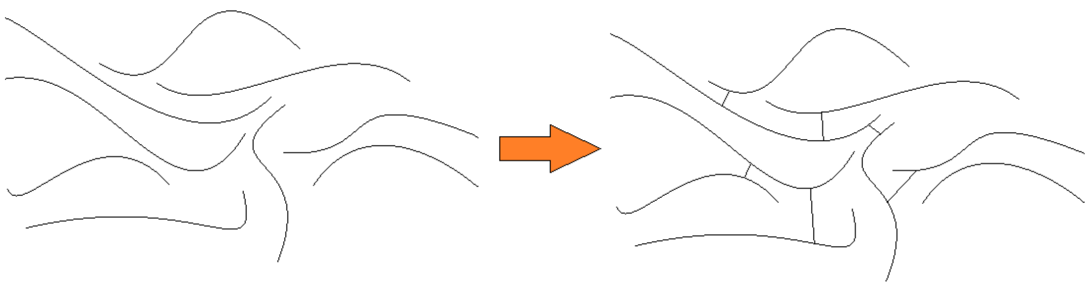

Figure 2. Introduced links between polymer chains turn polyethylene into XLPE.

The chemical process responsible for the crosslinking can be of different types. The most common types are silane crosslinking and peroxide crosslinking. The XLPE used in this thesis is created by peroxide crosslinking with dicumyl peroxide (DCP). The peroxide crosslinking process is initiated at temperatures above 140 °C, so normally temperatures around 180 °C are used for this process. At this temperature the peroxide will thermally decompose, creating free radicals [8][9]. The oxygen of the peroxides will subtract hydrogen from the polymer chains leaving connections for the chains to interconnect. Normal HV cables with rated voltages higher than 36 kV, are degassed for a few weeks to decrease the content of byproducts from the crosslinking reaction. In order for created test samples to have the same chemical properties as HV cables, a degassing process was necessary

When cooling down the polyethylene from 180 °C to room temperature after the crosslinking process, the cooling rate is essential for which crystalline structure is to be created. Using a slow cooling rate will create more lamella and spherulite structures in the material [10]. Using a fast cooling rate will create more amorphous structure with less ordered crystalline structures in the material. This is valid for both LDPE and XLPE.

The polyethylene pellets used in this thesis also contained antioxidants. Antioxidants reduce the amount of aging, in particular chemical aging [11]. Also other chemical specimens can be added to the material, such as voltage stabilizers or water tree retardants for wet designs. Voltage stabilizers are chemical specimens with the capability of absorbing the energy of high energy electrons, reducing the electrical treeing process in the material. Several Ph. D's and master theses are done on this subject at Chalmers, sharing the same test equipment and test method as this thesis [9][12][13].

2.1.3 Different types of degradation in high voltage cables

The degradation and breakdown phenomena described are valid for polymeric insulation types such as XLPE. In these insulations, a number of degrading processes can occur which do not destroy the insulation, but instead are able to trigger different breakdown mechanisms as described in chapter 2.1.4. These processes are often slow and become severe after several years of normal operation in high voltage cables.

The two aging processes referred to as physical aging and chemical aging are types of low level degradation. This means that they are present even if none or only low electric field strength is applied on the material. Physical aging is a process triggered by inner tensions between polymer chains, which are left in the material after the temperature is decreased below the melt temperature (T_m). These inner tensions will trigger a structural relaxation. The physical aging of the material can be measured in terms of free volume. Free volume is the measure of inefficiency of molecule packing in amorphous regions. As the material tries to relaxe continuously and the volume of the insulation is constant, this will cause a secondary crystallization in the material. Along with this crystallization come additional microvoids and discontinuities. Also additional interfaces between amorphous and chain folds will increase the number of electron traps, with the ability to trap more space charge over a longer time in the material [14].

Chemical aging occurs when the polymer chains in the material are subjected to chain scission, breaking them down into shorter chains. This process is often preceded by the formation of polymer free radicals. These radicals are very chemical reactive and can cause polymer chain scission. These radicals are also responsible for the crosslinking of the material, as described in chapter 2.1.2. Chemical aging can be caused by UV-light, mechanical stress, thermal stress or ionizing radiation such as high energy electrons. Often a combination of the above described factors is present. The chain scission also has the ability to create microvoids in the material [14].

In contrast to low level degradation, electrical aging occurs in the material when a higher electric field is applied. However these types of degradation are still present at low level since they can be caused by applied voltages below the electrical breakdown strength. It should also be noted that electrical aging has the ability to accelerate both physical and chemical ageing. The most severe forms of electrical degradation are electrical treeing, water treeing and partial discharges (PD:s). PD:s occur in microvoids and small air bubbles in the material. Since these voids often are filled witch air, small local flashovers will occur already at field strengths exceeding 3 kV/mm [2]. These local flashovers create erosion in the material by bombarding the edges with high energy ions and electrons. This bombardment can initiate the growth of electric trees. Electrical treeing and water treeing are two different degrading processes both creating tree like structures in the material. Electrical treeing and water treeing is described more thoroughly in chapters 2.2 and 2.3 respectively.

At last combinations of mechanical and electrical degradation can be mentioned. In reality the aging processes occurring in a high voltage cable is a combination of most of the explained phenomena. Mechanical aging by the application of mechanical stress to the polymer matrix can create defects and cracks in it. These defects are stress points where electrical aging can commence [2].

2.1.4 Different breakdown mechanisms in high voltage cables

The breakdown of a cable can be considered in three categories. Low level degradation (described in 2.1.3) is the first breakdown category, as well as a triggering event for quicker breakdown events. The 2 other categories are the deterministic models and stochastic models. The deterministic models focus on the quick breakdown events described in this chapter, whilst the stochastic models are used for obtaining time-to-breakdown in high voltage cables.
As all breakdown events occurring in the polymeric insulation are irreversible, they are to be avoided at all costs. The deterministic breakdown models include: electric breakdown, thermal breakdown, electro mechanical breakdown and partial discharge breakdown. Also an intrinsic breakdown is possible, referring to a material's ultimate breakdown strength [15].

The electrical breakdown mechanism relevant for polymer insulations is called avalanche breakdown. When sufficient electric field is applied to insulating materials, the carriers (electrons ions etc) in the material are able to acquire enough kinetic energy in-between collisions with the polymer matrix in order to ionize the material. As the probability for ionization increases, additional carriers will be created from the collisions. Also the amount of recombination is reduced as this probability increases. The small current, or flow of carriers, present in the insulation is then multiplied several times. Even though multiple evidences exist, this theory is considered controversial. The carriers, in this case electrons, with sufficient kinetic energy are referred to as 'hot electrons.' Both electro-luminesence and free radical generation have been observed in experiments [16][17], confirming their existence. In normal insulations the critical field levels are only present at local field enhancements such as tips of electrical trees or build up heterocharge near electrodes. The Fowler-Nordheim process, in which the electrode-polymer barrier is lowered allowing a tunnel injection of electrons from electrodes into the material, also contributes with an increased amount of carriers. It can be summarized that avalanche multiplication determines the breakdown strength, and that the breakdown is likely to start from electrode-polymer interfaces. When an avalanche is big enough a streamer develops, creating a short circuit part through the insulation.

Thermal breakdown is initiated in the materials as the heat input, in general created by joule heating, is not balanced with the dissipated heat. As this causes the temperature in the material to increase, the electrical conductivity increases exponentially as more carriers become available. An increased electrical conductivity causes more current to flow through the material, increasing yet again the heat input created by joule heating. As this process develops a thermal runaway can occur in the material [15]. The process is displayed below in figure 3.

$$\left(P_{th,injected} - P_{th,dissapated}\right) \uparrow \Rightarrow T \uparrow \; \Rightarrow \sigma \uparrow \; \Rightarrow I_{leaked} \uparrow \Rightarrow P_{th,injected} \uparrow \; \Rightarrow runaway$$

Figure 3. Thermal runaway process.

Electro mechanical breakdown is caused by the electrostatic attraction of the electrodes on both sides of the insulating material. As an increased electric field is applied to the insulations, the attractive force is increased as well as the joule heating of the material. The heating of the material causes the polymer to soften. Due the softening and the increased force a decrease of the insulation thickness can be present. This mechanism is eliminated by using sufficient insulation thickness as well as using crosslinked polyethylene. As described in 2.1.2 crosslinking prevents the melting of the material.

Partial discharge breakdown is initiated by small voids in the material. The way to breakdown is mostly by the development of tree like structures. Therefore the process is often referred to as electrical treeing. Electrical treeing is explained below in chapter 2.2.

2.2 Electrical treeing degradation

The following chapter describes the processes behind electrical treeing. The main part of this theory is adopted from Dissado and Fothergil [2]. For electrical trees do be developed, a high electric field is required. Electrical trees are generally initiated from contaminants, faulty geometry, voids or cracks, as insulation normally is dimensioned to withstand this type of defects. Electrical trees contain a connected structure of hollow tubules, forming a treelike structure with leftover graphite and other products. The stem of a tree typically is in the range of tens of micrometers in diameter, while the filament only is a couple of micrometers. Electric trees can have shapes such as bush and branch, separated by the shape of the tree. Higher fields generally create more bushy trees, while trees generated at lower fields generally have a more branch like shape. In order to describe the process, it is divided into 3 different stages, which are: inception, propagation and runaway. Electrical trees have been observed to grow in bursts. A wide variety of measurements have been done, supporting a clear model of the process.

2.2.1 Initiation

The initiation process begins with the injection of space charge, which occurs at field strengths exceeding 100 kV/mm [4][18][19]. When AC stress higher then this value is applied to the insulation, charge carriers can be injected or subtracted from the material in the vicinity of the stressed area. It is possible for this charge to be retained by deep traps. When this occurs, a heterocharge is created next half-cycle. The tree is then created by a local breakdown, described in two different ways by different theories. Electroluminescence is observed prior to the inception of electrical trees [20][21][22], and is explained by both theories as well.

- Electrons accelerate and reach kinetic energies up to 3-4 eV. These ‘hot electrons’ break polymer bonds by impact ionization or excitation. Electroluminescence is created by excited molecules returning to their original states [4].

- Charge recombination occurs in the material where electrons trapped from the previous halve-cycle recombine with holes injected the next halve-cycle. This process creates electroluminescence. Electroluminescence contains UV-light, which may able to breaks bonds and generate free radicals [23].

High enough electric fields will create local avalanches in the degraded area, and the treeing will begin.

2.2.2 Propagation

The area degraded by the treeing initiation is now further eroded by electron bombardment, creating a first tube. Ions produced in avalanches create positively charged bands along this channel's length. These ions neutralize new electrons injected from the electrode, and the growth of the tube will halt. Trapped electrons can still be extracted from the polymer at tip of the tube, making the tree propagate into all directions by creating back avalanches [24]. Electrons in these discharges can reach kinetic energies up to 10 eV at the discharge tip, which is sufficient for bond breaking. The branches continue to grow in all directions by extracting electrons. The ion bands disappear after a short period due to neutralization and diffusion, allowing for the forward discharges to recommence. This growth pattern makes the tree grow in bursts with both forward and backward discharges extending the tree. In many created channels, the discharge activity is extinguished, with possibility for reignition. All the discharges create gaseous and graphite decomposition products in the hollow channels. These channels with leftover products are clearly visible in figure 4.

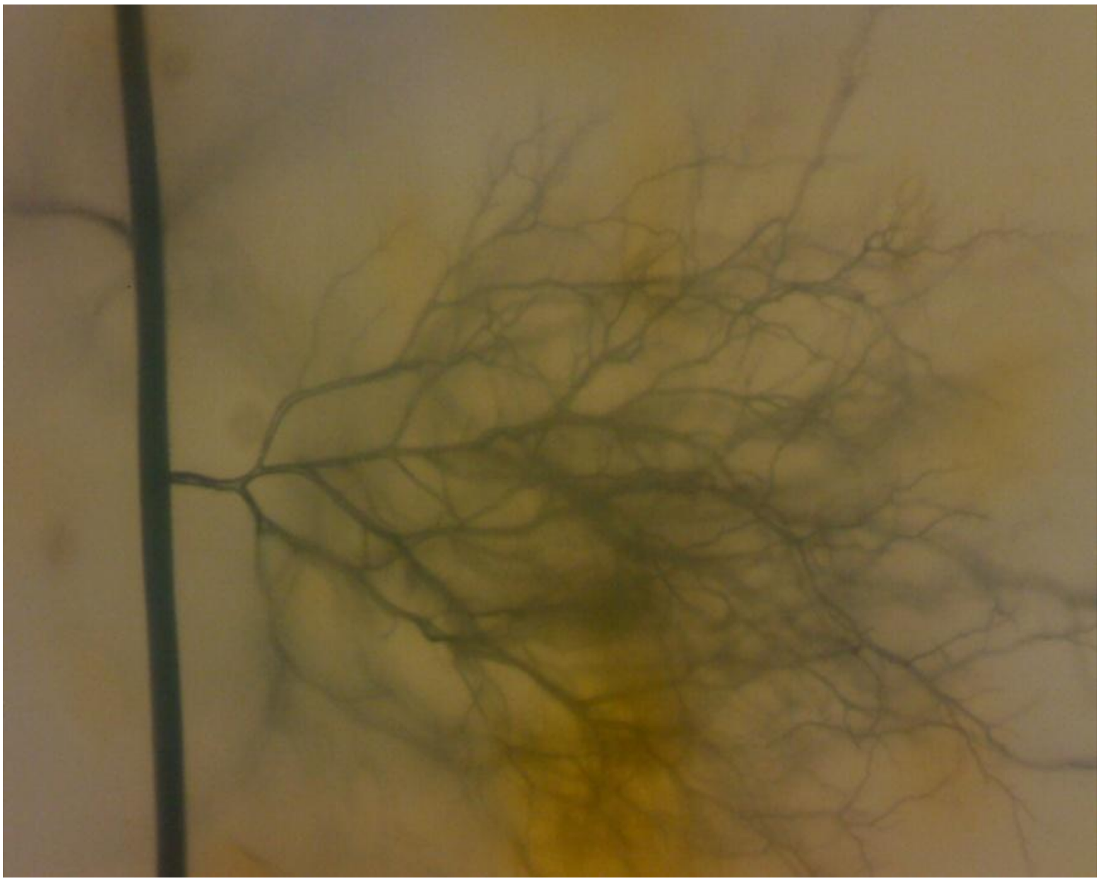

Figure 4. Electric tree with clearly visible channels and decomposition products, created by 20 kV aging with contaminants (yellow-brown areas).

As the tree develops, an increase in gas pressure is found inside the tree channels. This increase creates stagnation in growth, as overpressure is known to reduce avalanches [15]. For bush trees the growth stagnates more than for branch trees, showing that a somewhat smoothened out electric field due to the semiconducting decomposition products inside the channels exists.

2.2.3 Runaway and breakdown

As the tree increases in size, the electric field is moderated. This is due to the graphite and semiconducting decomposition products present on the tree walls, see figure 4. As the tree propagates, the field at its tip will increase. At a certain moment the growth speed will begin to increase, to create a runaway of treeing just before the breakdown is triggered in the material. The breakdown is triggered due to the weakening in the polymer, which at last will allow for a full streamer to develop through the material. After this a full short circuit of the insulation is created [2], an example is shown in figure 5.

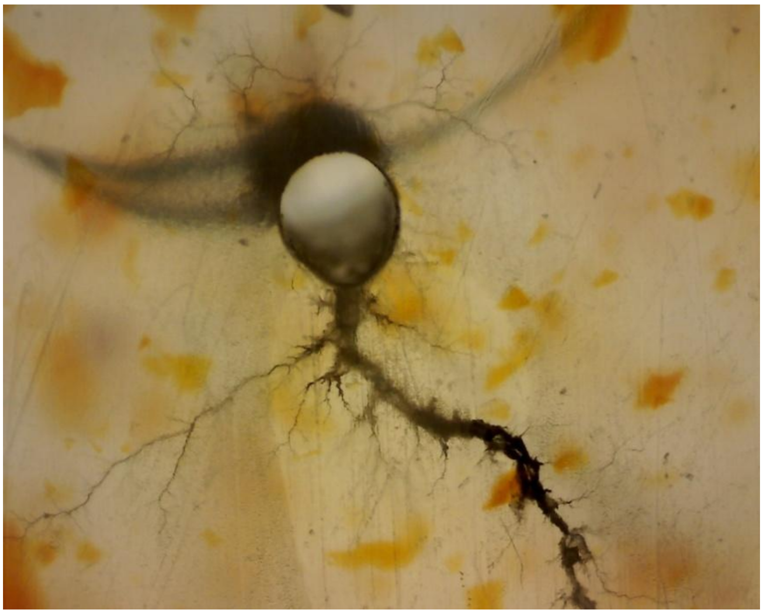

Figure 5. Electrical treeing sample subjected to a full and irreversible breakdown.

2.2.4 DC

The process described so far is valid for AC only. When DC stress is applied to the insulation, similar form of electrical treeing degradation takes place, only with slightly altered processes. Often trees thought to be created by DC stress are actually created by an AC ripple present in the DC. A known problem is that for DC the treeing inception voltage often exceeds the DC breakdown strength [22]. By using a faster ramp up rate of the voltage, the inception voltage is reduced since less space charge has time to accumulate in the material. Also small but undetectable microvoids in the material are known to lower the inception level. The main difference in the propagation of electric trees under DC stress is that only one-directional discharges and avalanches occur. Ramped up and down DC voltages can create pulses of injected charge carriers. The DC process begins with the creation of a tubular channel like in the AC case. The heterocharge present at the channel sidewalls is after a while neutralized by additional injected charge carriers from the electrode, as in the AC case. As the electric field is to be the highest at the tree tip, the tree propagates from the tip, one avalanche at a time with a possibility for branching. The propagation ceases when the created space charge reduces the electric field enough at all tree-tips. The time required for this space charge to disappear ranges within weeks for polyethylene [2][25].

2.3 Water treeing degradation

Water treeing degradation is the formation of a large number of electrolyte filled microvoids with possibly oxidized or chemically modified inner surfaces. The scattering in between these microvoids commonly form a diffuse tree shaped outline, hence the name water treeing. An applied electric field is essential for the development of water trees, but in comparison with electric trees, a much lower threshold for appearance is present. According to Dissado water trees may occur already at field strengths of 1.9 kV/mm [2]. Another key factor essential for water tree development is the presence of an electrolyte in the material. After a water tree has been created, it is in place permanently. It is possible though for a tree to disappear as the electrolysis is removed. The tree will then reappear when the material is resaturated with an electrolyte as the created voids have a hydrophilic nature. Water trees can be hard to detect as they contain transparent electrolyte. This calls for a method for making them more visible, which is often done by staining water trees with methylene blue (this is further described in chapter 3.2.3).

Water trees generally occur in two different forms. These shapes are bow-tie and vented. Trees are initiated from deformations or contaminants in the material, where the local electrical stress will be increased. Vented trees are generally created by deformations at the edge of the insulation while bow-tie trees are created by contaminants inside the insulation. There a lot of factors which influence water treeing significantly. Some factors are:

- Applied frequency (affects both initiation an propagation).
- Degree of crosslinking [8][26].
- Morphology of the polymer matrix [27].
- Magnitude of the applied electric field [28].
- Electrolyte’s chemical content.

As water treeing degradation is a slow process, experiments generally accelerate the process by increasing the frequency and using a high applied field (still low enough to prevent electrical trees from occurring). Finally it can be stated that water trees are not created by local electric breakdowns as electric trees are. Water trees slowly degrade and weaken the polymer material, allowing for earlier initiation of electrical trees. Also no fully conducting paths are created. Water trees create areas with higher conductivity as the rest of the polymer.

2.3.1 Water tree mechanisms

For the explanation of water treeing, a large number of different theories exist describing the process. These are stating the process to be a different combination of electrical, chemical and mechanical processes combined or only 1 or 2 of these [2][29]. Nowadays two main tracks exist describing the process, where Dissado’s electro-chemical [30] counters Crine’s electro-mechanical [31][32] explainaition.

The initiation of water trees occurs due to enlargement of nanovoids already existing in the material due to free volume. Dissado explains the process to begin with the dissociation of water in these sites forming radicals. As these radicals react with the polymer chain scission can occur forming polymer radicals. The broken chains can reconnect with other chains nearby, enlarging the void [30]. According to Crine treeing initiation commences instead by nanovoids in the material which assemble due to mechanical forces created in the polymer by the electric field, yielding bigger voids such as microvoids [31].

The propagation process of water trees involves the creation of additional voids. The connection between these voids is by excess aqueous electrolyte solvated in the material [2]. According to Dissado the void enlargement is halted by metal ions solvated in the electrolysis. These ions cluster up in the oxidized site, stabilizing it. As the applied electric field applies mechanical stress on nearby polar chains, segmental motion can occur since the local morphology now has been changed. Due to this additional free volume can be created, allowing for new oxidation sites and the transport of additional water [30]. Crine instead explains the propagation process by additional nanocavities joining together, and claims that if a complex chemical process exists, it is merely a secondary process [31]. As the filled voids partially conduct, the electric field will be enlarged at the tree tip, making the tree grow mainly in the forward direction in both cases.

2.4 Organic contaminants

Contaminants in high voltage cables can be divided into two groups:

1) Organic Contaminants (OC)
2) Inorganic Contaminants (IC)

IC consist mainly of metallic particles, or materials migrated from the semiconducting layer. IC are well known and are avoided at all costs due to their large impact on electrical breakdown strength. This thesis will focus on OC since much less is known in this area. OC are mainly created by thermal degradation of polyethylene, aging the material through chain scission [14]. OC in cables often originate from aged flakes in the supplied pellets, or from over temperatures during the extrusion/crosslinking process. Also processes in the cable production located after the extrusion process have the ability to create OC. It is possible for the contaminants to be badly adhered to the surrounding material. The bad adhesion will then form a local void in the material serving as a initiation site for PD:s. This makes the bad adhesion and the created voids the main cause for decreased electrical breakdown strength in the material [2]. An organic contaminant is shown in figure 5.

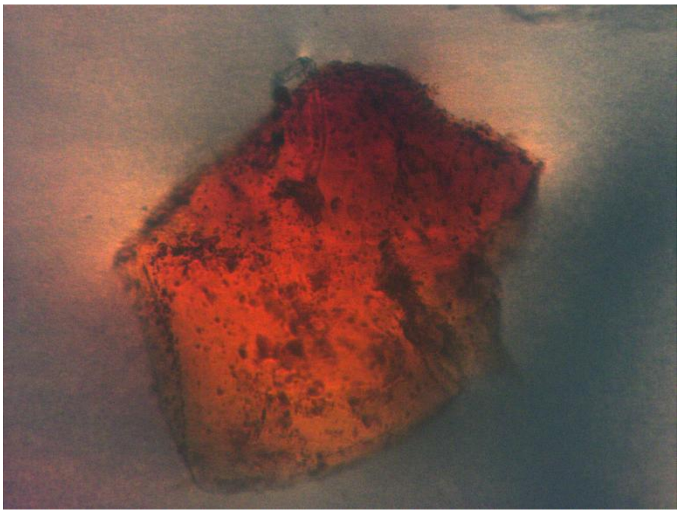

Figure 6. Organic contaminant placed in XLPE test sample, photographed with polarized light.

As OC are created, the dielectric properties of the material are changed. OC result in increased loss factor (tan δ) as well as in different conductivity and permittivity as XLPE. Also their bad adhesion, especially combined with humidity, has such an effect. The permittivity of OC changes less than the conductivity. A measurement on relative permittivity showed that it increased from 2.74 up to 2.93 after aging the material for 150 hours at 200 °C [33]. Reaching a relative permittivity of over 4 is unlikely to occur. The relative permittivity in inorganic contaminants (IC) can also be lower than for XLPE. The changes in permittivity and conductivity in the particles will create local field enhancements, likely of around 2-3 times.

During impulse tests on samples with OC, only 15% failed directly at the inclusion [34]. This proofs that OC not necessarily are electrically weak. It has been reported that tests using IR measurements on water trees created from OC, showed traces of ethylene glycol in the material. Ethylene glycol is known to have a large impact on water treeing [35]. Whether the glycol is a byproduct from water treeing or is originating from organic contaminants is not known. The mechanism involved creating the decreased breakdown strength for dry samples during AC stress also is unknown. Neither if mechanical stress might initiate voids due to the porosity of the OC. Finally, the OC impact on HVDC breakdown strength also is an unexplored territory.

2.5 Wire plan test method

For treeing tests, there are different approaches depending on the desired output. All approaches aim to represent a high voltage cable insulation system to a certain degree. Some test methods actually involve pieces cut off from real cables [36]. The advantage of these methods is that the morphology and physical properties are matched with those of real cables. The drawbacks are generally high sample costs and long test times. In order to increase reproducibility, decrease costs and reduce test times, small test samples with stressed fields are created. By using sharp controllable edges on electrodes in the samples, high field intensification is created, reducing the test times. Such typical test methods are the ASTM standard test method [37] or similar needle –plane or needle – needle topologies. These samples usually have easy correlation between applied voltage and electric field strength, as no complex field topologies are used.

The test method used in this thesis uses a wire plan topology, a sample can be seen in figure 7. The method was developed at Chalmers University [38][39]. The method has also been evaluated and improved in different diploma works and PhD studies [9][12][40]. The method uses an extremely thin wire to stress the field. A reduced amount of air bubbles inside the produced test samples are found in this method when compared to test samples with needles. Another advantage is that a bigger area is stressed with a high field, allowing for multiple trees to be created within one sample. This advantage also has a drawback, which is a more complex field topology. Also small kinks (chapter 4.1.1.4) can appear in the samples, altering the electric field. Due to this complex topology extensive field simulations are performed in appendix I.

3 Method

In this chapter the approach of the tests performed is described. First the sample manufacturing process is described in detail. Second the tests methods used for characterization of the samples and contaminants are listed. Next the method for the electrical field calculations is mentioned. The different electric tests performed are described afterwards. At last, the statistics used for the data analysis are explained. All tested samples in this project where of the wire plan topology, as described in chapter 2.5. The dimensions of the samples are shown below in figure 7.

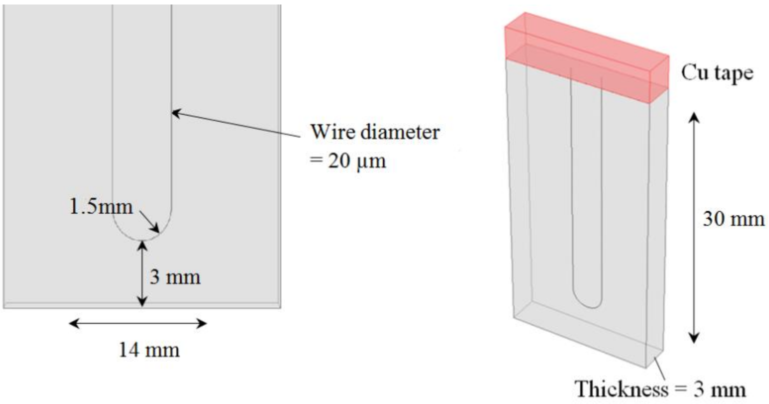

Figure 7. Dimensions of the manufactured test samples used in this project.

3.1 Sample manufacturing

For the testing of the material different test samples are manufactured. The samples were made at the Division of Polymer Technology at Chalmers. The samples were made in batches, with each batch containing 21 samples. A batch of samples is displayed in figure 8, (a). At first polyethylene halves were made from the provided materials. As these halves were assembled complete samples were made, and crosslinked to create XLPE. After the crosslinking, the samples were degassed and investigated with a microscope.

As the first batches turned out to have large fluctuations in the distance between the wire and the bottom of the sample, only half the amount was crosslinked at a time (b). For each batch the crosslinking process now had to be done twice. The empty spaces between the samples gave space for the excess material to flow into. Totally in this thesis, 7 batches were created with the original method (figure 8, (a)) and 14 batches with half the amount crosslinked at a time (figure 8, (b)). For the original method, the distance between the wire and the bottom varied between 1 and 6 mm. With half the amount crosslinked at a time, the wire bottom variation was reduced to between 4 and 4.6 mm. The influence of this variation on the electric field in the samples is further investigated in Appendix I.

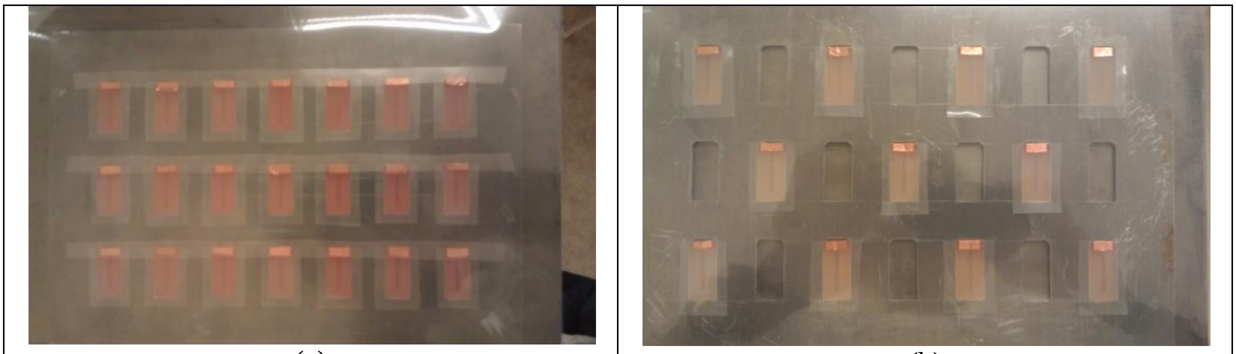

(a) (b)

Figure 8. A completed batch of samples ready for the crosslinking and joining process.

3.1.1 Contaminant manufacturing

The contaminants inserted with a homogenous distribution were produced at Chalmers, while the contaminants used for individual insertion were obtained from Sintef Energi AS. The manufacturing of the contaminants began with the production of thin XLPE films with a thickness of around 0.2 mm. The films were manufactured with a similar pressing procedure as described in chapter 3.1.3, except for somewhat shorter melting and crosslinking times. Next the films were degassed for approximately 12 hours by soaking them in methanol. The XLPE films where then inserted into an "*Elastocon EB 01 900W*" sample oven, aging them for different times (1-7 days) at 180 °C. Also some films were not aged in order to create pre-crosslinked grains for investigation of the morphology impact of the grain insertion. The aged films can be seen in figure 9.

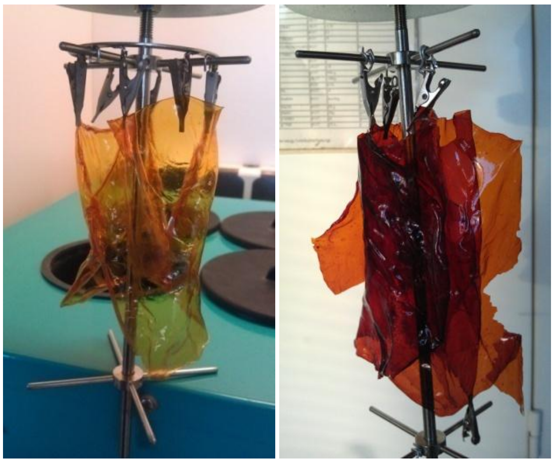

Figure 9. XLPE films aged for 1 (left) and 7 (right) days.

3.1.2 Material production

The pellets provided by Dow Chemical Company contained both peroxide crosslinking agents and antioxidants. Before usage, the pellets were ground into a fine powder. This was done by first cooling them in liquid nitrogen, after which they were ground in a retch rotating mill. The contaminants created in this thesis were also ground in this mill. For the reference samples, no contaminants were inserted, while for the homogenously contaminated samples a certain amount of contaminants was mixed with the clean powder.

3.1.3 Pressing procedure

For creation of two different strips, the ground polyethylene powder was weighed and placed into molds which were inserted into a press-oven. First, the preheated press-oven melted the powder for 3 minutes, after which a press-force of 200kN was applied in order to shape the different strips. After 6 minutes the temperature was ramped down to 20 °C, with a cooling rate of 7.33 °C/min. The total procedure took 21 minutes, as seen below in figure 10.

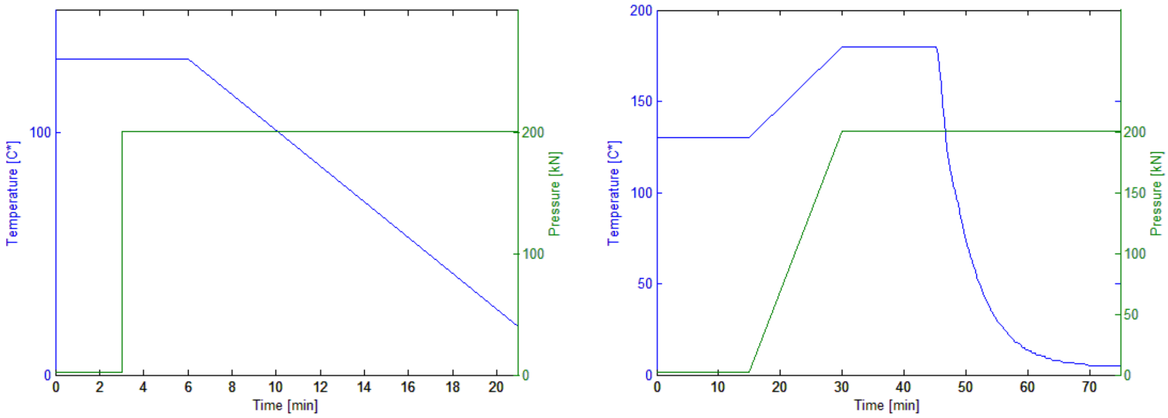

Figure 10. Pressing schedule for the polyethylene strips manufacturing process (left) and pressing schedule for the crosslinking process (right).

When the different strips were completed, a 20 μm tungsten wire was inserted in between the two strips. In some cases, also some contaminant grains were inserted in the vicinity of the wire. The two halves were then closed with the wire attached to a piece of copper tape.

After the samples were assembled, they were yet again placed in a mold and inserted into the press oven. The temperature in the pre-heated oven was first kept constant at 130 °C for 15 minutes. During the next 15 minutes both temperature and press-force were ramped up to 180 °C and 200 kN respectively, in order to start the crosslinking of the polyethylene. After another 15 minutes the crosslinking was complete. At this time the temperature was decreased as fast as possible in the press oven, to minimize the chemical aging that takes place due to the high temperature. For the first 2-3 minutes, the cooling rate was up around 35 °C/min, until the temperature had decreased to around 100 °C. Then the cooling rate was around 11.1 °C/min until room temperature was reached. After a total time of 75 minutes the procedure was completed. The whole pressing schedule is displayed in figure 10

In order for the press oven to decrease the temperature as fast as possible, the reference temperature of the oven was instantaneously switched to 0 °C at 45 minutes. Due to this the samples were cooled to a minimal temperature of 5 °C, which was the temperature of the cooling water. The rapid cooling was used in order to create as much amorphous regions as possible. The rapid cooling is also used to reduce the amounts of kinks in the samples. As the rapid cooling had been introduced recently, a gel content measurement was performed.

3.1.4 Degassing

After the completion of the samples, the samples were placed in a "*Binder*" vacuum oven. This was in order to remove the liquid crosslinking by-products created during the crosslinking process. Chemically, the crosslinking by-products often have a positive effect on electrical treeing resistance. If the by-products diffuse during operation, the effects are negative due to void formation and in particular their explosive nature. High voltage cables with rated voltages of over 36 kV, are normally degassed. The temperature of the vacuum oven was set to 75 °C, but due to a defect the temperature was generally somewhat lower.

3.1.5 Completed samples

Three different completed samples are displayed below.

Figure 11. Three different completed samples: reference sample (left), sample with separately inserted contaminants (middle) and sample with homogenously distributed contaminants (right).

Samples with no or differently inserted contaminants were used. Samples with no contaminants were used for reference tests. Samples with separately inserted contaminants were used for wet and dry aging tests. Samples with homogenously distributed contaminants were used for both AC and DC tests.

3.2 Evaluation of the manufactured samples and contaminants

A series of tests for investigation of the manufactured sample's and contaminant's characteristics were performed. These are gel content and HPLC (high performance liquid chromatography) measurements for the test samples, as well as the methylene staining. The contaminants have been characterized both electrically and through an IR scan.

3.2.1 Gel content measurement

To assure that the samples were fully crosslinked, a gel content measurement was performed. From 3 samples each, 0.3 g XLPE was microtomed, creating 30-150 µm thick sheets. From these sheets the uncrosslinked polyethylene was extracted with decalin (decahydronaphtalene). After 6 hours the decalin was replaced with new decalin and again the samples where boiled this time for 1 hour. The samples where then dried in an oven at 100 °C for 3 hours. The samples where weighed before and after the process.

3.2.2 HPLC measurements

HPLC measurements on the test samples were performed at Nexans in Halden. HPLC measurements are performed by solving the test samples in a solvent, and with a high pressure pump forcing the liquid through a column. In this column, different molecules are absorbed or adsorbed depending on their characteristics. The travel-time will now vary depending on the polarity of the molecules. At the end of the column, a detector is placed, measuring the amount of rest-products left in the liquid [41]. From this, the amount of crosslinking by-products left after the degassing process is determined.

3.2.3 Methylene staining

A methylene solution was prepared in advance at Nexans, containing methylene blue, sodiumcarbonate and distilled water. First the water aged and electrically tested samples were microtomed into thin slices of approximately 300 µm. These slices were then stained in the solution for 50-60 minutes. Afterwards the slices were cleaned, first with 50 °C water, next isopropanol and at last dried. Methylene blue stains the possible water trees, making them visible under a microscope.

3.2.4 IR measurements

After the aging process, the films where characterized with ATR (Attenuated Total Reflectance). ATR is a detection method used in conjunction with infrared spectroscopy (IR) or fourier transform infrared spectroscopy (FTIR). By checking the absorption of different wavelengths of infrared light, conclusions could be made of the chemical content of thin films. For comparisons between different films, a reference sample is needed for normalization. Absorbance spectra can also be converted to Transmittance spectra by simple means.

For studying the chemical content of thermally aged polyethylene different peaks become interesting. Carbonyl groups present in aged polyethylene are known to have a medium to strong peak at around 1720 cm^{-1}. This peak has been detected for light amber colored aged polyethylene, and is the result of double bounded oxygen to a carbon atom in the polymer chain [42]. In this study, this peak was investigated for the manufactured contaminants.

3.2.5 Contaminant electrical characterization

A series of aged films were also manufactured with the intention of determining the electric conductivity for aged XLPE in comparison with unaged XLPE. The main reason was to provide input data for the COMSOL simulations. These films were made with the same procedure as in chapter 3.1.1, but with more focus on quality of the films. After aging, the thickness was measured before inserting them into a "*Keithley 8009 fixture model"* connected to a measurement device for measuring the volume resistivity. The conductivity was then obtained by simply taking the inverse of the resistivity.

3.3 Electric field analysis

In order to further understand the field topology in the test samples, a finite element method [1] analyses was used to simulate the samples and investigate the influence of different imperfections. The imperfections could be small kinks on the wire or inexact dimensions of the geometry. Also the influence of small particles nearby the high voltage wire electrode was investigated. The simulated particles represent the organic contaminants investigated in this thesis. In a prior field analysis performed by Huuva [38][39], a scaling constant was calculated,

$$E_{max,nom} = K * \widehat{U}_{applied} \tag{1}$$

In the simulations performed in this thesis the scaling constant K was elucidated further:

$$K = K_\theta * f_{kink} * K_d \tag{2}$$

With the help of equations 1 and 2 the maximal nominal electric field for AC can be determined for all stressed locations along the outer edge of the wire. The simulations can be found in appendix I, and some results are shown in chapter 4. One issue is that the AC fields are simulated in the electrostatics modulus. The electrostatics modulus solves the Laplacian field, taking no consideration to injected charges. Disregarding the injected charges introduces an error into the calculations. Also, for modeling the electric field for DC, the electric current model is used. Once again no consideration is taken to the injected space charge, as it is a complex phenomenon which is hard to measure. Including the injected space charge would only complicate the simulations further, even though it is an essential factor when considering the electric treeing degradation phenomena.

3.4 Electrical Testing

Prior to the electrical testing, microscope pictures were taken of all samples used in this thesis. Also after the testing the samples were investigated with a microscope. Three kinds of electrical tests were performed. AC tests, DC tests and wet or dry aging tests. The respective tests are explained in the chapters below.

3.4.1 Test setup AC

The test setup used for AC testing of electrical treeing was already constructed in a previous project performed at the Division of High Voltage Engineering at Chalmers [38][39]. The test setup had also been improved in a master's thesis [40]. The test setup is shown in figure 12.

Figure 12. The HVAC test circuit at Chalmers (left) and a close-up on the voltage divider (right)

The test setup consist of a variable AC source (including a transformer), which is connected through a current limiting resistor. Connected in parallel to the test sample is a voltage divider, with a data acquisition (DAQ) system to measure the voltage. The test sample is mounted in a tank filled with transformer oil, with a lamp on one side and a camera on the other side. A schematic of the test setup is illustrated in figure 13. During the thesis work the light source was switched to a brighter LED lamp. This was necessary as some of the particles had low transparency due to inserted contaminants. Another issue was that the computer handling the filming through the camera and also the voltage measurement was heavily outdated. As film rendering took much memory space, only up to 15-20 minutes could be filmed at a time without experiencing frame drops. Whenever frame drops occurred the treeing initiation and growth could no longer be detected. Also for tests longer than 8-10 minutes the voltage could only be measured under short 10-20 second periods.

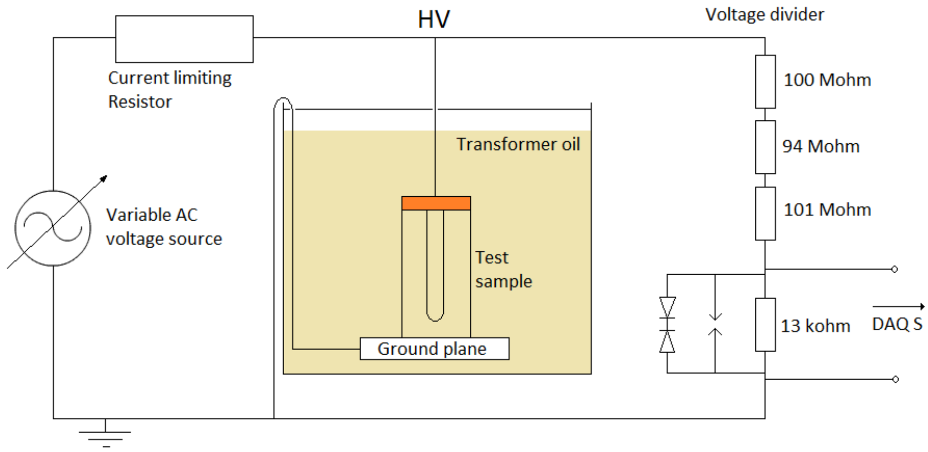

Figure 13. Test setup AC

As 15 minutes was the maximum time for filming, the voltage for the constant AC aging was set to 22.5 kV and later decreased to 20 kV in order to initiate the electric trees within this time.

3.4.2 Test setup DC

The AC test setup could be transformed to a DC test setup in the same way as described in [40]. The DC test setup is illustrated in figure 14.

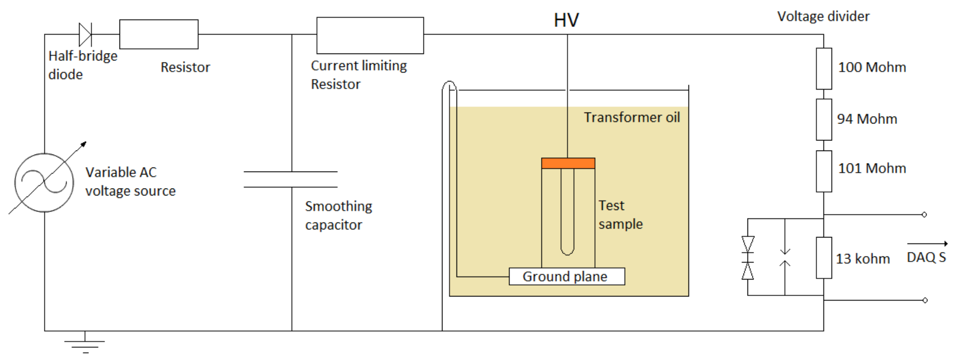

Figure 14. Test setup for DC tests

To the AC test setup, a diode, resistor and capacitor were added, creating a half-wave rectifier. The additional resistor was to limit the inrush currents to the capacitors, and also to add additional protection to the HV node at the capacitors. As positive polarity is known to inject less space charge into the test sample [40], only positive polarity was used. The full setup is shown in figure 15.

Figure 15. The HVDC test circuit, created by adding a diode, capacitors and a water resistor to the HVAC circuit

Using the control system for the transformer, the voltage was ramped up with the highest possible ramping speed (7.1 kV/s) to the desired voltage level. When the tests were finished and the AC source was turned off, the voltage slowly decreased when the energy from the capacitors dissipated in the circuit. When the voltage had decreased to around 10 kV, the circuit was grounded through a 17 kΩ resistor, first near the test sample, and last at the capacitors. The performance of the computer limited the duration of which the voltage could be measured, resulting in 120 or 240 seconds intervals (depending on the sampling frequency) of measured voltage.

3.4.3 Test setup for wet and dry aging

The electrical aging test setup was constructed at Nexans AS in Halden. Prior to the electrical testing the samples had been saturated with water. This had been done by soaking them in a water bath at 70 °C for 1 week. After the saturation the samples where quenched in 4 °C water in order to stop the saturation process, reducing the amount of water leakage before they were placed in the electric test setup. The electrical test setup created, using a variable AC source, is shown below in figure 16.

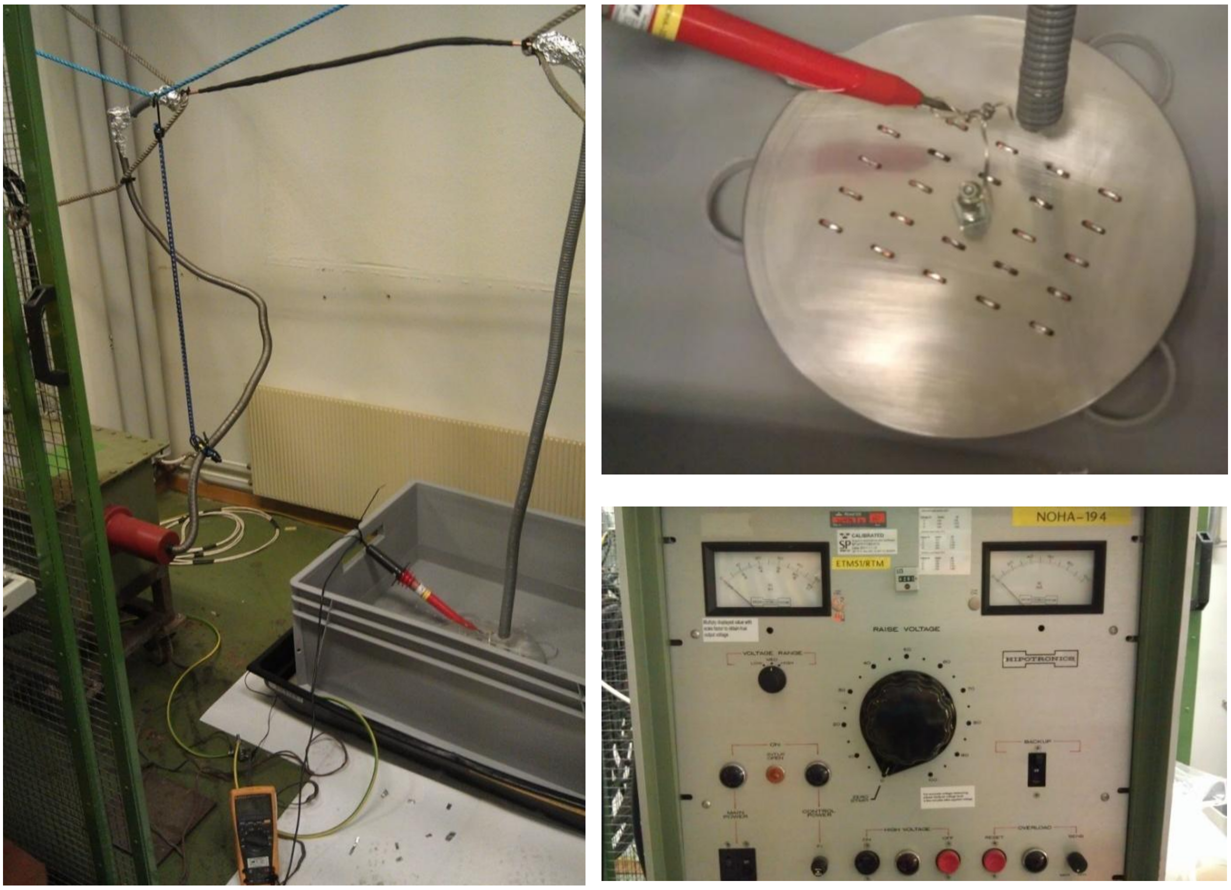

Figure 16. Water tree test setup. Showing the circuit layout (left), sample place holder (top right) and control unit (bottom right).

Because of the slow growth rate of water trees the samples were subjected to the applied voltage for 1 week. In order to age multiple samples at a time a place holder was manufactured (figure 16), fitting 24 samples. A 7 MΩ resistor was used in order to reduce the short circuit currents, in case of a breakdown in a test sample, to a minimum. The resistor was later replaced by a 3.8 MΩ resistor since the previous one broke. Due to these high ohmic resistances a voltage drop was present in the circuit. By using a high voltage probe ("*Fluke 80K-40*") with a scale factor of 1000x, the voltage could be measured with an ordinary multimeter. This was to ensure that the samples were subjected to the proper voltage. In this circuit the grounding plate was placed below the silicon oil filled tank. To prevent discharges the surface between the plate and the tank was greased up using insulating grease, eliminating possible air pockets. The circuit layout is shown in detail in figure 17.

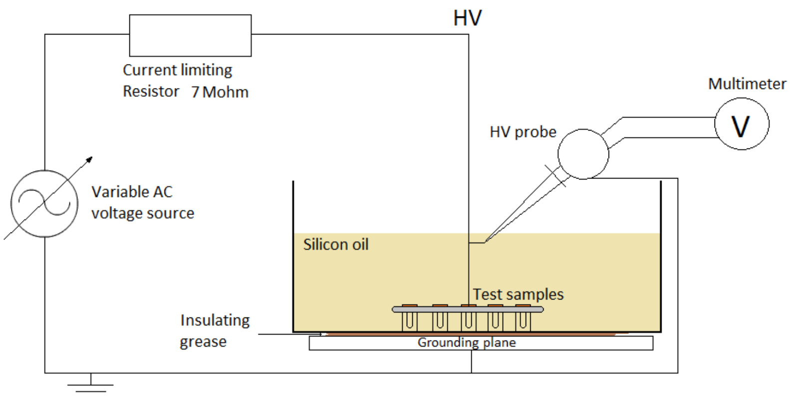

Figure 17. Water tree test setup

3.5 Statistics

As the treeing initiation varies considerably in between samples, different statistical analyses are necessary. The 2 and 3-parameter Weibull distributions are suitable for detecting initiation thresholds, such as a critical electric field for treeing initiation. This makes the Weibull distribution good for describing insulation performance in solid dielectric materials, so it is commonly used [43][44]. In this thesis the time to treeing initiation was mainly investigated. The normal distribution was used instead, since it allowed for a slightly simpler interpretation of the data.

All normal distribution plots used in this thesis where created in minitab [45] and are shown with a confidence interval of 95 % (95% CI). This confidence interval equals 2 standard deviations from the mean of the distribution. Also in each normal distribution plot, a box with the in table 1 described parameters is displayed in the same order as the different distributions are listed.

Table 1. Explanation of the displayed parameters for each normal plot.

Parameter	Displayed as	Explanation
mean	Mean	Indicates the most likely value
standard deviation	StDev	Indicates the spread in the data (higher means a bigger spread)
Number of data points	N	Amount of data points included in the distribution
Anderson-Darling statistic	AD	Quality of the fit (the lower the better the fit)
p-value	P	Indicate the statistical strength of the distribution. Small p-values favor a rejection of the fitted distribution.

The same distribution was used throughout the thesis for easy comparison in between different data series. The normal distribution might in some cases not have been the best fit for a particular data series, indicated by a high AD value or low p-value. If such a plot would have been changed to a different distribution, the made comparisons would have been more difficult.

4 Characterization and simulation results

In this chapter, various results are presented with valuable information about the quality of the test method. In the characterization results, different physical properties are found about both the test samples and the manufactured contaminants. In the simulation results some of the electric field simulation results are presented, containing information about the electric field in the AC test setup, DC test setup and the aging test setup.

4.1 Characterization results

The characterizations performed are listed in 2 chapters, with 4.1.1 presenting the results of the sample characterizations, and 4.1.2 presenting the results of the contaminant characterizations.

4.1.1 Sample characteristics

For the samples, the gel content has been determined. Also the degassing process has been evaluated by HPLC measurements and weight measurements. At last the degassing process's influence on the kinks in the samples is presented.

4.1.1.1 Gel content measurement

In all three samples only 80,4 % - 80,7% of the initial weight was left after the process. This corresponds to a average gel content of 80,6% present in the samples, which is a value comparable to the degree of crosslinking in ordinary high voltage cables.

4.1.1.2 HPLC-measurements

In the HPLC measurements, three typical compounds originating from the byproducts of the crosslinking process were detected. The amount of each compound, as well as normal values for a degassed HV-cable are displayed below in table 2.

Table 2. Results from the HPLC measurements compared with values for a normal HV-cable.

	Cumylalcohol [ppm]	Acetophenone [ppm]	α-metylstyrene [ppm]	Total [ppm]
Sample 1	1013,5	315,5	922,8*	2251,8
Sample 2	1009,1	309,9	-	1318,9
Sample 3	1035,9	323,3	-	1359,2
Average	*1019,5*	*316,2*	-	
St.dev	*14,37*	*6,73*		
Normal values from production	<3600	<1800	<80	5480

The amount of Cumylalcohol and Acetophenone left in the test samples was found to be a lot lower than the amount present in a degassed HV-cable. Even though a high amount of α-metylstyrene (*) was found for sample 1, no or extremely low traces of this compound were found in the other two samples. From the results it can be concluded that the samples used in this work had been degassed to a higher degree than in a normal high voltage cable.

4.1.1.3 Weight loss during degassing process

During the degassing of 5 batches of samples, the material was weighed on a daily basis. The last couple of days did not have a weight reduction, pointing towards the degassing being successful. The total weight reduction is shown in table 3. Similar results concluding 7 days to be sufficient degassing time were shown in a previous bachelor's thesis [46], where only 6% of the cross-linking by-products where left after 1 week of degassing.

Table 3. Weight data from degassing process.

Initial weight [g]	Total weight lost during degassing process [g]	Weight lost in %
151.2 g	1.7 g	1.12%

4.1.1.4 Kink appearance during the degassing process

In order to investigate if additional kinks were created by the degassing process, before and after pictures were taken with a microscope. It was found that most of the times, the kinks already in place were severed during the degassing process. This can be seen below in figure 18. The heat treatment during the degassing process, or probably the morphology change and relaxation of the polymer is likely to be the responsible for this process. As the matrix contracts, the excess length of the wire is shoved sideways, forming a kink. The influence of the kinks on the electrical field distribution can be found in appendix I. additional pictures of kink severance as well as in some cases kink appearance can be found in appendix II.

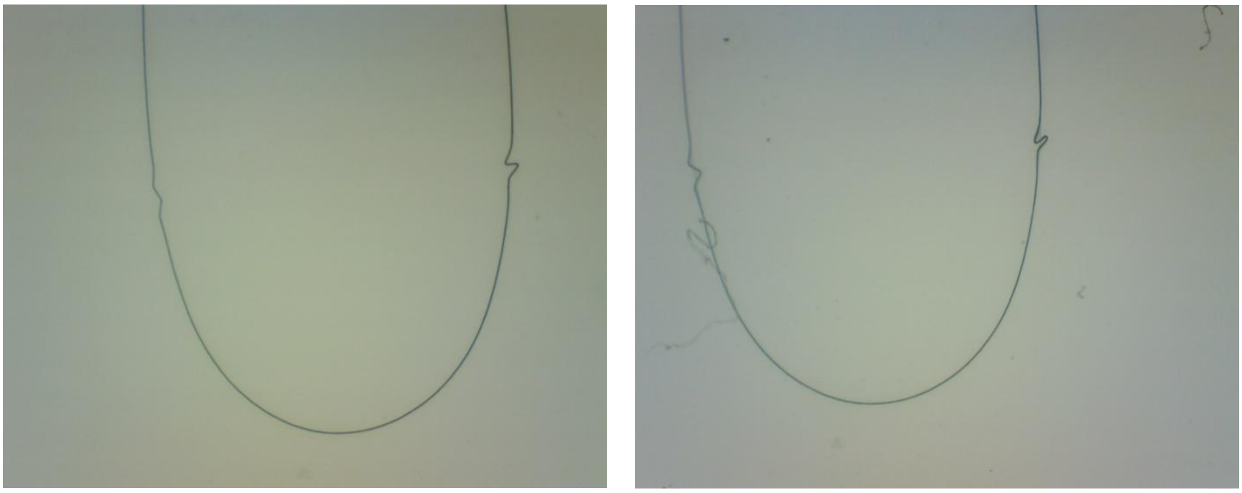

Figure 18. Microscope photo of the wire before (left) and after (right) the degassing process.

4.1.2 Contaminant characteristics

In this chapter, the produced contaminants are characterized with IR-measurements and conductivity measurements.

4.1.2.1 IR measurements

The result from the IR scan is shown in figure 19. The transmittance is measured as a function of the wavelength.

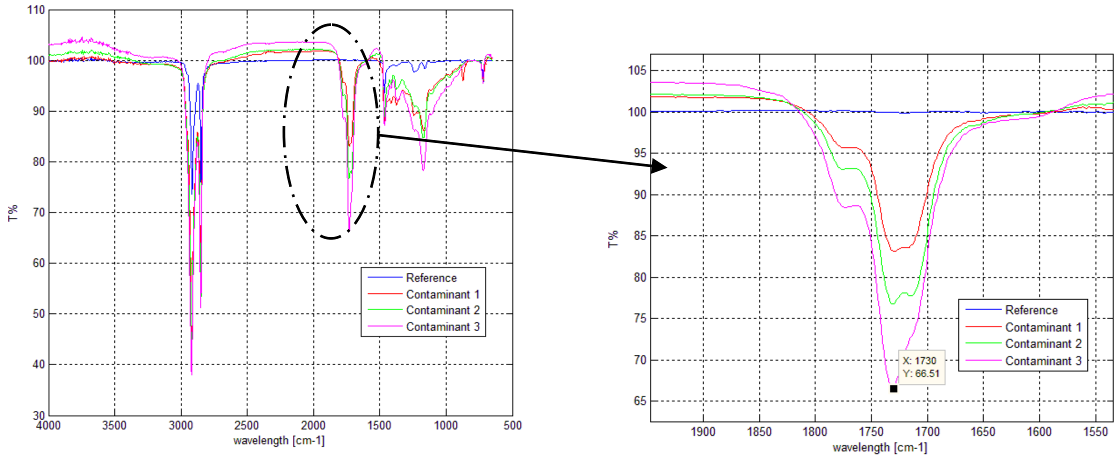

Figure 19. IR scan of the reference material and the different contaminants.

The triple peak found at 1650-1800 cm^{-1} is a typical result of the thermal aging. These peaks indicate a number of carbonyl groups, such as esters, ketones and γ-lactone, that have been created by the chain scission in the material [42][47].

For a comparison of the peak heights and area, the data is switched to the absorbance spectra. The result is shown below in table 4.

Table 4. Summation of the manufactured contaminants.

Name	Aging time	Aging temperature	Maximal absorbance peak height	Contaminant peak area
Contaminant 1	1 day	190 °C	0.1053	9.5092 A/cm
Contaminant 2	3 days	180 °C	0.1716	14.2434 A/cm
Contaminant 3	7 days	180 °C	0.2061	15.9579 A/cm

These contaminants were used for the tests with homogenous distributions, chapters 5.3 and 5.4

4.1.2.2 Conductivity measurements

As seen in figure 9, XLPE films will shrink and deform during the aging process. While the unaged reference film was smooth, the aged films had wavelike deformations, as well as cracks. Since voltages of up to 400V were applied during the resistivity measurements, only 2 of a total of 5 aged films could be used, and the other 3 were discarded to prevent breakdowns in the test fixture. Also, while measuring the resistivity of the film aged for 7 days, the film had a fold at 1 place, giving an increased thickness and therefore resistivity to the result. The result of the measurements is displayed in table 5.

Table 5. Resistivity measurements of unaged and aged XLPE films.

Aging time	Aging temperature	Film average thickness	Measured volume resistivity	Conductivity
0 days	-	0.196 mm	$3.5*10^{18}$ Ωcm	$2.86*10^{-17}$ S/m
3 days	180 °C	0.159 mm	$2.4*10^{16}$ Ωcm	$4.17*10^{-15}$ S/m
7 days	180 °C	0.149 mm	$4.4*10^{16}$ Ωcm	$2.27*10^{-15}$ S/m

As the obtained results for the aged films were highly inaccurate, only the magnitude of the conductivity was used as an input for the COMSOL simulations. These results indicate that a conductivity increase of 100 times is likely to occur, but to be certain also an increase of 10 times was used for the inserted particles in the simulations. The full simulation is found in appendix I.

4.2 Field simulation results

The complete simulations performed in this thesis can be found in appendix I. As mentioned before, no space charge was implemented in the simulations, which in reality would account for an increase (AC) or decrease (DC) of the electric field. From the simulation, a series of equations were derived with Matlab [48] for calculation of the electric field in the test samples. Equation (4) focuses on the electric field at different positions along the wire. Equation (5) scales the electric field if the wire-ground distance varies from its original value (3mm). Equation (6) introduces a kink factor, creating the amplification of an eventual kink.

$$E_{max,nom} = (K_\theta * f_{kink} * K_d) * \hat{U}_{applied} \tag{3}$$

Where:

$$K_\theta = -0.7693\theta^2 + 2.4167\theta + 12.3623 \tag{4}$$

$$K_d = (14.5 + {}^{4}/_{d} - 0.5 * d)/14.382 \tag{5}$$

$$f_{kink} = \begin{Bmatrix} (0.0014 * l + {}^{4}/_{r} - 0.006 * r + 1.4) \\ 1\ (if\ no\ kink) \end{Bmatrix} \tag{6}$$

Here θ is the angle along the outer edge of the bended part of the wire, d is the distance between the wire and the ground plane and l and r are the length and the toroidal radius of an optional kink. These derived field approximations are used in chapter 5 to calculate the electric field in the samples. The electric field magnitude present in the samples can be seen in figure 20 as a surface plot. It can be concluded from these calculations that the electric field is highly concentrated to the area around the wire.

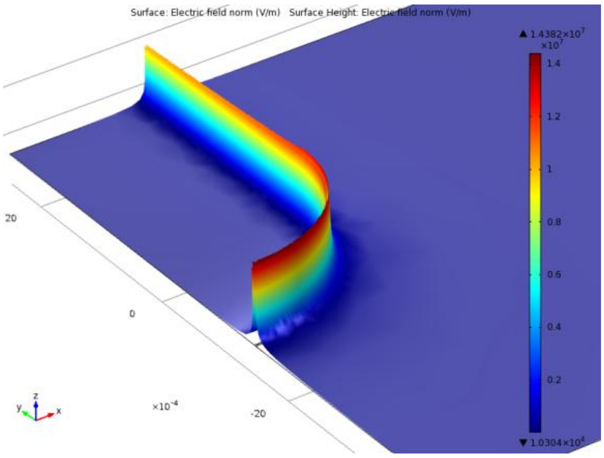

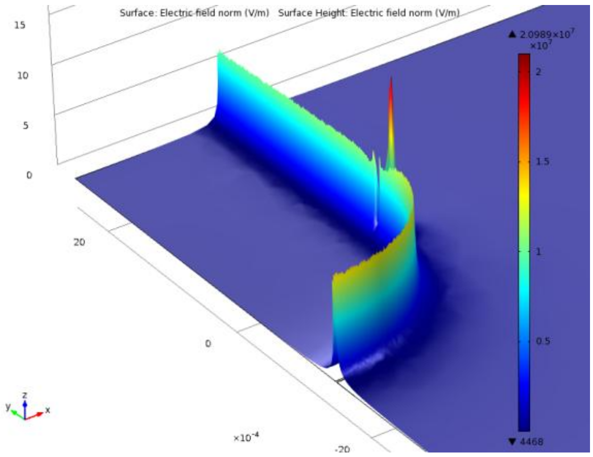

Figure 20. Electric field magnitude present in the sample, with (left) no kink and (right) kink

These AC simulations provided valuable information about the electric field, and factors affecting it such as kinks etc. The effect of a typical kink can be seen figure 20. It was also found that the kink only affected the field locally, as the electric field further away from the kink only decreased slightly. The value at the tip of the wire (closest to the ground plane) was found to be 14.382 kV/mm and was comparable with the result found from a 2 dimensional circle-plane simulation (14.606 kV/mm was obtained by 2d the simulation).

For investigation of the impact of contaminants on the electric field, a series of simulations where done. In the AC case, the field was slightly affected by a permittivity change. For DC however, the conductivity change of inserted particles is big enough to change the electric field. Two examples of field modifications imposed by inserted particles can be found in figure 21.

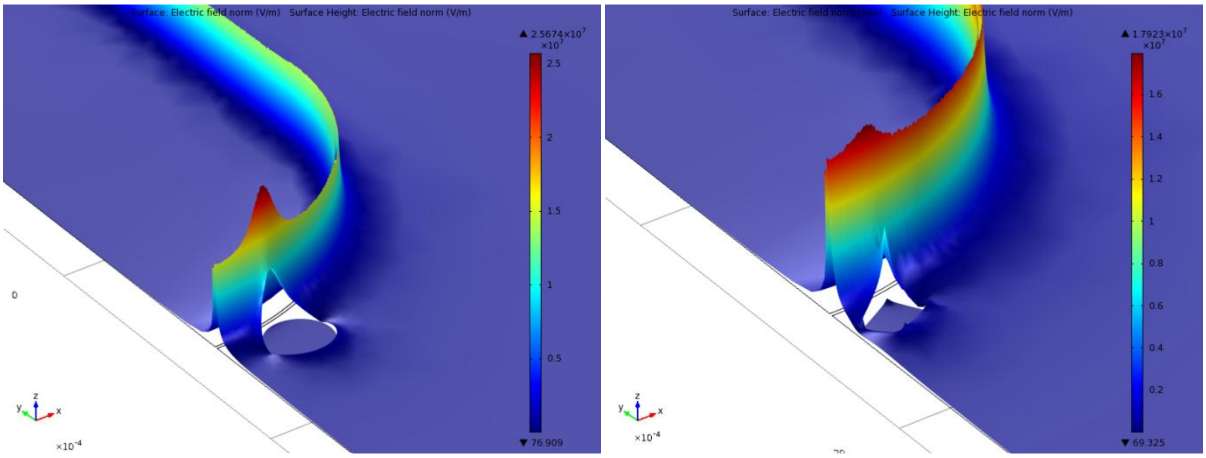

Figure 21. Electric field impact of a (left) spherical or a (right) sharp contaminant with a 100 times increased conductivity

It can be concluded that in order to notice the electric field influence of the contaminant, it is necessary for the contaminant to be located in the close vicinity of the wire. Also a conclusion could be that big, round particles provide the largest field amplification at the wire. As for sharp particles, the field at the contaminant can also be enlarged to a noticeable extent.

5 Electrical and optical results

In this chapter, all results from the electric tests are presented, as well as optical observations made on the tested samples. At first a series of reference tests were performed. Second, tests with inserted contaminants along with wet or dry aging are presented. At last, the test results with a homogenous spread of contaminants are presented, first for AC, and finally for DC. All mentioned AC voltages are described in terms of rms.

In all results trees initiated at kinks were excluded. Kinked locations were found to introduce electrical trees much earlier in comparison with unkinked locations along the wire. This trend is highly dependent on the increased electrical field at the kinks (see appendix I for a full evaluation). In figure 22 it can be seen that the kink locations were often the first location to initiate trees when subjecting the samples to a ramped up AC voltage.

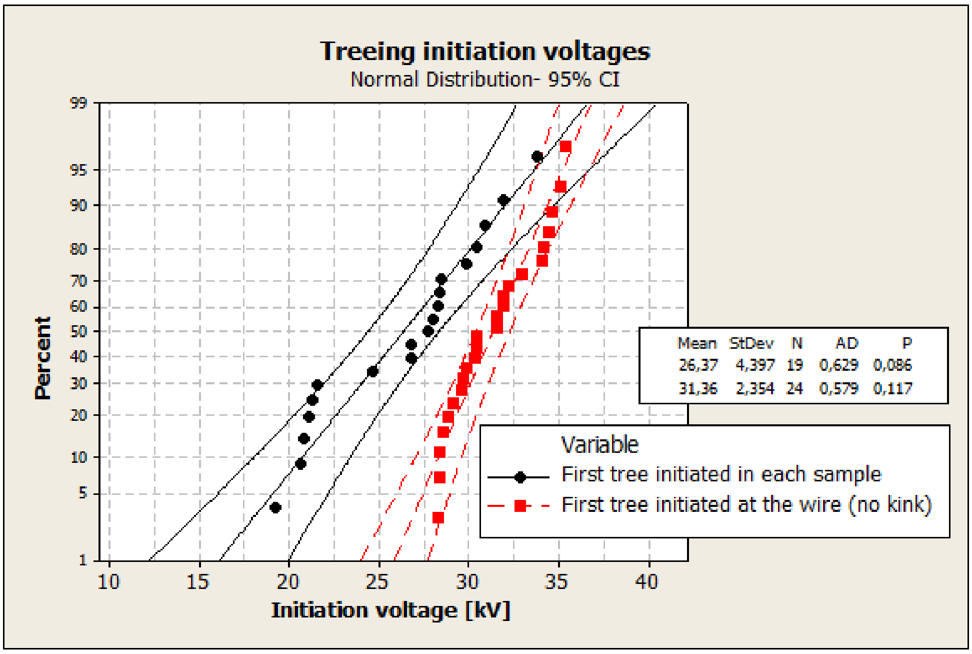

Figure 22. Tree initiation voltages for reference tests with ramped voltage (chapter 5.1.1)

An attempt has been made to apply the derived equation for the electric field at a certain kink, but the process turned out to be too complex and time consuming. Also the deviation in between different kink initiated trees after the application of the formulas was too big. The explanation for this could be a change in the morphology at the kink location, as well as that simplifying a kink top with a halve toroid is not exact enough.

5.1Reference tests

A number of reference test were performed. This was in order to become familiar with the test method, and to investigate the characteristics of the supplied materials. Also a successful method was derived for constant AC aging of the material.

5.1.1 Ramped AC reference tests

For the ramped AC tests, a ramping rate of 250 V/s was used. This was the lowest possible ramp rate possible in the test setup. The measured voltage for a typical Ramped AC test is shown below in figure 23.

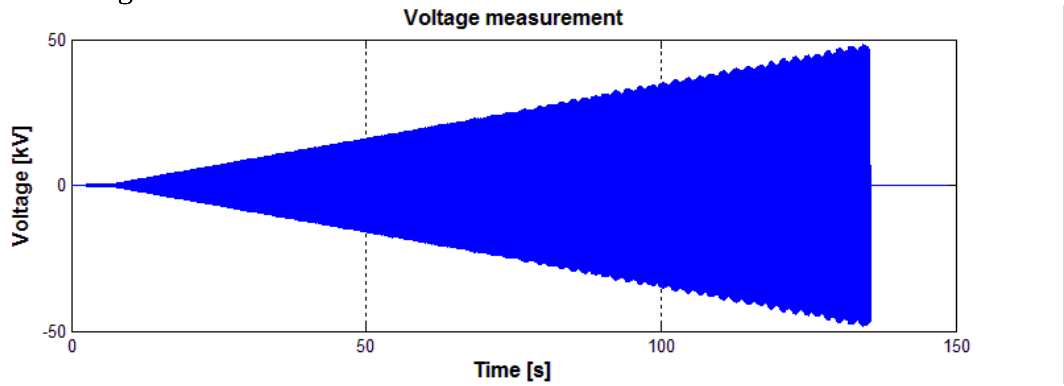

Figure 23. The measured voltage profile for a ramped AC test.

The voltage was turned off when enough electrical trees were initiated in each sample, and before the trees initiated an avalanche breakdown in the material. From the detected treeing initiation voltages (TIV) corresponding electric field magnitude was calculated in three different ways.

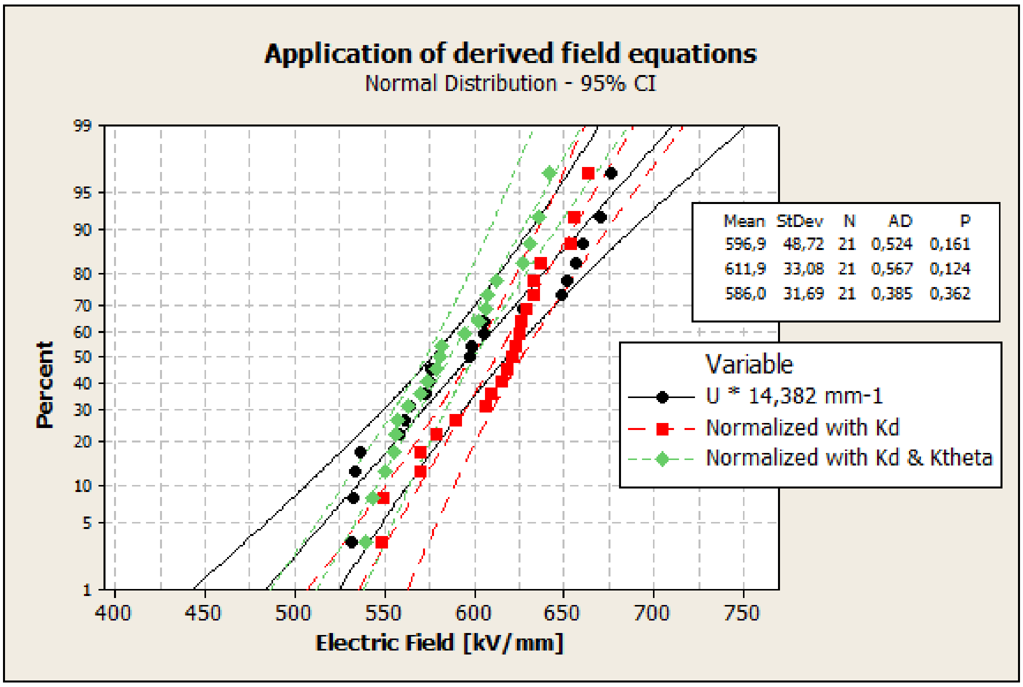

Figure 24. A Normal distribution plot comparing the treeing initiation field calculated in three different ways.

The circle data points correspond to the calculated data when only a single scaling constant was used. The square data points display the calculated field when only the derived wire to ground scaling constant (Kd) was applied. The diamond data points are when both Kd and the angle variation was used (K_θ). It can be seen in the figure that the biggest reduction in the standard deviation (StDev in the figure) is created as Kd is introduced. The introduction of K_θ also reduces the standard deviation. This indicates that both trends could be present in the samples. Some typical trees created during the ramped AC tests can be found in appendix III, pictures 1-4.

5.1.2 Constant AC reference tests

The first constant AC test was performed with 22.5 kV rms applied to the samples. A typical voltage profile for a sample test is shown below in figure 25. At first the voltage is ramped up with a ramping speed of 250 V/s. This ramping speed is to make the eventual trees initiated before 22.5 kV is reached relatable with the results obtained in 5.1.1. When a voltage of 22.5 kV is reached, the voltage is kept constant until enough trees are detected in the sample.

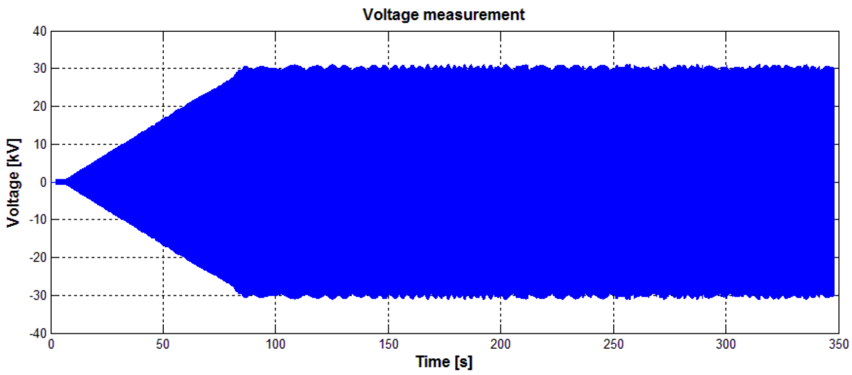

Figure 25. Voltage measurement obtained from a 22.5 kV constant AC aging test

To detect the changes in the samples the time from that the high voltage is applied until the treeing initiation is detected is measured. 22.5 kV is reached after 76 seconds, and in a few cases trees initiated before this time. It should also be noted that a voltage drop of around 1.3 kV rms was found over the current limiting resistor, hence only 30 kV peak was measured to be applied on the samples. The time to treeing initiation is plotted in figure 26, related to the electric field applied in each sample.

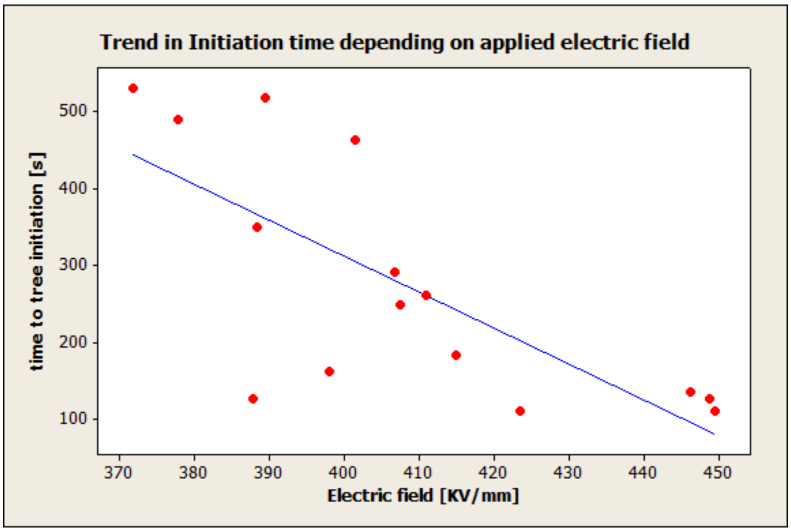

Figure 26. Figure showing a relation between time to treeing initiation and applied electrical field.

A higher applied electric field on a sample is most likely to initiate treeing earlier compared with a lower electric field. The difference in field is mostly created by different distances between the wire and the ground plane. In order to eliminate the differences in electric field in between samples, a different manufacturing method was necessary to reduce the time to treeing deviation in the samples. The different method is described in the beginning of chapter 3.1. By only inserting half the amount of samples into the crosslinking press procedure, the field variation was reduced. The result of the test series is shown in figure 28. Some trees initiated by 22.5 kV are shown in appendix III, pictures 5-8.

A new reference test series was performed with the new manufacturing method (as described in the beginning of chapter 3.1). Also a lower voltage level was chosen, since test on contaminated samples showed treeing initiation before the constant voltage level was reached. The voltage was set to 20 kV, and again a voltage drop of around 1.2 kV was found over the current limiting resistor. The measured voltage is displayed below.

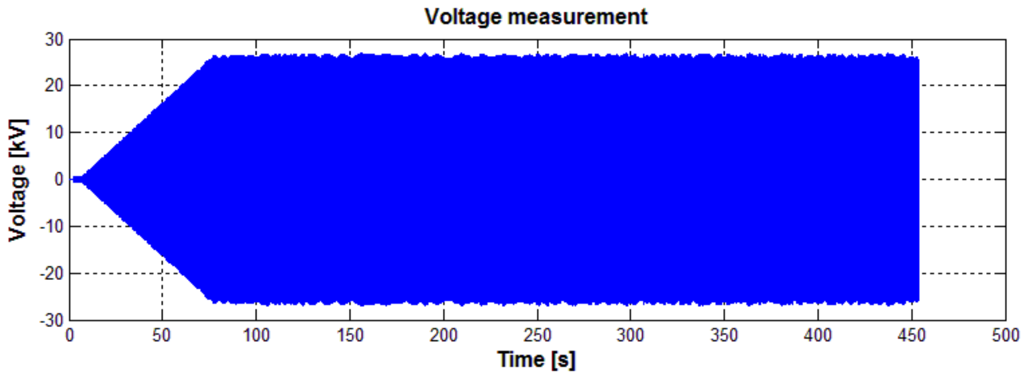

Figure 27. Voltage measurement obtained from 20 kV constant AC reference test. This particular voltage profile was used for all following constant AC tests.

The changed applied voltage and improved manufacturing method, ensured that the maximal electric field now varied between 360 and 382 kV/mm for the test samples. The result of this reference test is shown in figure 28.

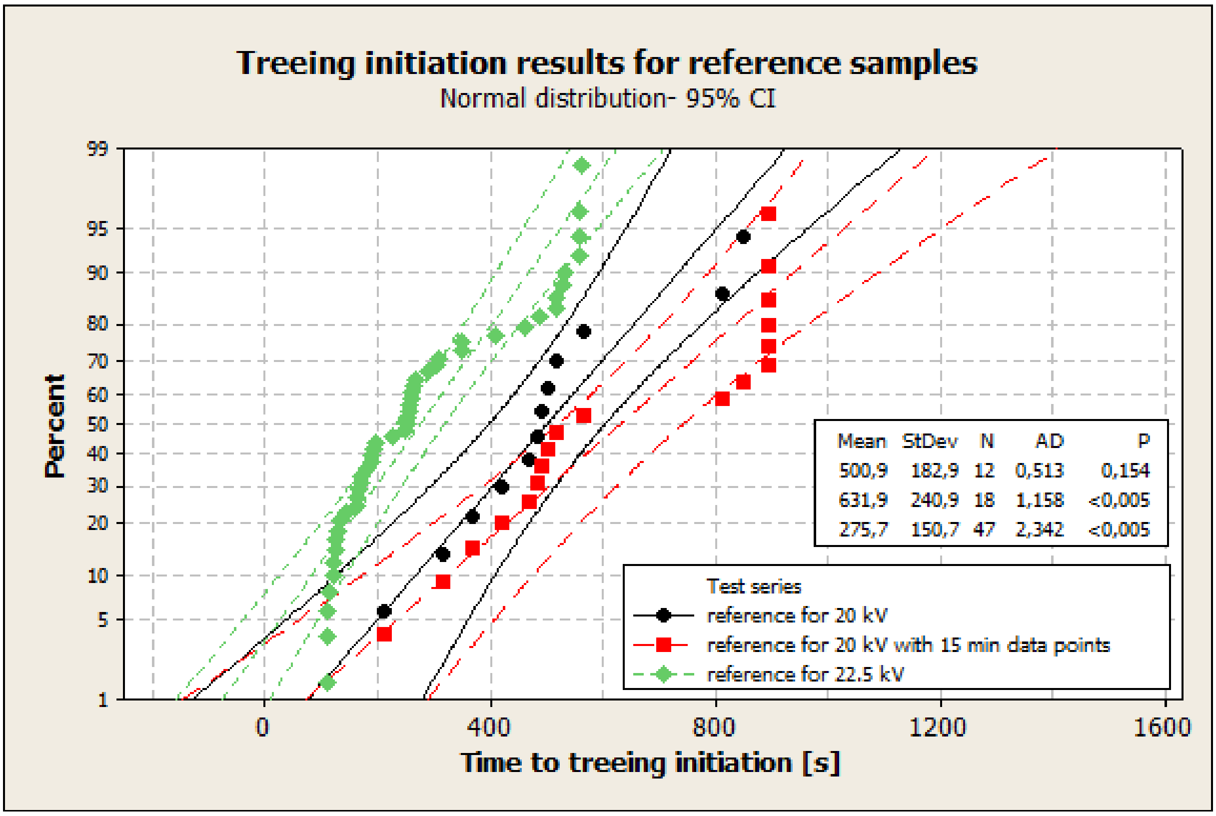

Figure 28. Treeing initiation results for aging of reference material with 22.5 and 20 kV.

The lower voltage level resulted in a much later treeing initiation, along with a much lower amount of initiated trees within the 15 minute test time. Also in around 6 samples no trees were initiated before 15 minutes, at which the voltage and camera were turned off to prevent frame drops. As for most tests, small polluted particles moved around in the oil and interacted with the wire, indicating that bad contact was not the case for these samples. For these 6 samples an additional fit including 6 data point at 15 minutes is displayed in figure 28. Even though this fit has data based on unobserved values, its purpose is showing us the smallest impact including the uninitiated trees could have. As the 20 kV reference is used throughout the thesis, this possible effect of the uninitiated trees should taken into consideration when comparisons are made. The test also showed 4 samples where the trees were initiated earlier than expected showing the possible effect of an “unclean” environment during the manufacturing. Pictures of the trees initiated by 20 kV can be found in appendix III, number 9-12.

5.2 Wet and dry aging with contaminants

A series of tests with separately inserted contaminants was performed. These contaminants contained the thermally aged XLPE provided by Sintef Energi AS. A special manufacturing method ensured that the contaminants had no sharp edges, and they were all 400-560 µm in diameter. Using the different test setups described in chapter 3.4, the samples were aged in wet or dry environments, and afterwards tested using the 20 kV AC voltage profile shown in figure 27. For the wet and dry aging, a voltage of 6 kV was applied for 1 week per test series. 6 kV is according to the electric field calculations just low enough for avoiding electrical treeing. This result was verified when 10 kV was used, and electric trees were detected after 1 day of testing. One of these trees is shown in pictures 13 and14, appendix III. The tests with inserted contaminants are divided into 2 test series, since the results from the first test series indicated that additional tests were necessary. The different manufacturing method was used for the second test series, resulting in less variation in distance between the wire and the ground plane. By performing two test series the influence of the wire-plane distance variation and of the rewetting of the samples was now investigated as well.

5.2.1 First test series

The first series contained a dry aged and AC tested series and a wet aged and AC tested series. For the wet aged series, the samples were saturated in 70 °C water with controlled NaCl content, prior to the wet aging and prior to the AC testing. The dry aged samples were not water saturated. For the wet and dry aged series, samples with inserted contaminants were also compared with samples without inserted contaminants. An example of found electrical trees is shown in figure 29.

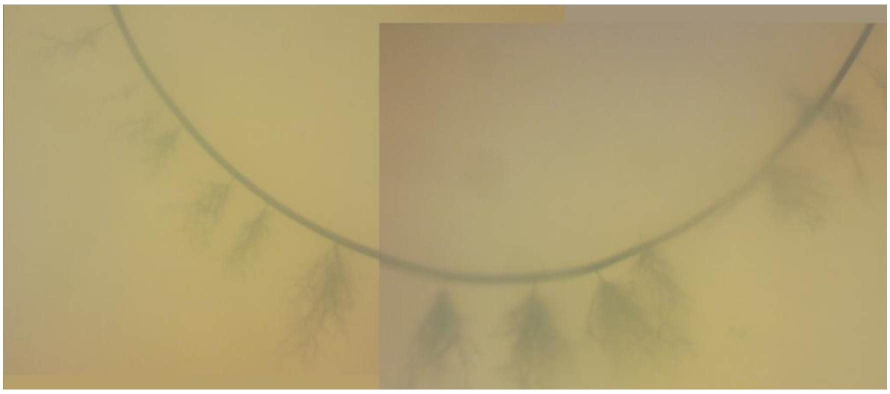

Figure 29. A high number of electric trees initiated in water aged and water re-saturated sample.

Already from the first tested sample, seen in figure 29, a high amount of initiated electrical trees could be observed. Also, locations near kinks could initiate trees before trees were initiated at the actual kinks.

5.2.1.1 Electric results

The treeing initiation results from the first test series is shown below, compared with the reference for 20 kV aging

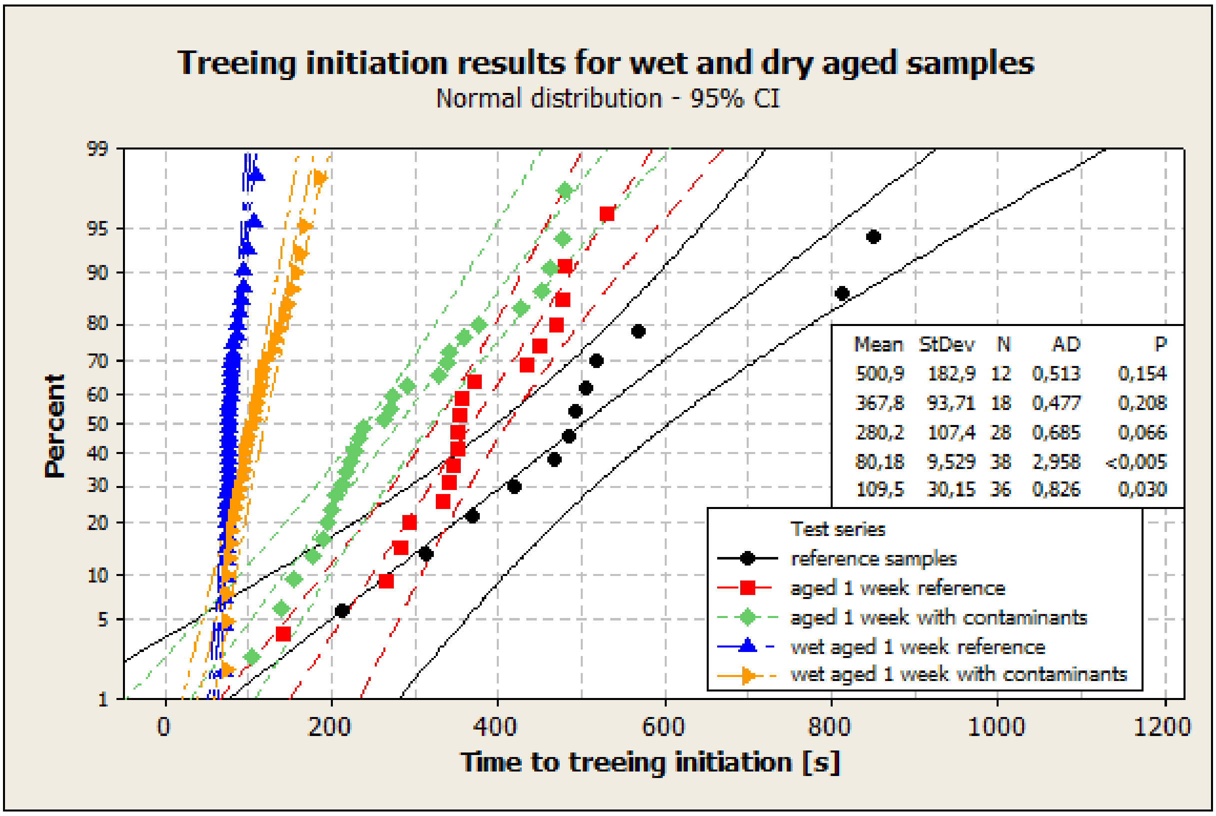

Figure 30. Test results for the first test series aged at Nexans and tested at Chalmers.

The test results indicate that both the aging procedures, and in particular wet aging both increased the amount of electric trees initiated in the samples, as well as they decreased the initiation time for these trees. The difference between the samples with and without contaminants is however arguable, since for dry aging the contaminants seemed to have decreased the initiation time, while for the wet aging the electric trees were initiated later. This could be the effect of the selection of the samples, where samples with shorter distance between the wire and the ground plane were selected for one series, and vice versa. In order to fully see the impact of the contaminants, the optical results need to be studied. If the earlier initiation of the wet aging is depending on the formed water trees in these samples, or is a result of the rewetting performed prior to these tests is unknown. For this reason the wet aged samples in the second test series were dried instead of the rewetting in the first test series.

5.2.1.2 Optical results

From all the tests, only one tree was found were the initiation clearly was affected by a contaminant. This tree is shown in figure 31, originating from the dry aged test series.

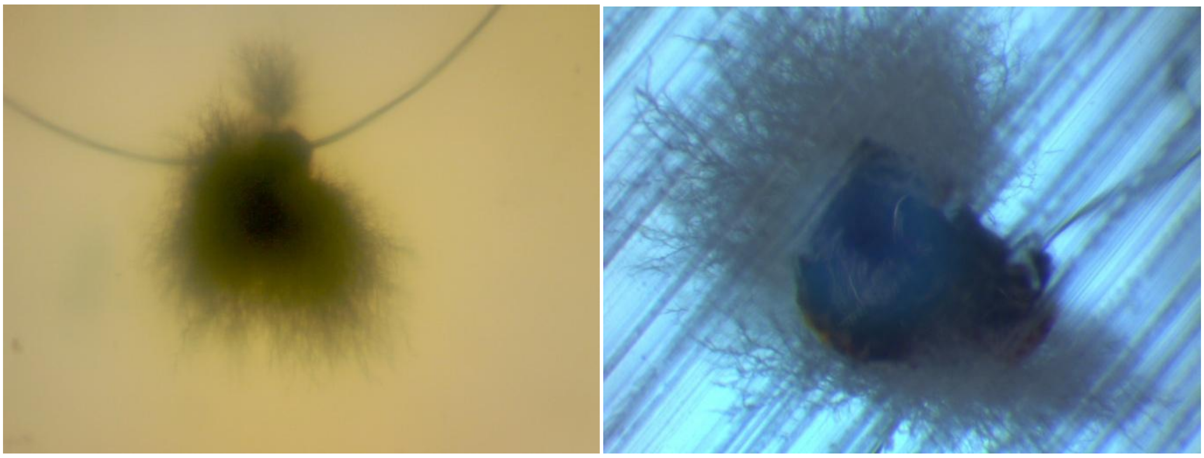

Figure 31. The only electric tree initiated from a contaminant, normal picture (left), microtomed and investigated from another direction (right).

It is difficult to determine if the tree channels had propagated along the surface of the contaminant, or through the contaminant. It is likely that the tree channels grow on the surface of the contaminant, since contaminant may have bad adhesion to the surrounding polymer. The lack of samples with contaminant affected trees called for another test series, as found in chapter 5.2.2. Pictures 15-30 in appendix III show a selection of samples used for the analysis.

The water tree samples were stained with methylene blue to disclose possible water trees. The results of some typically observed trees are shown in figure 32.

a) Electric trees and small vented water trees

b) Electric trees initiated from water tree

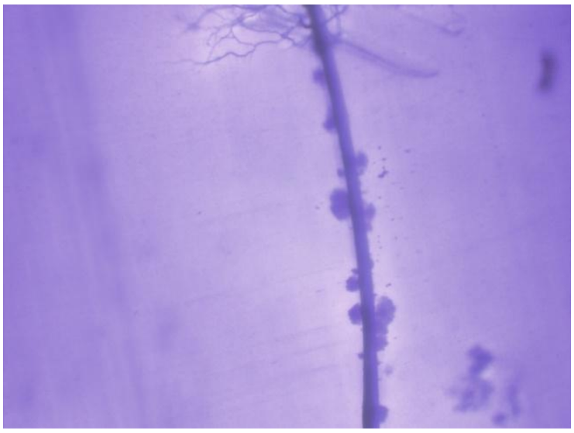

c) Vented water trees

d) Contaminants remained untreed

Figure 32. Electric trees and water trees stained with methylene blue.

From these results it is indicated that water trees are formed. The size of the water trees is in the range of 20-40 μm, which is extremely small. This was likely due to the water in the samples diffusing out into the oil after a couple of days. Also, no increased frequency was used, which is a known factor accelerating water tree growth. Finally, the small size could also be caused by the electric field topology in the samples. High electric fields are known to create small and dense trees, while lower fields create bigger, diffuse trees [2]. In some cases, electrical trees could be detected to be initiated from water trees. Unfortunately, both due to the small size of the water trees and due to the location of the contaminants, it is dubious if the contaminants were affecting the tree growth at all.

5.2.2 Second test series

As only 1 tree was found clearly affected by a contaminant in the first series, another test series was performed. As mentioned a different manufacturing method was used with the hope of obtaining more samples with contaminants located near the wire. Using this different method also reduced the wire-ground variation in the samples. Again one series of samples was subjected to wet aging while the other series was aged dry. This time the wet aged samples were not resaturated with water, but instead dried prior to the 20 kV AC testing. This was to reveal a possible influence of the rewetting process.

The moisture content in the samples was also measured after the wetting before the wet aging, 7 days later after being soaked in oil (A, B and C) and for dry samples.

Table 6. moisture content in samples after 7 days in transformer oil.

Sample	A	B	C	After wetting	Dry samples
Moisture content	30.1 ppm	29.2 ppm	24.9 ppm	142 ppm	8 ppm

These results indicate that although a lot of moisture is lost during the wet aging process, the samples still contain more water than dry samples, after the wet aging is complete.

5.2.2.1 Electric results

The treeing initiation results are displayed in figure 33, compared with the unaged reference samples. As before, a voltage of 20 kV was used.

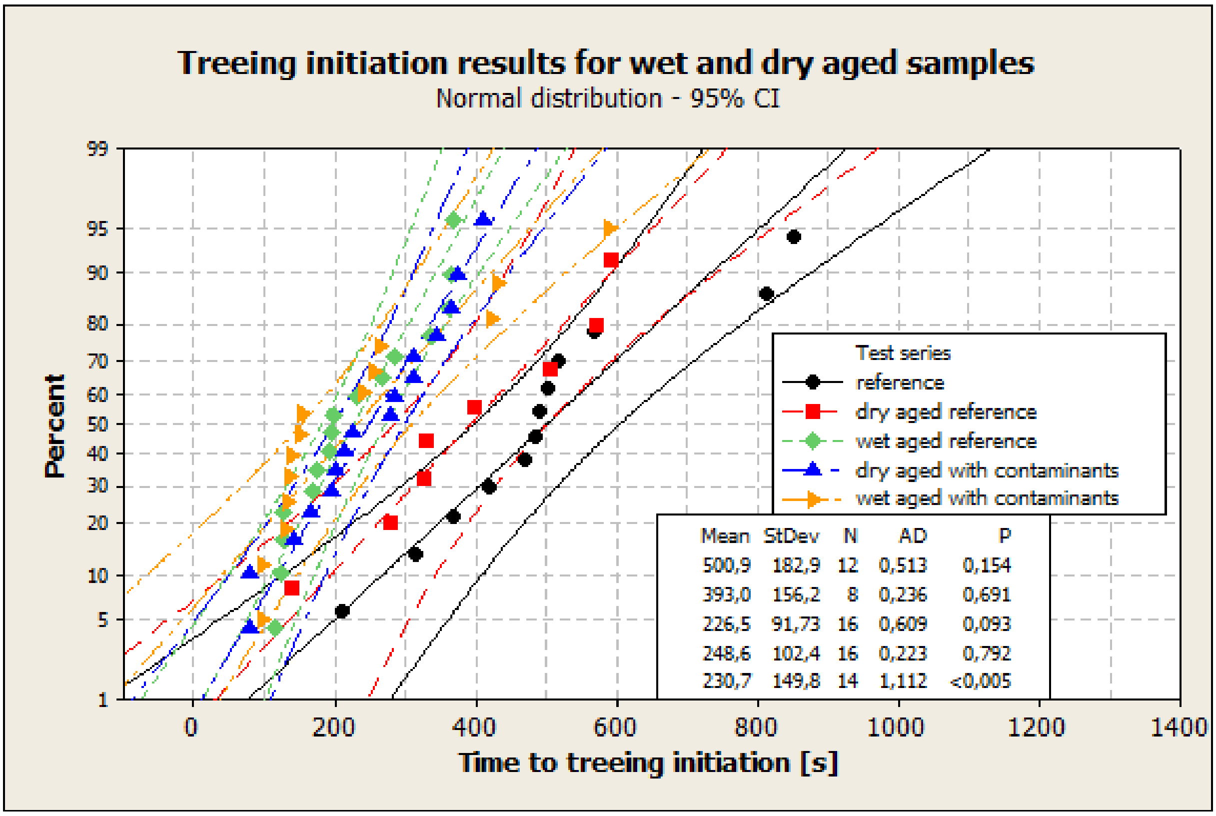

Figure 33. Test result for the second test series aged at Nexans and tested at Chalmers.

By comparing these dry aged samples with the first dry aged test (figure 30), it could be found that a lower amount of electrical trees was now initiated from an equal amount of samples. This might mean that the samples were electrically stronger for this test series. Less difference is found between the wet and dry aged samples, when compared with the first test series. This is likely the cause of that the samples were dried before the testing, instead of the resaturation. This concludes that the moisture content in the samples during the testing probably had an impact on the tree development. A clear difference between samples with and without contaminants was not detected in this series either. Even though the dry aged reference seems to initiate trees later, a lot of the confidence interval is still shared with the dry aged samples with contaminants.

5.2.2.2 Optical results

This time no methylene staining was done. The reason was that the water trees already had been studied, and the water tree size was observed to be too low for them to be affected by contaminants. This time more trees were found possibly affected by contaminants. The trees are shown below in figure 34.

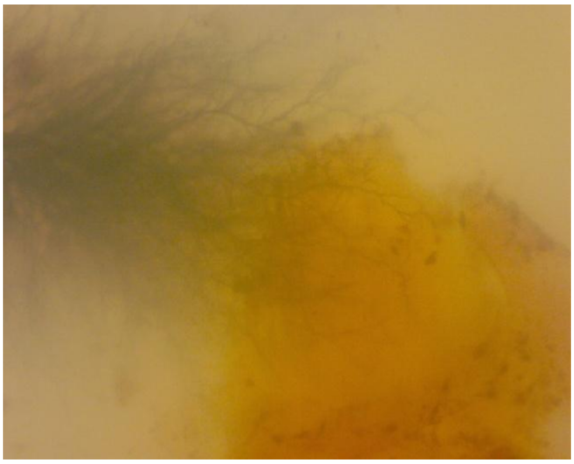

a) Electric tree with channels possibly on the surface of the contaminants, observed in a wet aged sample.

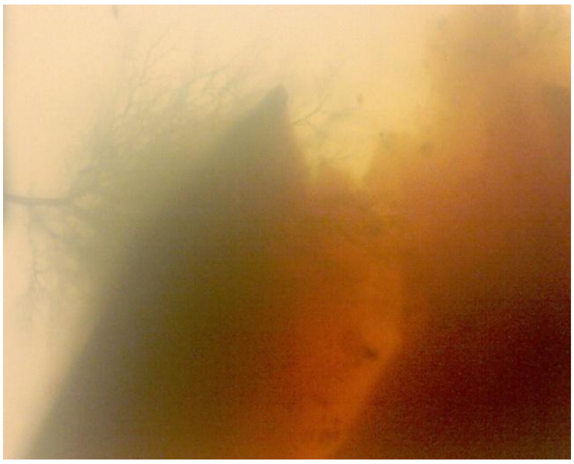

b) Electric bush tree with channels propagated into contaminants, observed in a wet aged sample.

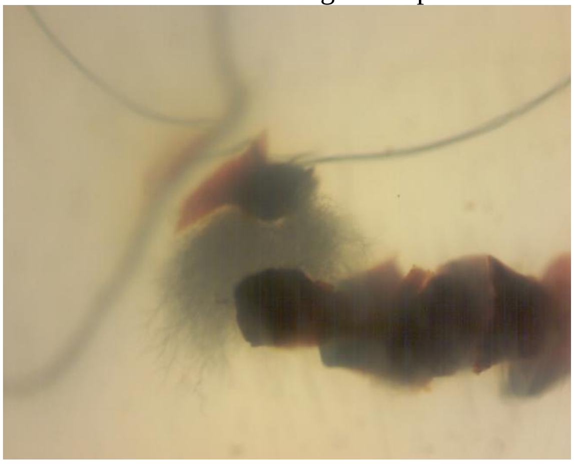

c) Electric tree initiated from kink and seemingly propagated out from a contaminant at 2 locations, observed in a dry aged sample.

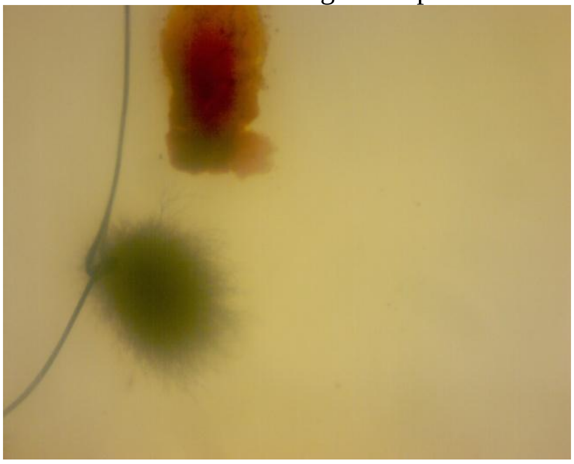

d) Electric bush tree with a small branch aimed towards the contaminant, observed in a dry aged sample.

Figure 34. Trees initiated affected by contaminants.

From these results, it could be possible to claim that the contaminants did affect the treeing propagation. If further conclusions are to be made from this data however, the lack of contaminant affected trees from the entire test series is still a problem. Beside the conclusion about the contaminants, it could probably be stated that the wet aging degraded the material more than the dry aging. This conclusion is both based on the data from figure 33, and the observed initiated trees, some can be found in appendix III, pictures 31-46.

5.3 Homogenous contaminant distribution tests with AC voltage

A series of tests with contaminants or prematurely crosslinked particles evenly distributed through the entire samples were performed. The completed samples were aged with the same waveform as seen in figure 27, at a constant voltage of 20 kV rms.

5.3.1 Contaminant distribution in test series

Different contaminants were used with different degree of oxidation. The contaminants are listed in table 4 in chapter 4.1.2.1. Contaminant 1 was aged thermally for 1 day, and contaminant 3 for 7 days. These contaminants were spread out uniformly through the entire test sample with 2 different concentrations. This resulted in 4 different combinations, as seen below.

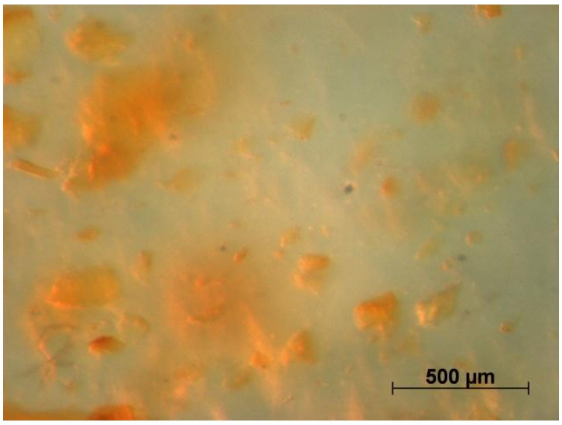

a) 2% wt of contaminant 1

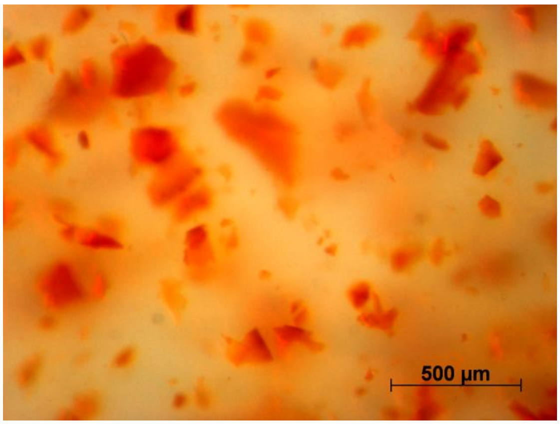

b) 2% wt of contaminant 3

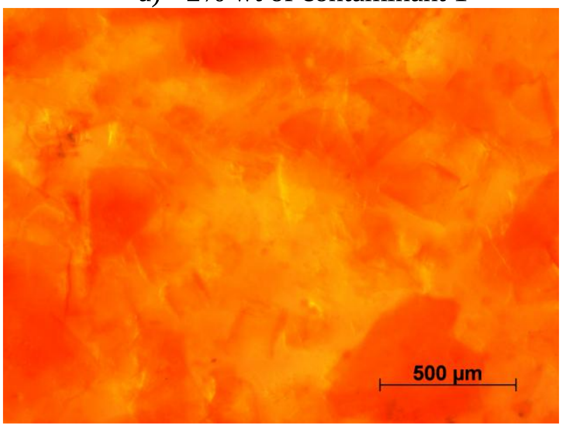

c) 20% wt of contaminant 1

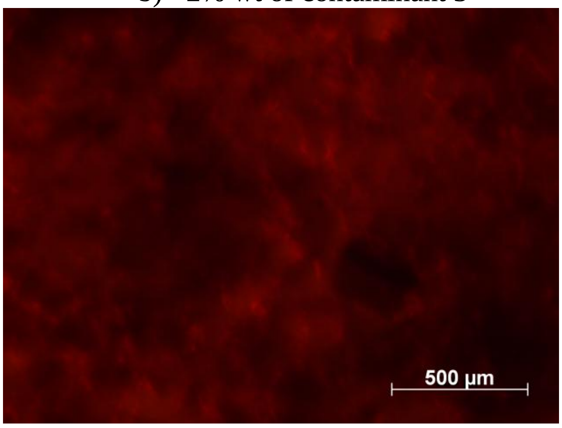

d) 20% wt of contaminant 3

Figure 35. Sizes and distributions of contaminants in test samples.

As visualized the contaminants were spread out evenly in the test samples. Also the sizes of the contaminants varied between 50-500 µm, and sharp edges were a normality.

5.3.2 Electric results

The treeing initiation was measured for the 4 different combinations. The result is shown in figure 36, as compared to the reference from chapter 5.1.2.

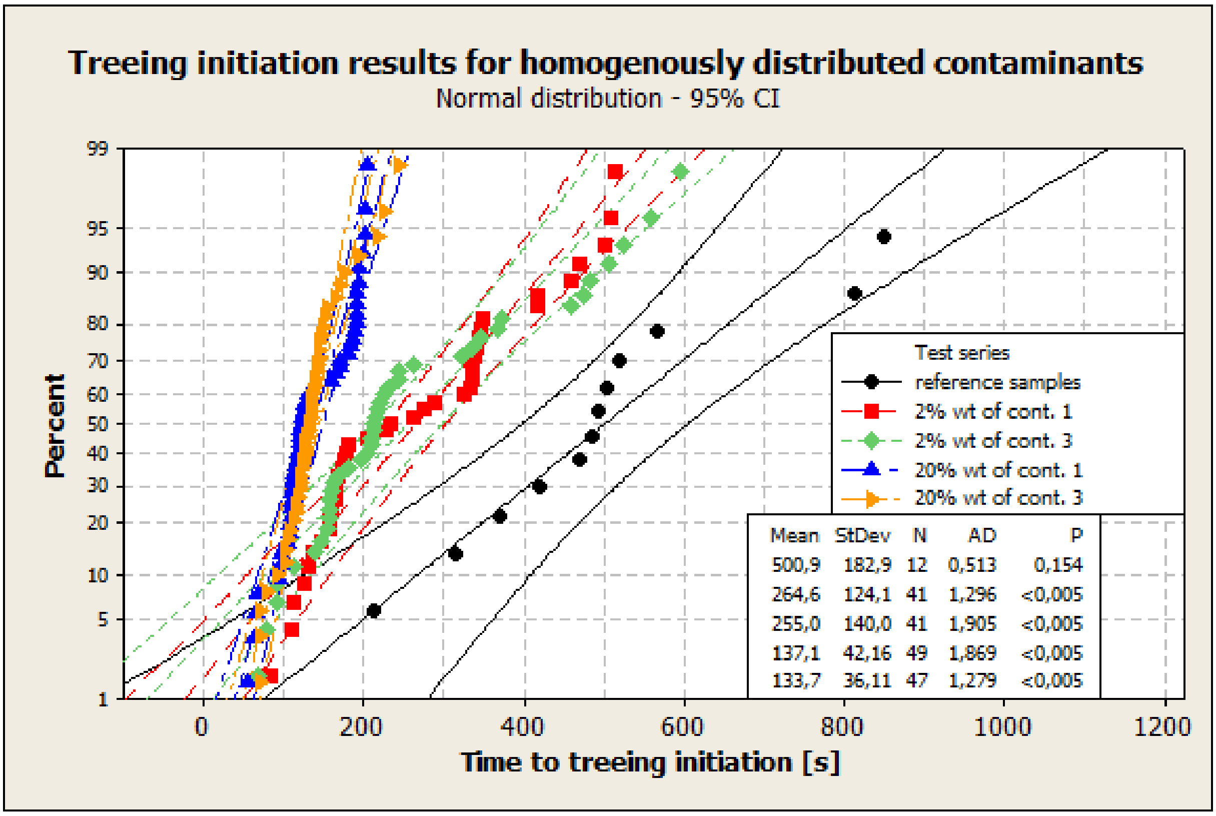

Figure 36. Treeing initiation results for samples with homogenous distributed contaminants.

The higher concentration resulted in a much earlier treeing initiation. For 2% wt, the trees initiated somewhat later, although some trees were also initiated early. A possible explanation is that the early initiation is depending on the amount of particles located in the close vicinity of the wire. No or insignificant impact was found of the degree of thermal aging of the contaminants on the treeing initiation time.

5.3.3 Optical results

The samples were microtomed, since the tree channels were difficult to detect. Afterwards, the channels were visible for microscope photography, as seen in figure 37. Additional and unmicrotomed pictures used for the analysis can be found in appendix III, pictures 47-62.

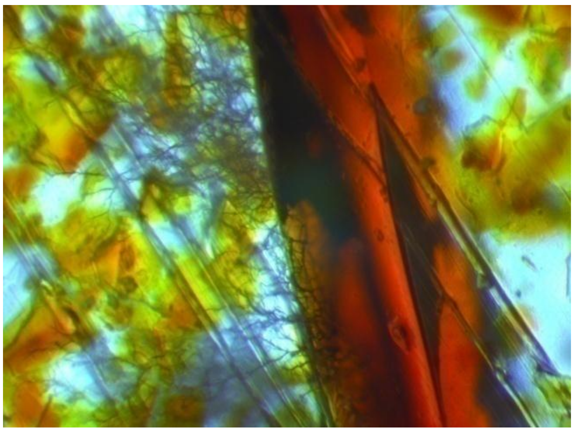

a) Electric tree propagated along contaminant

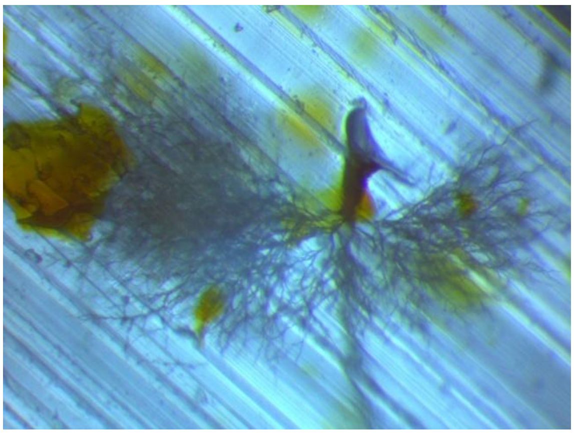

b) Unsymmetrical electric tree

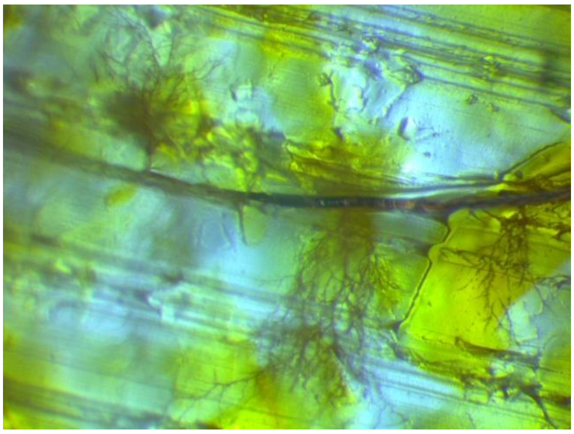

c) Electric trees propagated along contaminants

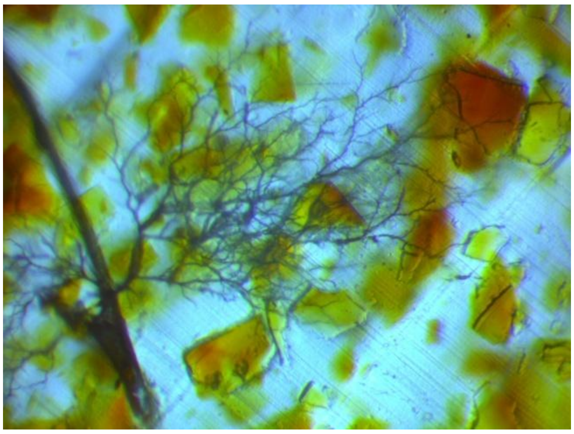

d) Electric tree propagated through contaminants

Figure 37. Different electric trees revealed by microtoming.

Some typical trends could be detected, in some cases an increased number of treeing channels along contaminants could be seen, as well as electrical trees with much more distorted shapes. A possible explanation is that the contaminants had distorted the electrical field in the sample. Although, since no clear difference in the treeing initiation time was found between contaminants 1 and 3, the best explanation for the observed phenomena is the worsening of the morphology in the material. The densely treed areas were likely caused by not necessarily big voids, but bad adhesion. It is speculated that an increased amount undetectable microvoids, due to bad enclosement of the particles in the polymer matrix is the main factor behind the observed phenomena.

5.3.4 Tests with inserted pre-crosslinked particles

To investigate the impact of unaged particles inserted into the samples, crosslinked particles were made without thermal aging. Pre-crosslinked particles are known to also worsen the quality of high voltage cables. Again the concentrations of 2% wt and 20% wt were used in these tests. The result is shown below in figure 38 as compared to the reference.

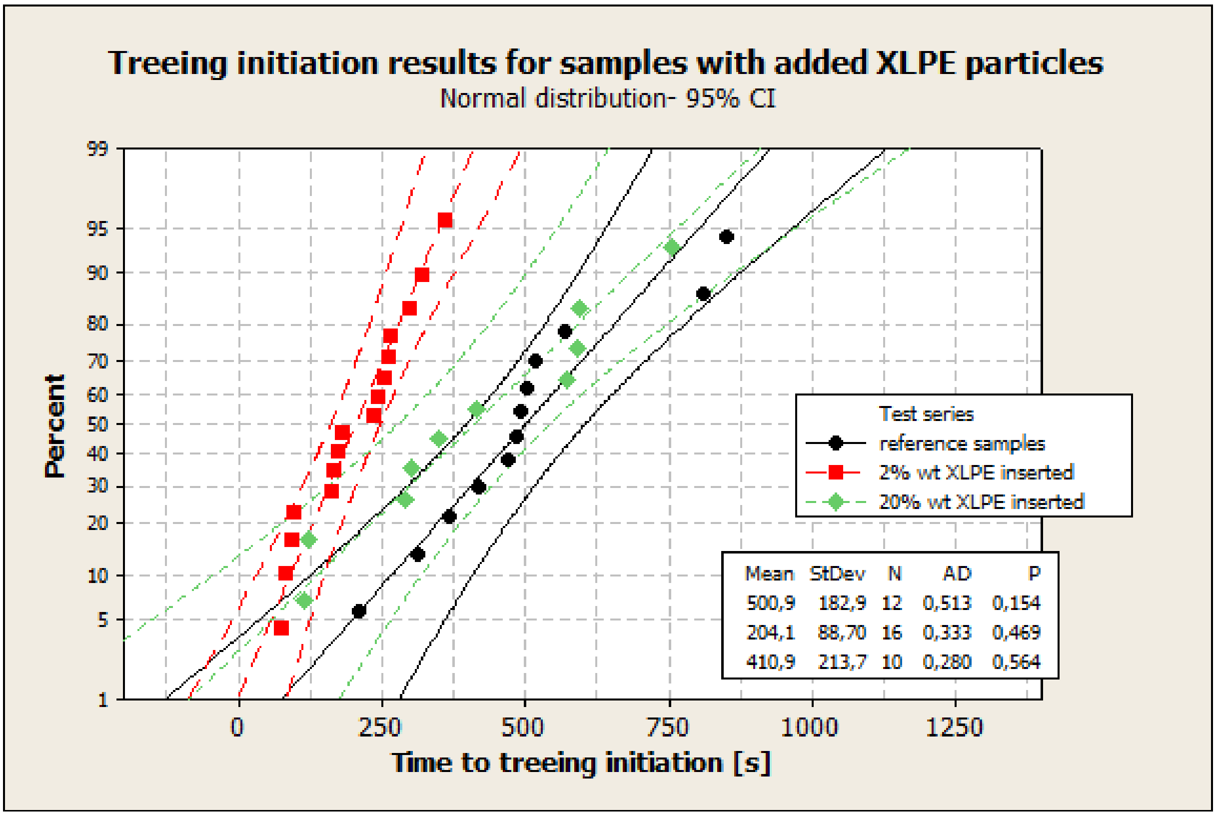

Figure 38. Treeing initiation results for samples with inserted pre-crosslinked particles.

It could be observed that the initiation started earlier when adding these particles, although the effect is not nearly as severe as when adding contaminants. It was also observed that the samples with 20% wt particles added treed later than the samples with 2% wt added. This is likely the effect of another factor, as for example a large amount of severe kinks were present, especially for the series with 20% wt added. The kinks often developed large bush-trees, which in turn could have delayed the treeing initiation. Also in all samples trees were initiated before 15 minutes, showing that an earlier initiation is present when compared to the reference samples. Pictures 63-70 in appendix III show some of the tested samples were the trees and in some cases large kinks can be observed.

Explaining why the initiation didn't occur as early as when inserting thermally aged particles, could be done by comparing it with a similar test result. This result originates from a study where particles of high molecular weight polyethylene where added in a series of tests [49]. For these tests no difference in AC breakdown voltage was found when compared to reference tests. The suggested explanation is shared also for the in this thesis performed tests: Uncrosslinked polymer chains were present in the inserted particles. As these polymer chains might connect with the polymer matrix, a better adhesion and lower amount of microvoids could probably be found in the vicinity of the particles, as for the insertion of organic contaminants. For organic contaminants the polymer chains are likely to be more degraded and will not connect to the polymer matrix to the same degree.

5.4 Homogenous contaminant distribution tests with DC voltage

For the tests with DC voltage, 4 batches including reference samples as well as samples with 10% wt addition of pre-crosslinked particles or contaminants were used. This concentration was chosen since the electrical trees were expected to be small in size due to space charge in the samples, allowing for better optical detection of these trees as when using 20 % wt addition. Also if lower concentrations such as 2% wt were to be used, the impact of the contaminants might not be as powerful. The test circuit used for these experiments is described in chapter 3.2.4. First a series of DC breakdown strength tests were performed in order to choose a suitable voltage level for the electrical tree tests. Next an attempt is made for growing electric trees in the samples.

5.4.1 DC breakdown strength

A DC voltage was applied for measuring the DC breakdown strength of the test samples. The voltage profile is shown below in figure 39.

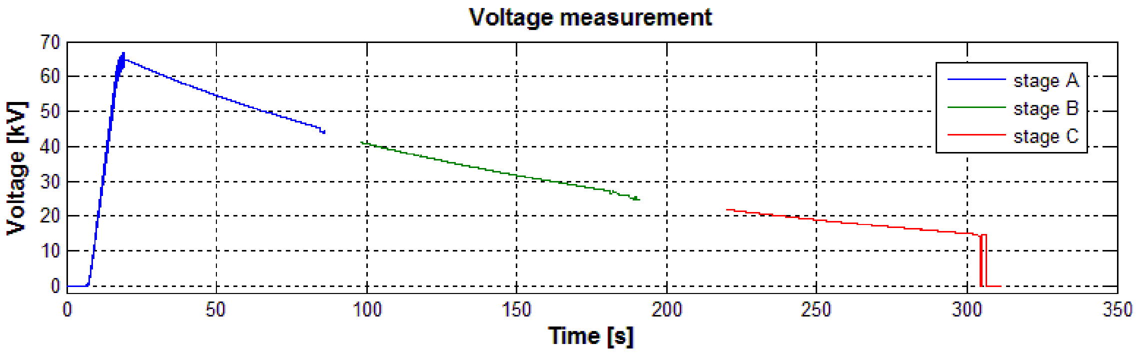

Figure 39. Applied voltage for DC breakdown test, suggested that no breakdown occurred.

At first, the voltage was ramped up with a ramp rate of 7.1 kV/s. The ramping stopped at 67 kV as the AC source is turned off, to prevent powerful discharges in the circuit as these might damage the equipment. Next, during stage B the voltage slowly decreases as the energy from the capacitors was dissipated in the circuit. Finally, at stage C the voltage was low enough for grounding the circuit through a resistor. When breakdowns occurred, the voltage profile looked different, and the circuit could be grounded much earlier as a chunk of the energy from the capacitors was released. The results from the breakdown tests are shown below in table 7 and table 8.

Table 7. DC breakdown test results in kV. W stands for samples that withstood 67 kV voltage.

		Sample number									
		1	2	3	4	5	6	7	8	9	10
Batch	Reference	W	W	52.8	W	W	W	W	57.3	60.6	W
	10% wt XLPE	W	W	W	56.4	W	W	W	W	W	W
	10% wt c2	W	59.9	66.6	W	62.7	W	62.8	W	62.3	57.2
	10% wt c3	65.4	W	56.7	48.7	50.9	W	53.7	60.3	55.5	53.3

Table 8. Average breakdown voltage and number of withstands summarized from table 6. * indicates averages calculated from 1 and 3 breakdowns respectively, and is likely below the real breakdown level.

	Reference	10% wt XLPE	10% wt c2	10% wt c3
Average breakdown	56.9 kV*	56.4 kV*	61.9 kV	55.6 kV
Number of withstands	7	9	4	2

From these tests a probable influence of the contaminants on the DC breakdown strength in the samples was found. It can also be stated that as before for AC, the insertion of pre-crosslinked particles for DC did not necessarily weaken the material. At last a possible difference was found between contaminant 2 and 3, indicating that the degree of aging could be an influencing factor as well. This could be due to the different conductivities of contaminant 2 and 3, possibly changing both the electric field and the amount of current dissipated in the samples and the contaminated sites. Some tested samples are shown in pictures 71-74 in appendix III.

5.4.2 DC treeing experiments

As the space charge in the test samples often changes the treeing inception level to be close to the DC breakdown level, a special approach was necessary. As no voltage reversals were possible in the test method, an opposite space charge was injected manually by applying -5 kV DC in 3 sessions. Each session included 8 samples, with 2 from each batch. The DC voltage was applied for 4.5, 8 or 22 hours for the three sessions. Hopefully, some of the negative space charge was retained in deep traps. Afterwards the samples were subjected to a voltage below the DC breakdown level found in chapter 5.4.1 for 5 minutes. The AC voltage fed into the circuit was 39 kV rms for samples with contaminant 3, and 43 kV rms for the other samples. The DC voltage measured was around 50.3 kV and 56.1 kV respectively, with a 2 kV ripple. A voltage profile measured for a tested sample with 10% wt of contaminant 2 is displayed below in figure 40.

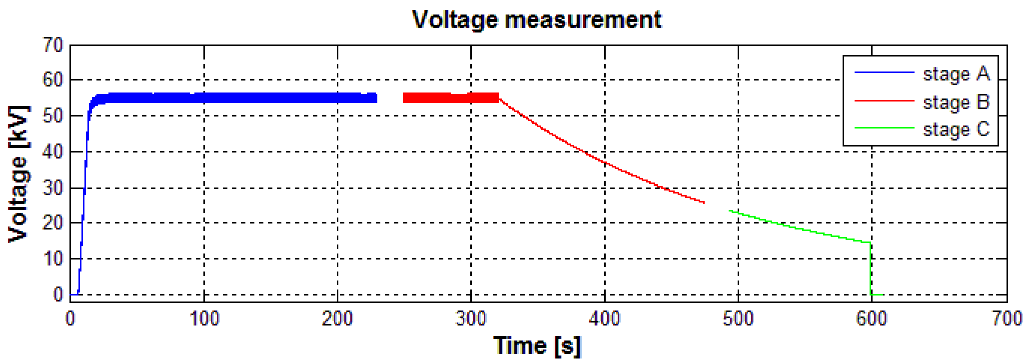

Figure 40. Applied voltage for DC treeing test.

When afterwards observing the samples in a microscope, a few possible trees could be detected. Better observations were necessary, so the samples were microtomed. The trees found after the microtoming are displayed below in figure 41.

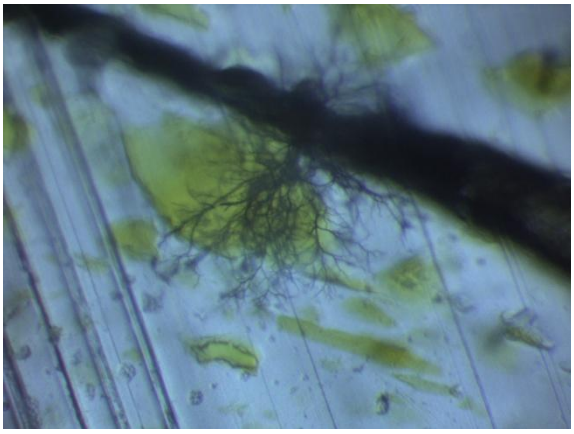

a) Bush DC tree created by a self-sustained

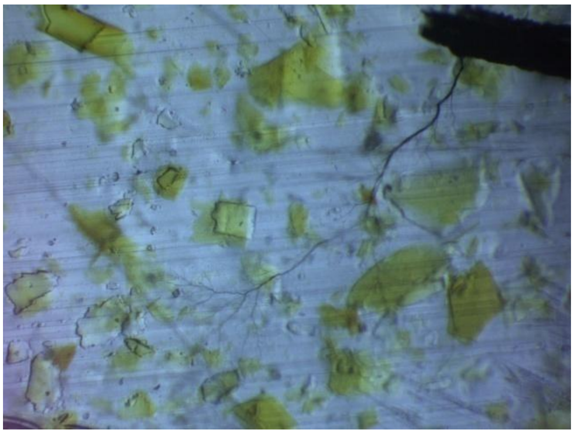

b) DC tree created by a breakdown in the breakdown in the oil. test sample.

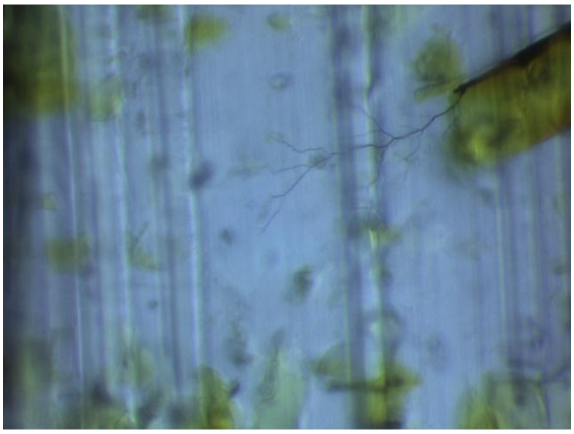

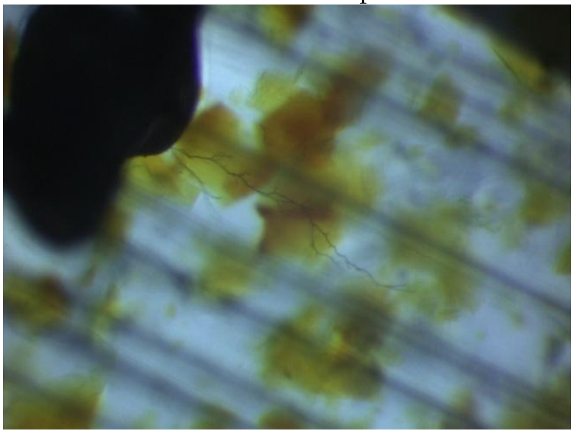

c) DC tree propagated from the wire

d) DC tree found near a breakdown channel.

Figure 41. Created DC trees revealed by microtomation.

Due to the low amount of observed DC trees, it is not possible to make conclusions on the propagation of DC trees. In some cases the trees were likely caused by a breakdown, rapidly grounding the wire, while the space charge remained in the sample. Trees were only found in the samples with contaminant, since the applied voltage was adjusted to their breakdown voltage. For the reference samples and samples with added XLPE particles, the applied voltage for the treeing tests was likely to low to initiate any trees. Due to the limited amount of initiated trees it is unclear if the space charge saturation was a successful method or not. Additional pictures of DC trees initiated by the DC treeing tests are found in appendix III, pictures 75-82.

6 Discussion

Topics discussed are the results of the electrical field simulations, the optical observations made and some aspects regarding the test samples and the impact of organic contaminants.

6.1 Electric field simulations

The accuracy of the COMSOL simulations is to be discussed. The derived value for the electrical field for the 3 dimensional calculations was found to be close to the value for a 2 dimensional circle-plane topology. This might indicate that the 3 dimensional simulations were accurate when the effect of space charge is to be ignored.

Deriving equations from the simulations might have introduced an error to the result, but since this error was small compared with the error introduced by the neglecting of the space charge effects, no further investigation was made about this error. When the first 2 of the derived equations were applied to the results from a ramped up AC test, the standard deviation was reduced in the results. This didn't give any conclusions about the quality of the approximations, but indicates that the described trends probably exist in the test samples. The approximated equation derived for calculating the electric field at kinks showed unsuccessful. Although its unsuccessfulness, the kink equation and simulations showed that pointy and long kinks provided the biggest field amplification.

For the electrostatic (AC) simulations, a background field could be applied to the material. For the electric current (DC) simulations, this background field could not be applied. This background field simulates the effect of an infinity sized high voltage plane connected to the top of the samples, exactly where the copper tape begins. Even though this field's impact on the scaling constant was low, a difference could be seen in the electric field distribution along the wire. When no background field was applied, the electric field along the wire decreased slower when moving further away from the tip. This effect was translated into the different test setups. When using the wet and dry aging test setup, the high voltage electrode had a shape similar to the described high voltage plane. The high voltage electrode for the AC and DC test setup was smaller. For wet and dry aged samples, most trees were initiated at the curvature of the wire, indicating that this area could have been stressed more than areas higher up in the sample. Unaged samples did not share this trend to the same extent.

As mentioned before, the effect of space charge has not been included in the simulations. Including this effect would not have improved the quality of the simulations, but is essential to consider when conclusions are made from the tests.

The variance in the wire-plane distance could be eliminated for ramped up tests. For constant AC and DC tests this didn't work, so a different manufacturing method was necessary. This was one of the reasons why a second tests series was performed for the wet and dry aging tests. Fortunately the altered manufacturing process had already been implemented when the samples with homogenously distributed contaminants for the AC and DC tests were made.

6.2 Optical observations

Electric trees and water trees propagate from the wire in three dimensions. When the trees are observed in a microscope, the trees can only be investigated from 2 directions (front and back of sample or microtomed slice). To make good conclusions about the propagation of the trees, especially when organic contaminants are involved, the used observation method is extremely important. The observation methods used in this thesis are:

- Using different focus depths on the test samples. This is suitable for reference samples or samples with good enough transparency. For samples with a high concentration of contaminants it is hard to fully figure out how the trees have propagated. Even though some conclusions can be made from these observations, it is unsuitable to present different pictures for each created tree in the thesis.
- For samples with higher concentrations of contaminants, microtomation becomes suitable. Microtomation will cut slices from the test samples so only a thin slice with trees inside remains. In this way, all the tree channels will be in focus, and obscuring contaminants in a different depth level will be eliminated.
- The best observations are made manually using a microscope with depth vision. Unfortunately these observations could not be translated into the presented pictures. This is why in some cases conclusions made about the propagation of electrical trees are hard to detect in the presented figures.

6.3 Sample issues and contaminants

For the tests with separately inserted contaminants, contaminants were placed in the close vicinity of the wire, prior to the crosslinking process. During the crosslinking process, the wire tended to move around 1 mm upwards in the sample. The contaminants often remained in the same place as before the crosslinking process. This turned out to be a problem, since the contaminated areas in most cases remained unaffected by the different trees initiated from the wire.

When comparing the samples with homogenously inserted contaminants with samples with separately inserted contaminants, the advantages and disadvantages of both methods can be discussed. The advantage of the homogenous insertion is that, independently of the wire's movement during the crosslinking process, some contaminants will always be found in the near vicinity of the wire. The disadvantages of the homogenous insertion are worse visibility of the trees and that more contaminants are used for creating the samples. The advantage of the separate insertion would be better visibility and less contaminants used for the sample manufacturing. The disadvantage of the separate insertion is, as discussed before, that samples with contaminants near the wire were scarce.

When evaluating the quality of the insertion of contaminants, no visible voids were observed. The creation of such voids due to inefficiency of the manufacturing process was an in advance expected variable. Fortunately no visible voids were created, leading to a low amount of discarded samples unsuitable for electrical testing.

Voids created by possible oxidization of the material after the crosslinking process could affect electrical degradation as well. As these voids might be present in high voltage cables due to local over temperatures after the crosslinking process, these voids might be interesting to study. Since the organic contaminants were manufactured and inserted before the crosslinking method, a different approach could be necessary. These approaches are further discussed in chapter 8.1, untouched topics.

The DC treeing tests showed to be challenging due to several factors. At first, really high voltage levels had to be used due to the injected space charge. Secondly, the DC trees were extremely small in size, often only consisting of a few tree channels. This characteristic made them extremely difficult to observe. DC treeing initiation detection was practically impossible, and might have been the cause of some of the breakdowns in the samples.

The ramping speed used was the fastest possible in the test setup. As no polarity reversals were possible in the circuit, another approach was tested to reduce the impact of the space charge. By applying the opposite voltage for a longer period of time to the test samples, hopingly some opposite charge was left when the treeing test were performed. It is unclear if the space charge saturation had an effect on the DC treeing initiation. Maybe voltages even closer to the breakdown voltage should have been used. The space charge saturation could possibly be a method for further evaluation in future work.

7 Conclusions

A series of conclusions has been listed, both about the test method and about the organic contaminants in general.

7.1 Test method

The degassing and the crosslinking process used in the method were measured to be successful. Also the degassing process was found to have an influence on the development of kinks in the samples.

The COMSOL simulations provided essential information about the electric field in the test wire-plan test setup. For ramped up tests, the simulations provided approximated equations suitable for calculating the electric field for each electric tree initiated in the sample. The simulations also provided information about the field impact of different distances between the wire and the ground plane. Also increased knowledge about the impact that kinks have on the electric field is found. Finally, from the conductivity measurements and the simulations with organic contaminants, information is obtained about the influence of the contaminants on the electric field in the wire-plan test setup.

The wire-plan setup shows a different aspect of the contaminants and their influence on electrical degradation as setups using different field distributions might show. By stressing a bigger area as for example a needle-rod setup, and still having easy reproducibility and good visibility, the impact of the morphology of the material is easily detectible. Compared to a setup using a more homogenously distributed field, the propagation of the trees through locally contaminated areas becomes interesting.

The current test method is unsuitable for full tree propagation studies as the resolution of the optical detection system is arguable. Instead the conclusions about the propagation could only be made after the electrical testing was completed, using a microscope and in some cases a microtome.

The used wet aging setup allowed to grow water trees in the ranges of 20-40 μm. For better contaminant studies bigger water trees are to be created, forcing a change in this setup. This topic is further discussed in future work.

The aging of the samples in the wet and dry aging setup was found to have an impact on the electric treeing. In the aged samples and in particular in the wet aged samples, a higher amount of electrical trees were initiated earlier in the reference. Also the moisture content in the samples during the testing showed to have an impact on the electrical treeing

7.2 Organic contaminants

Neither water trees nor electric trees were observed to initiate directly from the contaminants. This does not imply that the contaminants had good resistance to electrical degradation and breakdown. This may be caused by the highly concentrated electric field in the wire-plan test method.

Due to the test method, the results from the wet and dry aging with and without contaminants yielded a limited amount of data. In some cases trees were found affected by the contaminants. From these trees a tree-enhancing impact of the contaminants could be found, but the limited amount of data makes this impact unclear.

7.2.1 AC tests

For the AC tests with a homogenous distribution of the contaminants, no big impact was found of different amount of thermal aging of the contaminants. Different concentrations of the contaminants indicated that the samples with higher concentrations had worsened morphology in the material. Also from the optical observations, several cases could be found were an increased amount of tree channels was found on the contaminants' surfaces. From these AC test results possible conclusions of the contaminants' impact on AC breakdown strength could be made:

- A loss of adhesion between the organic contaminants and the XLPE insulation may likely be the main cause for an increased amount of degradation in the material, resulting in a reduced AC breakdown voltage
- The permittivity change originating from the thermal aging in the contaminants could also have an impact on the process and in particular on the electric field distribution, but this was not the main factor of the reduced AC breakdown voltage in this case.

7.2.2 DC tests

For the DC tests with homogenously distributed contaminants, a difference in DC breakdown strength was found. This difference could be found when comparing the reference samples with samples with contaminants. Also a possible difference between samples with different amount of thermal aging of the contaminants was found. From the conductivity measurements of the contaminants, a possible conductivity increase of approximately 100 times to the reference material could be found. From the optical observations performed after the electrical testing, no particular growth pattern could be distinguished. From these DC test results, possible conclusions about the contaminants' impact on DC breakdown strength could be made:

- The conductivity increase of the organic contaminants has a big enough impact on the electrical field distribution to possibly influence the degradation and DC breakdown voltage.
- The conductivity increase of the organic contaminants could also locally increase the amount of charge carriers at the contaminated sites. This might have an impact on the degradation and DC breakdown strength as well.
- The loss of adhesion between the contaminants and the XLPE insulation is an accelerating factor for the degradation, but this might not be the most severe factor for the short-term DC breakdown strength.

7.2.3 Conclusions for pre-crosslinked particles

The insertion of pre-crosslinked particles didn't show as severe AC and DC breakdown strength influences as the organic contaminants did. This could be explained by:

- The pre-crosslinked grains still contained uncrosslinked polymer chains. As some of these chains might have had connected with the polymer material during the crosslinking process, the adhesion of these particles might be better than for organic contaminants.

- The pre-crosslinked grains have similar permittivity and conductivity as the XLPE insulation. Due to this, the electrical field is probably not influenced by these particles, resulting in less degradation and breakdown strength influence.

8 Future Work

For future work within the area of organic contaminants, a lot of interesting topics are still untouched. Also additional tests on the same subjects as in this thesis could be of interest, for obtaining additional evidence for the mentioned conclusions about organic contaminants. For additional testing using the same or a similar test method, some possible improvements are listed.

8.1 Untouched topics

No mechanical stress testing was performed in this thesis. Mechanical stress is present in dynamic cable applications, such as cables connected to offshore wind farms or oil rigs. As organic contaminants could have a higher porosity as the XLPE used in the thesis, applied mechanical stress might be able to damage the contaminants more than the XLPE. The mechanical stress should be applied in a repeatable way with possibly different amounts for different test series. After the application of the mechanical stress, electrical testing might reveal a difference in treeing initiation times when compared to unstressed samples.

As the contaminants were created and inserted prior to the crosslinking process in this thesis, no microvoids were found in the samples. If possible, samples could be made with organic contaminants created after the crosslinking process. By subjecting the test samples to overtemperatures during or after the test method, another perspective on thermal aging could be found. Also extremely local overtemperatures could maybe be applied by applied by using a heated needle or rod and connecting this rod to a sample for a certain amount of time. If feasible, this local overtemperature might create contaminants with voids in the material. Although the inserted contaminants in this thesis had bad adhesion to the material, the adhesion of a contaminant created after the crosslinking process might be far worse.

For a full investigation of the DC performance of XLPE with organic contaminants, wet or dry aging with a DC voltage applied to the samples might be interesting. The samples could be tested afterwards with AC or DC voltage to detect a possible difference in the treeing initiation time.

As the test method used in this thesis stressed the material with an electric field highly concentrated to the wire, a different field topology might reveal other effects of the contaminants. By using a homogenous field distribution in a test sample, the electric field could instead be the highest at the actual contaminants. This field topology could be achieved by inserting a thin film with contaminants in between two rogovski profiled electrodes or rogovski cups. To eliminate air pockets in between the film and the electrodes, insulating grease could be used, as well as applying a pressure to the sample. Using this sample-setup it would be more likely to develop bow-tie trees originating from the contaminants, which are found in high voltage cables.

8.2 Test method improvement

Since the size of the created water trees was in the range of 20-40 μm, an impact from the contaminants on water tree development was hard to find. Growing bigger and longer water trees could reveal this impact. It could be possible to use an increased frequency in the wet and dry aging test setup. Another option is to age the samples for a longer time, such as 2 to 3 weeks. If the samples are to be aged for longer times than 1 week, re-saturation of the samples with water would be necessary. Also adding a layer with water in the test setup could show to be a viable option for keeping the environment wet. If water is to be added in the test setup, it should be noted that it is to be removed again for dry aging tests.

For AC treeing studies, only treeing initiation studies were possible with the current test setup. If an optical detection system with a better resolution was to be installed, also propagation studies could be done on the subject. For these tests samples with around 2% wt contaminants added homogenously, or separately inserted contaminants are suitable. It is possible that contaminants not only have an impact on treeing initiation, but also propagation, as densely treed areas were found on the borders of the contaminants in this study.

Also the DC treeing studies could benefit from an upgrade of the optical detection system. As the DC trees created in the current setup were undetectable by the system, many tests were performed “in the dark” with no knowledge whether trees were initiated or not until further investigation in a microscope afterwards. A better detection system might however be sensible to the extremely high voltages used for the DC tests. For this reason, DC aging followed up by AC testing might be an alternative as well.

For the samples with separately inserted contaminants, a sample with contaminants located in the close vicinity of the wire was almost impossible to get with the current pressing scheme. For most samples, the wire moved 1 mm upwards during the crosslinking process, while the contaminants remained were the wire originally was located. Experimenting with different ways to insert the contaminants could reveal a way to create samples with contaminants in the close vicinity of the wire. For example, contaminants could be inserted into 1 of the polyethylene strips, at the position were the wire is expected to be located after the crosslinking process. The advantages of these samples would be that they would have both good visibility as well as a bigger impact of the contaminants.

All samples used in this thesis had several kinks at different positions along the wire. As the electric field was found to be increased at these sites, no electric trees initiated at these kinks could be used for analysis. Even though the derived kink approximation calculated in this thesis might work for ramped up AC voltage, it is unusable for constant AC voltage. For extremely clean samples, the electric trees were initiated first at the kinks, and in some cases only at kinks. If the amount of kinks was to be reduced in the samples, the quality of the test method would improve a lot. As a lot of kinks were found to be severed or even created during the degassing process, a possible change in the degassing process could possibly reduce the amount of kinks in the test samples.

At last, a possible addition to the test method could be a heated silicon oil bath along with a microscope. The heated oil will make the samples fully transparent, and the full structure of the trees could easily be detected.

References

[1] “COMSOL Multiphysics version 4.2” Comsol AB, Sweden, 2011.

[2] L.A. Dissado; J.C. Fothergill; “Electrical degradation and breakdown in polymers”, *IEE Materials and Devices Series 9*, Peter Peregrinus, pp. 601, 1992.

[3] N. Ahmed; N. Srinivas; ”Cable insulation”, *Wiley Encyclopedia of Electrical and Electronics Engineering*, J. Webster, Editor, John Wiley & Sons Inc., 2001.

[4] N. Shimizu; C. Laurent; "Electrical tree initiation," *Dielectrics and Electrical Insulation, IEEE Transactions on* , vol.5, no.5, pp.651-659, Oct 1998.

[5] T. Worzyk; “Submarine Power Cables” *Springer Berlin Heidelberg*, 2009.

[6] N. Hampton; R. Hartlein; H. Lennartsson; H, Orton; R. Ramachandran: ”Long life XLPE Insulated Power Cable”, *Jicable*, Georgia Institute of Technology, June 2007.

[7] J.M.G. Cowie; V. Arrighi; “Polymers: chemistry and physics of modern materials”, *Boca Raton, CRC press,* third ed., 2008.

[8] S. Nilsson; ”The Effect of Crosslinking on Morphology and Electrical Properties in LDPE Intended for Power Cables”, Thesis for the Degree of Doctorate of Engineering, *Department of Chemical and Biological Engineering*, Chalmers University of Technology, 2010.

[9] M. Jarvid; ”Voltage Stabilizers Inhibition of Electrical Treeing in XLPE at High Voltages by Molecular Voltage Stabilization”, Thesis for the Degree of Master of Engineering, *Department of Chemical and Biological Engineering*, Chalmers University of Technology, 2010.

[10] A.E. Woodward; “Atlas of Polymer Morphology”, *Hanser Gardner Pubns*, May 1989.

[11] L.R. Mason; T.E. Doyle; A.B. Reynolds; "Effect of antioxidant concentration and radiation dose on oxidation induction time," *Electrical Insulation, Conference Record of the 1992 IEEE International Symposium on”,* vol., no., pp.169-172, 7-10 Jun 1992

[12] V. Englund; “Voltage Stabilisers for XLPE Cable Insulation”, Thesis for the Degree of Doctorate of Engineering, *Department of Chemical and Biological Engineering*, Chalmers University of Technology, 2008.

[13] M. Andersson; ”Investigation of Voltage Stabilizer in XLPE cable insulation” Thesis for the Degree of Master of Engineering, *Department of Chemical and Biological Engineering*, Chalmers University of Technology, 2012.

[14] S.H. Hamid; “Handbook of polymer degradation”, *New York : Dekker cop*., edition 2, 2000.

[15] E. Kuffel; W.S. Zaengl; J. Kuffel; “High Voltage Engineering: Fundamentals”, *Butterworth Heinemann, Elsevier Ltd.*, Second edition, 2009.

[16] R. Cooper; C.T. Elliot; “Directional Electric Breakdown of KCI Single Crystals”, *Appl. Phys. 1*, pp. 121, 1968.

[17] L.L. Alston; “High Voltage Technology”, *Oxford University press*, 1968.

[18] J. Andrianjohaninarivo; M.R. Wertheimer; A. Yelon; "Nucleation of Electrical Stress in Polyethylene," *Electrical Insulation, IEEE Transactions on* , vol.EI-22, no.6, pp.709-714, Dec. 1987.

[19] G. Krause; S. Gottlich; K. Moller; D. Meurer; "Space charge phenomena in partially crystalline polymers: on-line measurement of charge carrier motion under high AC-field stress," *Conduction and Breakdown in Solid Dielectrics*, 1989., Proceedings of the 3rd International Conference on , vol., no., pp.560-564, 3-6 Jul 1989.

[20] N. Shimizu; H. Katsukawa; M. Miyauchi; M. Kosaki; K. Horii; "The Space Charge Behavior and Luminescence Phenomena in Polymers at 77 K," *Electrical Insulation, IEEE Transactions on* , vol.EI-14, no.5, pp.256-263, Oct. 1979

[21] Y. Shibuya; S. Zoledziowski; J.H. Calderwood; "Light emission and deterioration in epoxy resin subjected to power frequency electric fields," *Electrical Engineers, Proceedings of the Institution of* , vol.125, no.4, pp.352-354, April 1978

[22] D. Mary; C. Laurent; G. Teyssedre; S. Bamji; A. Bulinski; M. Abou Dakka; L. Cisse; "Threshold of space charge injection and electroluminescence in polymeric insulation," *Electrical Insulation and Dielectric Phenomena, 2004*. CEIDP '04. 2004 Annual Report Conference on , vol., no., pp. 249- 252, 17-20 Oct. 2004

[23] S.S. Bamji; ”Electrical Trees, Physical Mechanisms and Experimental Techniques”, *in Wiley Encyclopedia of Electrical and Electronics Engineering*, Vol. 6, pp. 264-275, 1999

[24] N. Hozumi; T. Okamoto; H. Fukagawa; "TEM observation of electrical tree paths and micro-structures in polyethylene," *Electrical Insulation, Conference Record of the 1988 IEEE International Symposium on* , vol., no., pp.331-334, June 1988.

[25] L.A. Dissado; "Understanding electrical trees in solids: from experiment to theory," *Dielectrics and Electrical Insulation, IEEE Transactions on* , vol.9, no.4, pp. 483-497, Aug 2002.

[26] F. Ciuprina; G. Teissèdre; J.C. Filipini; “Polyethylene crosslinking and water treeing”, *Polymer,* Volume 42, pp. 7841-7846, April 2001.

[27] J.J. de Bellet; G. Matey; L. Rose; V. Rose; J.C. Filippini; Y. Poggi; V. Raharimalala; "Some Aspects of the Relationship between Water Treeing, Morphology, and Microstructure of Polymers," *Electrical Insulation, IEEE Transactions on* , vol. EI-22, no. 2, pp. 211-217, April 1987.

[28] C.T. Meyer; "Water Absorption during Water Treeing in Polyethylene," *Electrical Insulation, IEEE Transactions on* , vol.EI-18, no.1, pp.28-31, Feb. 1983.

[29] S.L. Nunes; M.T. Shaw; “Water Treeing in Polyethylene – A Review of Mechanisms”, *Electrical Insulation, IEEE Transactions on*, vol. EI-15, issue 6, pp. 437-450, 1980.

[30] A. Eccles; L.A. Dissado; J.C. Fothergill; J.A. Houlgreave; "Water tree inception-experimental support for a mechanical/chemical/electrical theory," *Dielectric Materials, Measurements and Applications*, 1992., Sixth International Conference on , vol., no., pp.294-297, 7-10 Sep 1992

[31] J.-P. Crine; J. Jow; "A water treeing model," *Dielectrics and Electrical Insulation, IEEE Transactions on* , vol.12, no.4, pp. 801- 808, Aug. 2005.

[32] K., Abdolall; "The polymer-water interaction in water treeing: an NMR study," Electrical Insulation, 1988., Conference Record of the 1988 IEEE International Symposium on , vol., no., pp.267-271, 5-8 Jun 1988.

[33] J.O. Bostrom; E. Marsden; R.N. Hampton; U. Nilsson; "Electrical stress enhancement of contaminants in XLPE insulation used for power cables," *Electrical Insulation Magazine, IEEE* , vol.19, no.4, pp.6-12, July-Aug. 2003

[34] S. Kitai; S. Asai; K. Hirotsu; "Voltage life characteristics of XLPE", *Proceedings of the Twenty-First Symposium on Electrical Insulating Materials*, pp. 267-270, 1988.

[35] G. Katsuta; A. Toya; S. Katakai; M. Kanaoka; Y. Sekij; "Influence of defects on insulating properties of XLPE cable", *Proceedings of the 3rd International Conference on Properties and Applications of Dielectric Materials*, Tokyo, pp. 485-489, July 1991.

[36] R.D. Naybour; "Assessment of polyethylene based insulations for wet environments", *Power Cables and Accessories 10kV - 500kV, Third International Conference on*, vol., no., pp. 36-40, 23-25 Nov. 1993.

[37] ASTM D3756 – 97 “Standard Test Method for Evaluation of Resistance to Electrical Breakdown by Treeing in Solid Dielectric Materials Using Diverging Fields”, 2010.

[38] R. Huuva; V. Englund; S.M. Gubanski; T. Hjertberg; "A versatile method to study electrical treeing in polymeric materials," *Dielectrics and Electrical Insulation, IEEE Transactions on* , vol.16, no.1, pp.171-178, February 2009.

[39] R. Huuva; ”New Test Arrangement for Measuring Electrical Treeing in Polymers”, Thesis for the Degree of Licentiate of Engineering, *Department of Materials and Manufacturing Technology*, Chalmers University of Technology, 2007.

[40] A.B. Johansson; A. B. Sandberg; “Detection of Electrical Treeing in XLPE Exposed to AC and DC Stress”, Thesis for the Degree of Master of Engineering, *Department of Materials and Manufacturing Technology*, Chalmers University of Technology, 2010.

[41] C.M. Marvin; “HPLC: a practical user’s guide”, *Interscience*, second edition, jan 2007.

[42] J.O. Bostrøm; E. Marsden; R.N. Hampton; U. Nilsson; H. Lennartsson; "Electrical stress enhancement of contaminants in xlpe insulation used for power cables", *IEEE Electrical Insulation Magazine*, Vol. 19, No. 4, pp. 6-12, Aug 2003.

[43] "IEEE Guide for the Statistical Analysis of Electrical Insulation Breakdown Data," *IEEE Std 930-2004 (Revision of IEEE Std 930-1987)* , vol., no., pp.1-41, 2005.

[44] R. Ross; "Bias and standard deviation due to Weibull parameter estimation for small data sets," *Dielectrics and Electrical Insulation, IEEE Transactions on* , vol.3, no.1, pp.28-42, Feb 1996.

[45] "Minitab 16 Statistical Software", Minitab Inc., U.S.A., 2010.

[46] L. Kronlund; P. Kvist; " A study of electrical treeing in XLPE using wire electrodes - Impact on electrical treeing inception voltage by sample preparation and voltage stabilizers", Thesis for the Degree of Bachelor of Engineering, *Department of Chemical and Biological Engineering*, Chalmers University of Technology, 2011.

[47] J.V. Gulmine; L. Akcelrud; "FTIR characterization of aged XLPE", *Polymer Testing*, Volume 25, Issue 8, pp. 932-934, December 2006.

[48] "Matlab R2010b" MathWorks, U.S.A., 2010.

[49] R.W. Coppard; J. Bowman; R.T. Rakowski; R.T. Durham; S.M. Rowland; "The effect of included flaws upon the ac breakdown of polyethylene", *Proceedings of the 3rd International Conference on Conduction and Breakdown in Solid Dielectrics*, pp. 55-60, July 1989.

Appendix

List of appendices:
Appendix I: COMSOL simulations.
Appendix II: Additional pictures of kink appearance during the degassing process.
Appendix III: Additional pictures of electrical trees created in the thesis.

Appendix I - COMSOL simulations.

All analyses used stationary studies, with 1kV applied to the electrode. Conveniently this stress creates electric field strength in the magnitude of a couple of kV/mm.

1 Field layout with no imperfections

Due to the small size of the wire, several simplifications of the original test sample geometry were made in the 3 dimensional (3D) simulations. It was impossible to create sufficient mesh to adequately simulate the entire sample. Instead, only a quarter of the sample was created, as shown in figure 1.

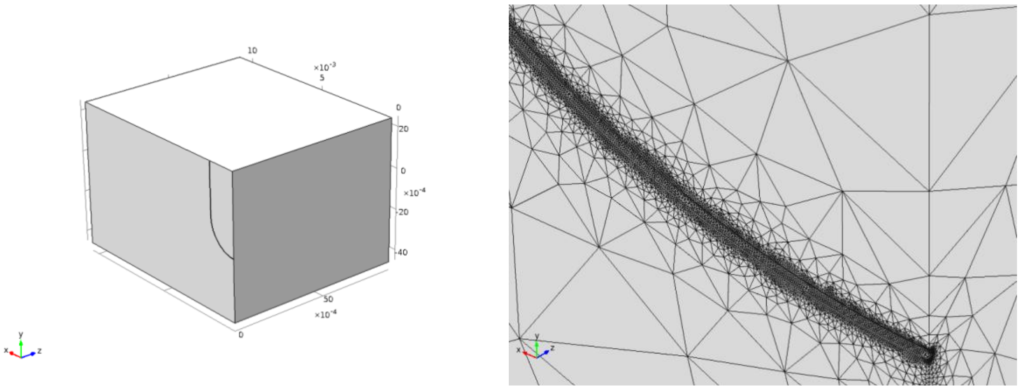

Figure 42. Domain for 3D simulations. Also a zoom in (right) on the refined mesh around the wire.

The lower boundary was set to ground to simulate the ground plane, and the wire boundaries were set to the applied potential. The two symmetry boundaries where set the zero charge/symmetry. The two outer boundaries were set to distributed capacitance with an equal relative permittivity to the material (ε_r = 2.3) in order to allow equipotential lines to be unperpendicular to these boundaries. The top boundary was also set to distributed capacitance, with the reference potential of 1 kV and a thickness of 2 cm. This boundary condition creates a background field around the sample which in reality is created by the high voltage terminal holding the sample in place. In order to properly distribute the mesh in the sample a scale of 0.03 was applied to the wire.

The result was a maximal nominal electric field of 14.382 kV/mm, located at the tip of the wire electrode. This value is slightly lower than the maximal field for a wire-plane geometry, which would be around 15.5 kV/mm. The reason for this is that some field lines now seek to connect the wire-electrode further away from the ground plane, lowering the maximal nominal electrical field in the sample. The resulting electric field is displayed below in figures 2 (left) and 3 as a surface plot and a streamline plot. The surface plot is displaying the nominal electric field magnitude at the surface seen in figure 2 (right). The same plane (xy-plane) is used for all surface plots in the simulation, as it provides the data points with the most interesting and interpretable results.

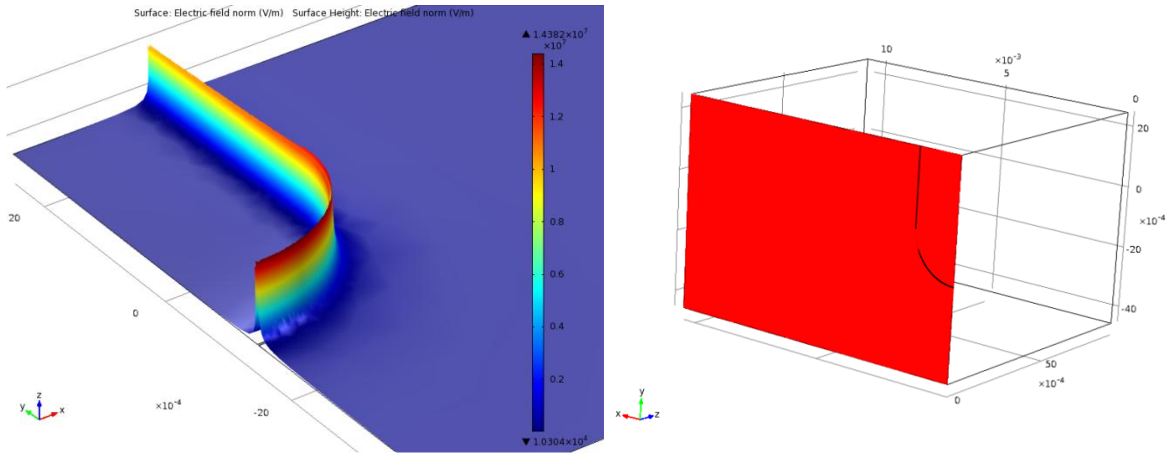

Figure 43. Field layout in the vicinity of the 20µm wire (left), and the cut plane for this data (right).

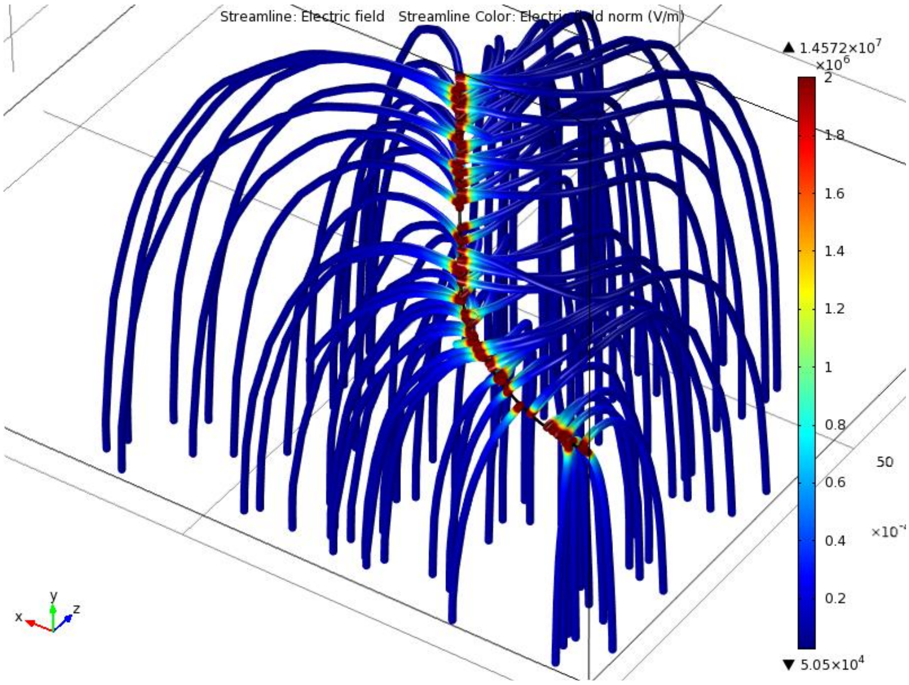

Figure 44. Electric field direction and magnitude (color) originating from the wire.

Next the field along the outer edge of the wire is calculated, and shown below in figure 4. Due to the inaccuracy of the mesh, the data has become distorted. However the actual distribution should look a lot like the fitted curve shown in the figure.

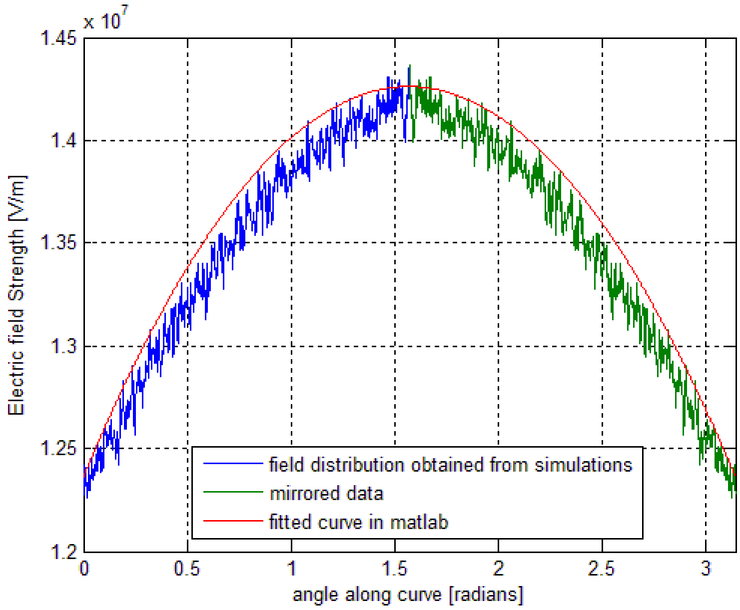

Figure 45. The maximal electric field distributed along the outer edge of the wire.

The fit performed in matlab resulted in the following equation, determining the angle scaling constant in mm^{-1} as a function of the angle θ.

$$K_\theta = -0.7693\theta^2 + 2.4167\theta + 12.3623$$

For:

$$0 \leq \theta \leq \pi \tag{1}$$

As said before, the highest nominal electric field was found to be 14.382 kV/mm in the test sample. Since the applied voltage is 1kV this would make a scaling constant of 14.382 mm^{-1} in the sample. This is a value similar to the obtained value by Huuva. However, the scaling constant is not 100% exact since this simulation does not account for unsymmetrical ground electrodes. Another factor could be eventual differences of relative permittivity of the samples and the transformer oil, creating surface charges on the boundary of the test sample.

2 Using a 10 micrometer wire instead

If a wire with a 10 micrometer diameter was used instead, a similar field distribution was found. The field was now somewhat higher and the high field was limited to the wire even more. A field strength of 24.99 kV/mm was found in the simulations.

3 The influence of kinks on the electric field

A common problem in the test method is the appearance of kinks on the metal wire (see also chapter 4.1.1.4). The kinks create local “hot spots” where the electric field strength is amplified. In order to further investigate the amplification of the field at the kinked locations, a 3D simulation was made on a typical kink located at the edge of the transition between the straight and curved part of the wire, with the result shown below in figure 5. A local amplification is found at the top of the kink, but also two minor amplification points are found at the stretched area where the wire is bended outwards.

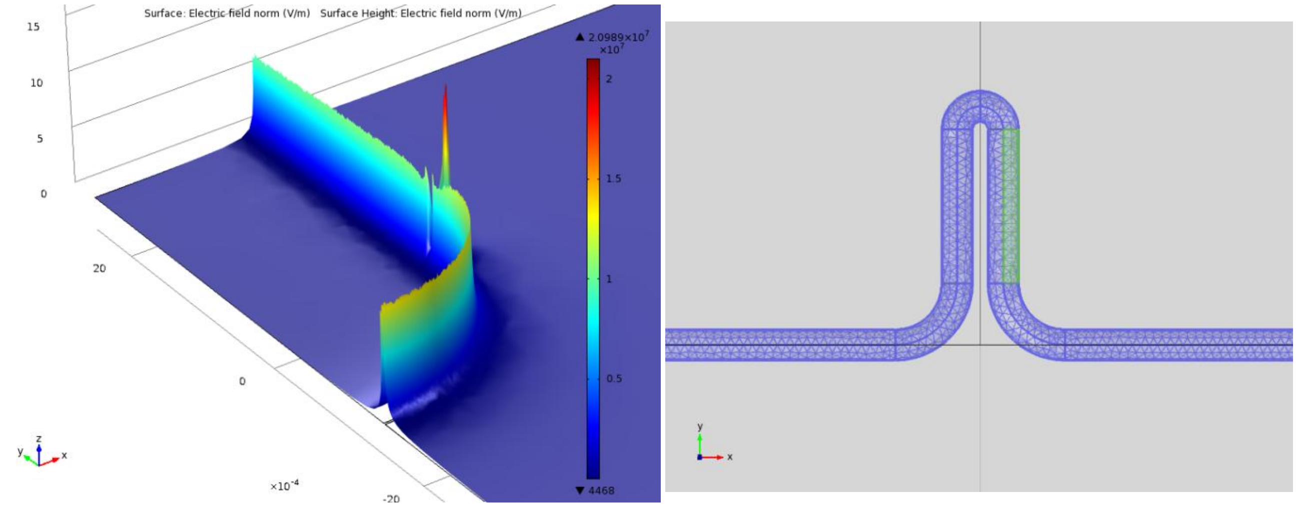

Figure 46. Visual layout of a typical kink(length = 100 µm, radius =15µm).

In the simulations, the length of the kink (the marked area in figure 5) is varied, as well as the major radius of the upper halve-toroid. The results are shown below in table 1, where the change in the maximal nominal electric field is shown. Also the increase of the field in % compared to the reference of 12.362 kV/mm (original field at the kinks location derived with equation 1) is displayed.

Table 9. Maximal nominal field strength for different kink dimensions.

Variation of the kink length (radius = 15µm)			Variation of the kink upper toroid diameter (length = 100 µm)		
Length [µm]	E_max [kV/mm]	Increase [%]	Radius [µm]	E_max [kV/mm]	Increase [%]
20	19.347	56.5	13	21.357	72.8
60	20.346	64.6	**15**	**20.989**	**69.8**
100	**20.989**	**69.8**	20	19.906	61.0
140	21.422	73.3	30	17.980	45.4
200	22.378	81.0	40	17.088	38.2

From these simulations it can be concluded that the kinks longer than 100 µm and with small radiuses lower than 15µm contribute with the biggest field amplification of over 70 %. Next the influence of a kink at the top of the wire electrode is investigated.

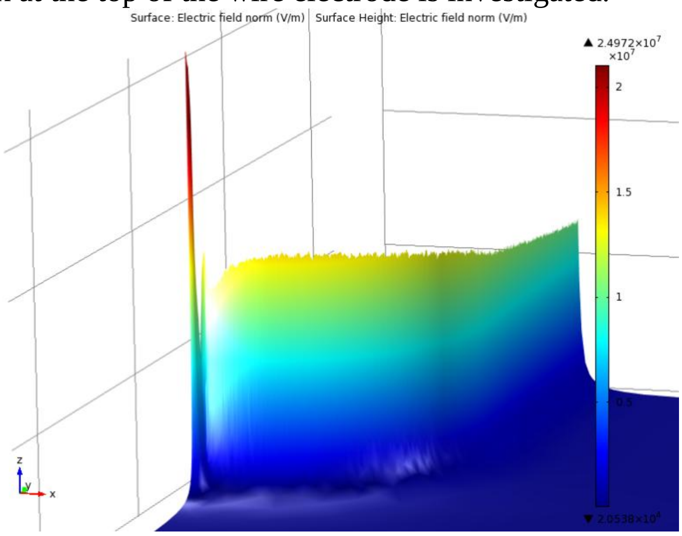

Figure 47. Visual layout of a typical kink at the top of the wire (length = 100 µm, radius = 15 µm).

Here the fields are compared to the reference field 14.382 kV/mm in order to obtain the % of field enhancement

Table 10. Data for variation of kink dimensions for a kink at the top of the wire

Variation of the kink length (radius = 15μm)			Variation of the kink upper toroid diameter (length = 100 μm)		
Length [μm]	E_max [kV/mm]	Increase [%]	Radius [μm]	E_max [kV/mm]	Increase [%]
20	22.958	59.6	13	25.775	79.2
60	24.027	67.1	**15**	**24.972**	**73.6**
100	**24.972**	**73.6**	20	23.686	64.7
140	25.709	78.8	30	21.595	50.2
200	26.753	86.0	40	20.370	41.6

The kink at the tip contributed to a bigger field amplification compared with the kink on the side. The variable variation displayed in the tables show the same trends for the kink at the tip and the kink at the side. The difference in the field amplification was found to differ only a couple of percents between the tip and side kinks. The values from the tables were plotted as a surface plot in matlab, and an approximate fit to the surface was made. The fit is shown in the equation below.

$$f_{kink} = f(l,r) = \begin{Bmatrix} (0.0014 * l + {}^{4}/_{r} - 0.006 * r + 1.4) \\ 1\ (if\ no\ kink) \end{Bmatrix} \quad (2)$$

The kink function with its respective field amplification values is shown below in figure 7 as a surface plot. As stated before, the most severe kinks are found to be the longest kinks with the sharpest tips, since they contribute with the biggest amplification of the field.

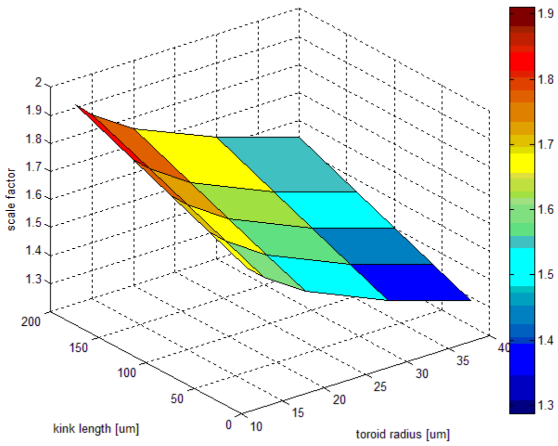

Figure 48. Surface plot of the kink factor depending on the kink's length and sharpness

Also it was investigated if a kink will affect the electric field in the rest of the sample. For this, again the field along the outer edge of the sample was studied. The result is shown below in figure 8. The angle along the curve corresponds to the different positions along the curved part of the wire. It can be seen that the field in the rest of the sample is relatively unaffected by a kink. In the figure the field decreases drastically at the location of the kink. The reason for this is that the plotted data is only for the area approaching the kink. In the vicinity of a kink, the electric field is reduced.

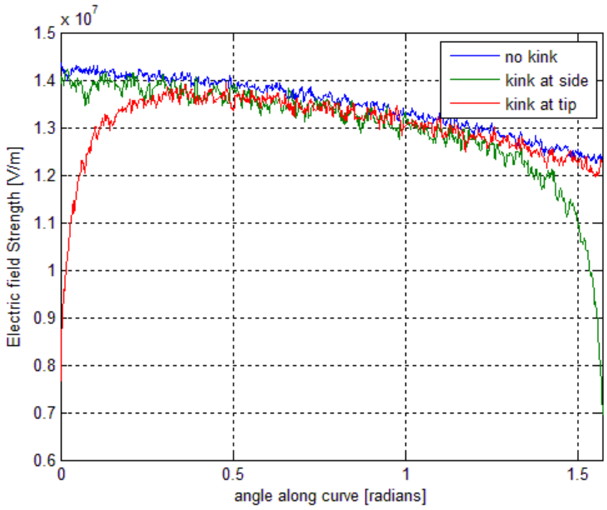

Figure 49. Electric field strength along the outer edge of the wire

4 The influence of inexact geometry dimensions

In order to investigate the influence of inaccurate ground-electrode distances in the samples, this distance was varied from 1 to 6 mm. Normally ground-electrode distances of below 2 mm are not used for the samples. This is to avoid electrical breakdown in the test samples. However the distance sometimes exceeded 5-6 mm, due to the wires floating towards the high voltage electrode during the joining process (see chapter 3.1). The result from the simulation is shown below in figure 9.

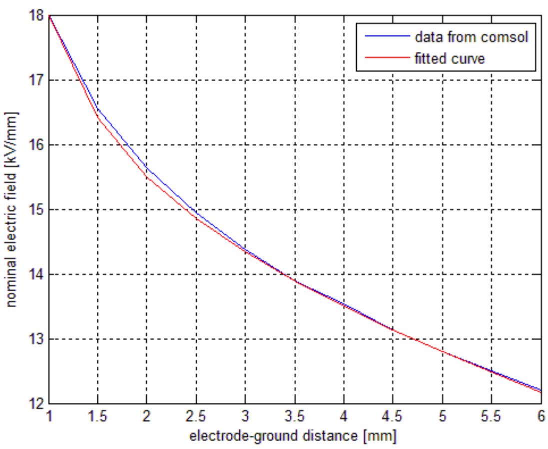

Figure 50.Variation of the distance between the ground plane and the wire electrode.

As seen in figure 9, only small changes in the maximum nominal electrical field are obtained. For an increase in distance of 1mm the field is reduced around 10 %. This is due to that the wire diameter is mostly controlling the magnitude of the field. From the figure the distance scaling factor K_d is determined as shown below in formula 3.

$$K_d = (14.5 + {}^{4}/_{d} - 0.5 * d)/14.382 \tag{3}$$

Different inexact geometry dimensions do not affect the field strength as much as the electrode to ground distance, since the sample is immersed in transformer oil during the electrical testing. The transformer oil has similar relative permittivity as that of XLPE in the sample.

5 The influence of small particles

For investigating the effect of inserted particles and their influence on the electric field, a series of simulations is performed including a small domain with different permittivity or conductivity in the vicinity of the wire. In all simulations the particles are exactly on the xy-plane, in order to detect the maximal influence when using the same cut plane as used for previous surface plots. The geometry used is the same as in part 1 of this appendix, besides the insertion of this small domain.

5.1 AC simulations

As a slight permittivity change might be present in the contaminants, the influence on the electric field is investigated. The selected COMSOL physics used for these simulations is once again electrostatics, simulating the laplacian field. The influence of a particle with a different permittivity is seen in figure 10.

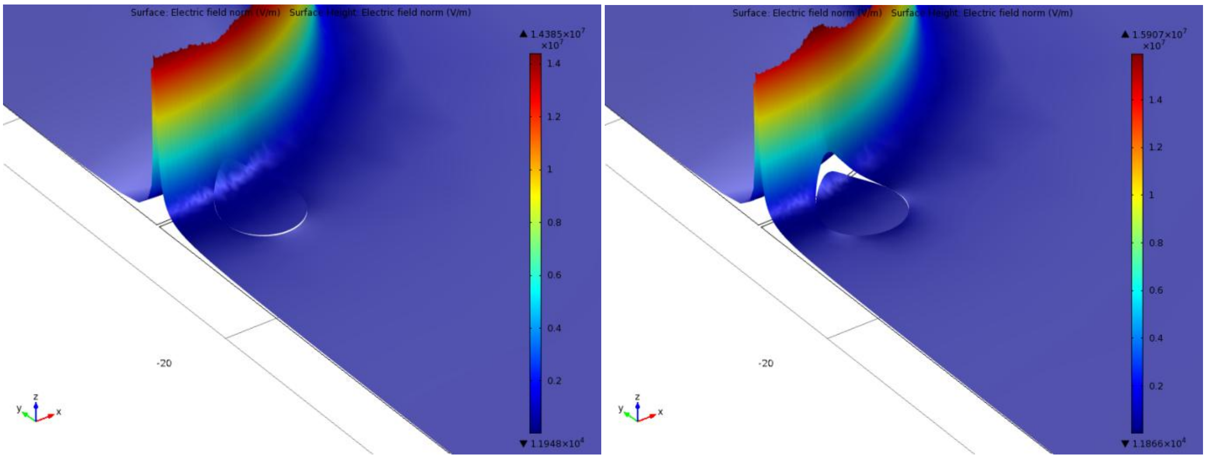

Figure 51. Insertion of a spherical domain with a diameter of 0.4 mm near the wire. The relative permittivity of this domain is set to 1.6 (left) and 4 (right), in comparison with 2.3 for the rest of the XLPE

From the simulations it can be concluded that an inserted particle with different permittivity as the rest of the material has a slight ability to increase or reduce the electric field at some locations. Although it should be mentioned that a relative permittivity of 4 for an organic contaminant is rare, normally it is lower.

5.2 DC simulations

As organic contaminants are known to have increased conductivity, their impact on the DC electric field is to be investigated. For simulation of this field, the COMSOL physics were changed to the electric current model. The conductivity used for the material and for the contaminant was obtained from the conductivity measurements (chapter 4.1.2.2). Using the electric current model, the background field from the electrode could no longer be included in the calculations, as the distributed capacitance boundary condition doesn’t exist. This resulted in a somewhat higher field along the wire. Also the electric field is more uniformly distributed along the wire. The maximal nominal electric field was found to be 15.6 kV/mm when 1 kV was applied to the wire. Again it is important to mention that no space charge is included in these simulations, which in reality has the ability to reduce the electric field. The results from these simulations are summarized in table 3.

Table 11. Electric field results for the simulations, using the electric current model with insertion of different contaminants.

<table>
<tr>
<td>a)
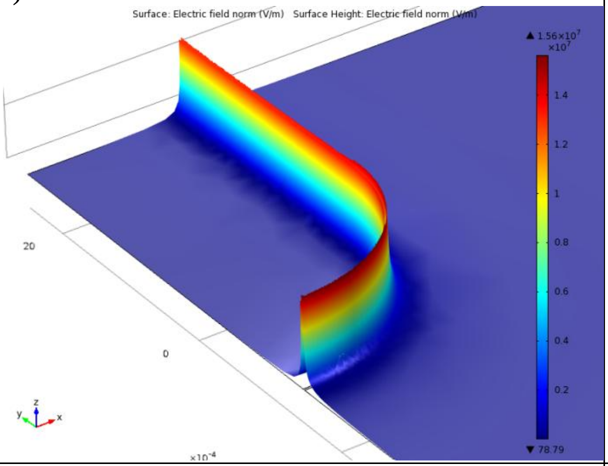
</td>
<td>b)
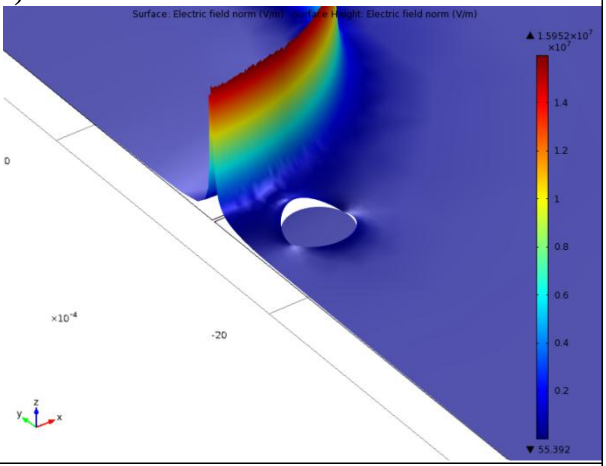
</td>
</tr>
<tr>
<td>c)
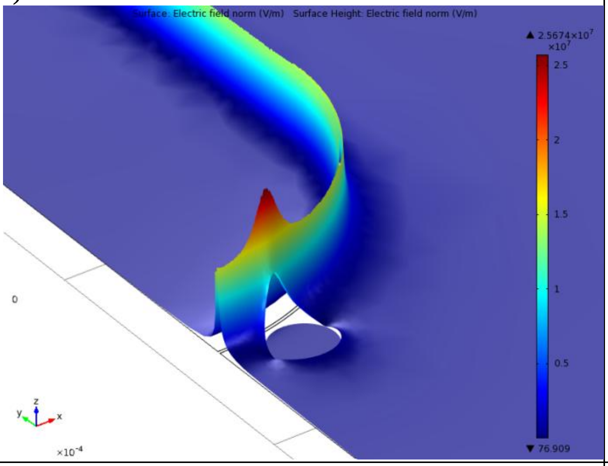
</td>
<td>d)
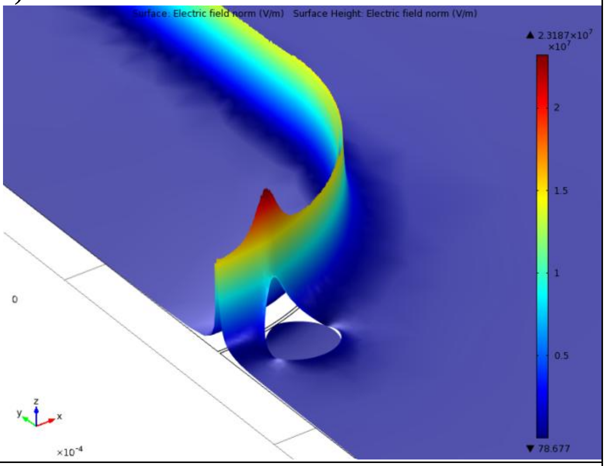
</td>
</tr>
<tr>
<td>e)
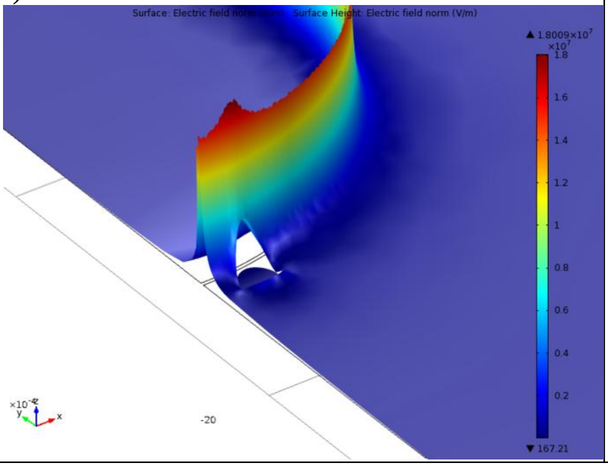
</td>
<td>a) Without contaminant
b) Contaminant further away from the wire, diameter 0.4 mm 10 times increased conductivity.
c) Contaminant close to the wire, diameter 0.4 mm 100 times increased conductivity.
d) Contaminant close to the wire, diameter 0.4 mm 10 times increased conductivity.
e) Contaminant close to the wire, diameter 0.2 mm 10 times increased conductivity.
f) Square like contaminant close to the wire, 10 times increased conductivity.
g) Square like contaminant close to the wire, 100 times increased conductivity.</td>
</tr>
</table>

f)

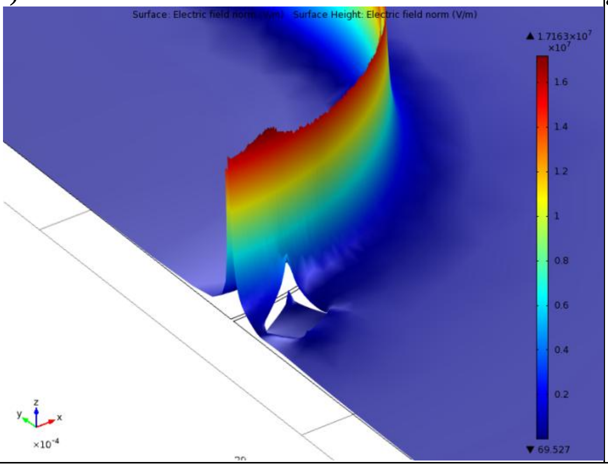

g)

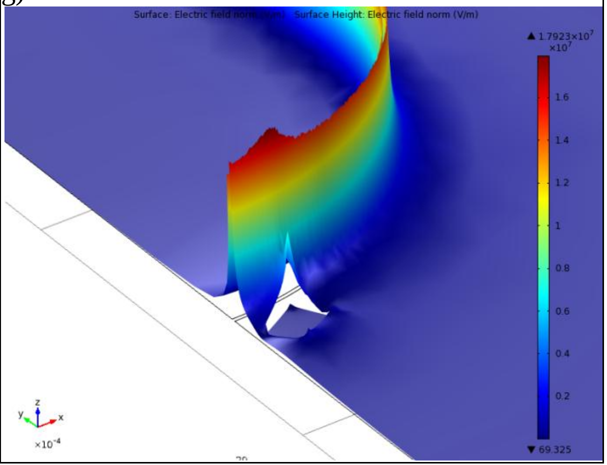

From (b) it can be concluded that in order to achieve an increase of the electric field, the contaminant needs to be located close to the wire. From (c) and (d) the result is shown when the conductivity of the particle is ten and a hundred times higher than the reference XLPE. It can be concluded that the field amplification is quite similar for these 2 cases when big, round particles are used. In (e) the diameter is halved, resulting in I similar field amplification at the wire. The electric field along the contaminant is however increased. For (f) and (g) a particle with sharp edges is inserted. The result in (g) shows that when sharp particles with a high conductivity increase are inserted, a field magnitude comparable to the magnitude at the wire is present. The increased conductivity simply allows the equipotential lines to be more spread out within the contaminant due to the increased current flow.

Appendix II - Additional Pictures of kink appearance during the degassing process

Table 12. Kinks created or severed during the degassing process. The pictures are a selected series showing some typical changes. A total of around 100 samples were investigated.

Sample	Before degassing	After degassing
D13		
E13	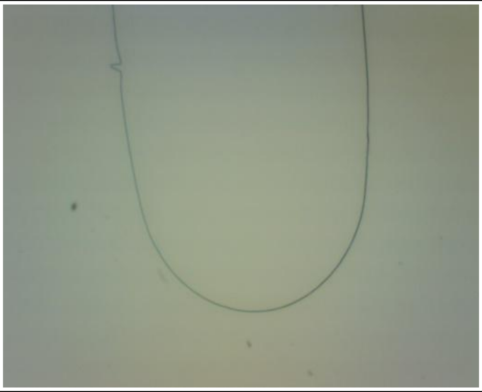	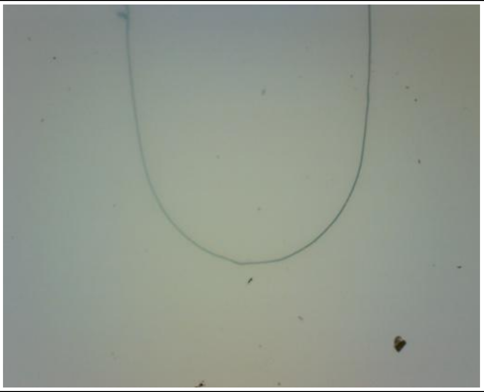
F13		
G13		

Appendix III: Additional pictures of electrical trees created in the thesis

Table 13. Selection of typical electric trees and water trees observed in the thesis work. The description is found at the end of the table. Around 4 pictures are selected from each test series.

1) 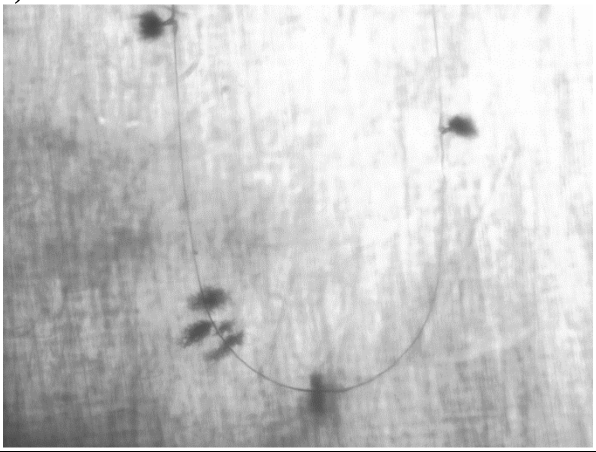	2) 
3) 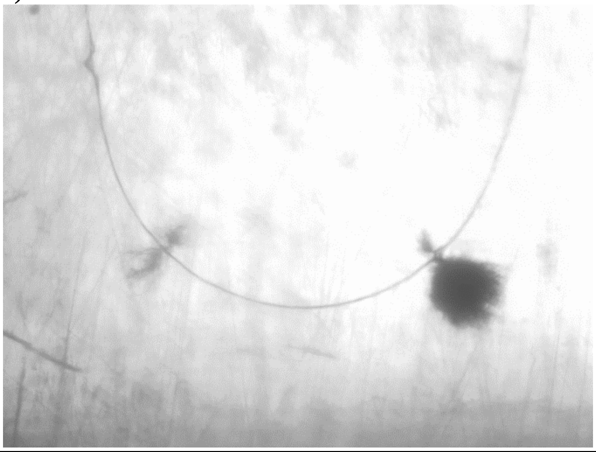	4) 
5) 	6) 

7)


8)


9)
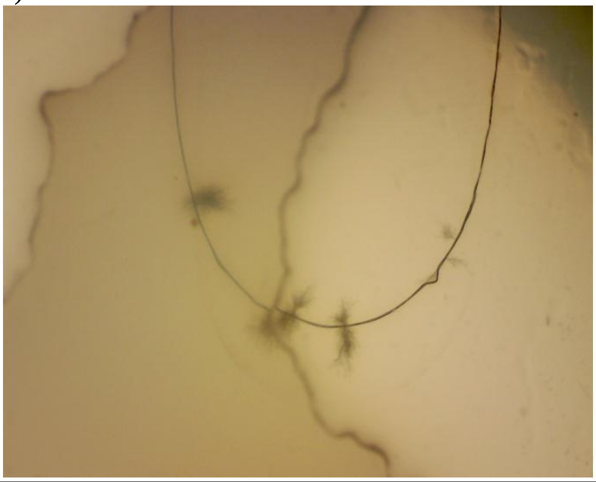

10)
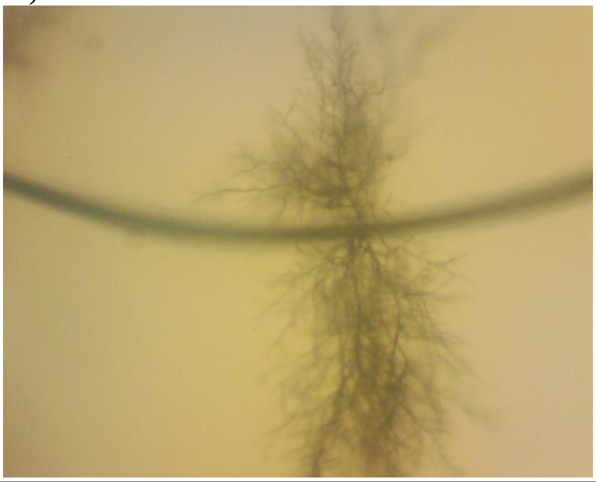

11)


12)


13)

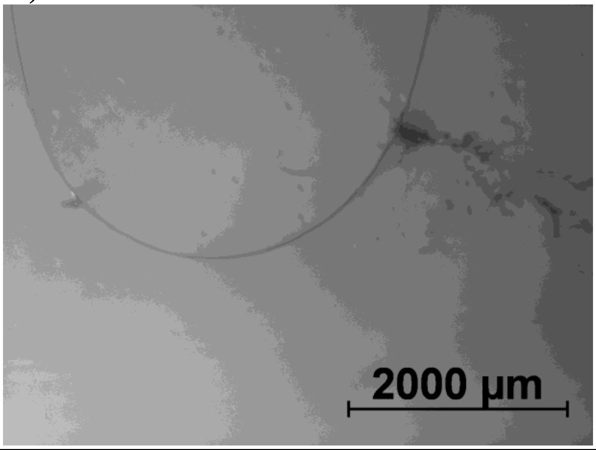

14)

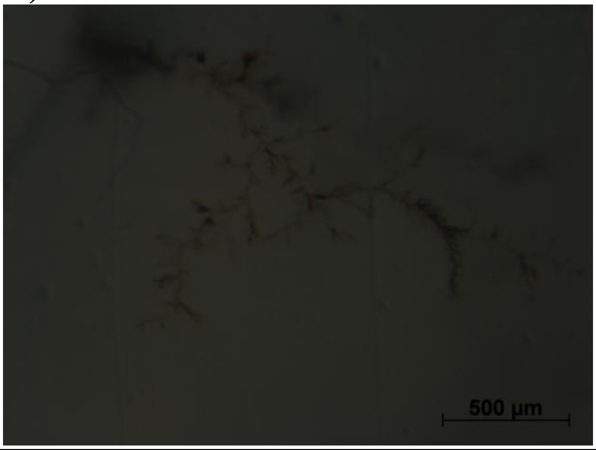

15)

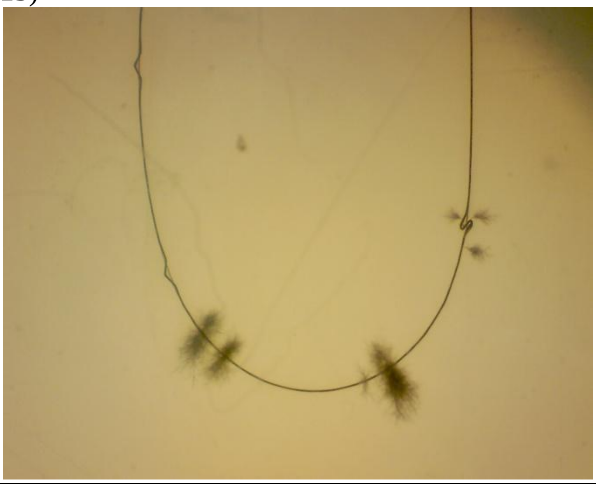

16)

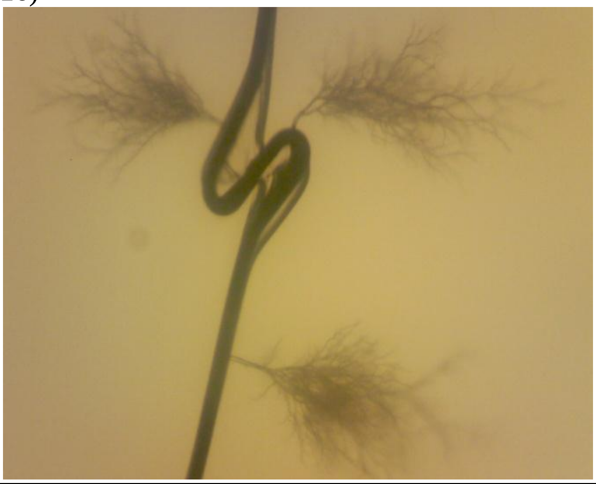

17)

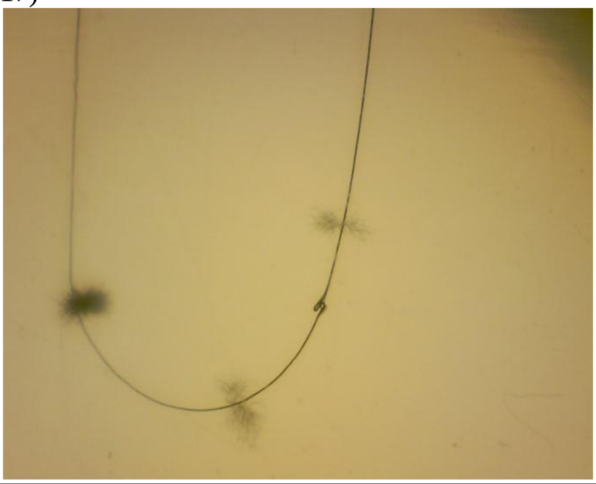

18)

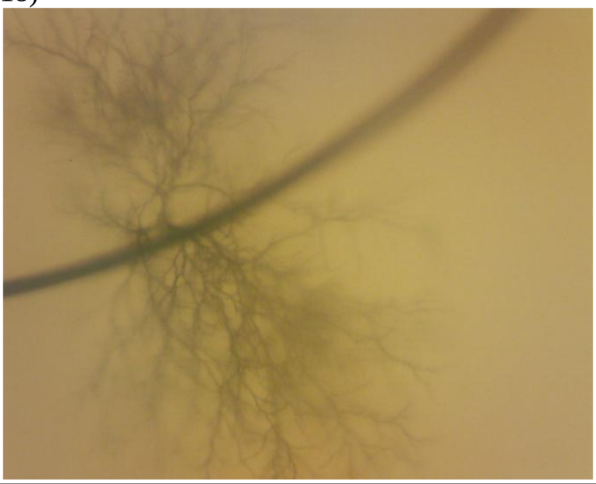

19) 	20) 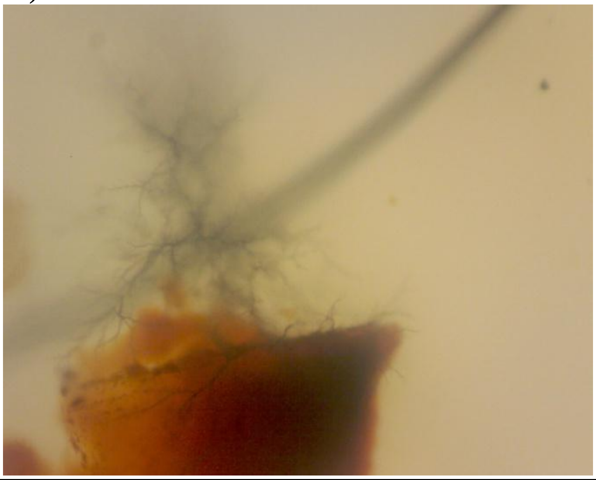
21) 	22) 
23) 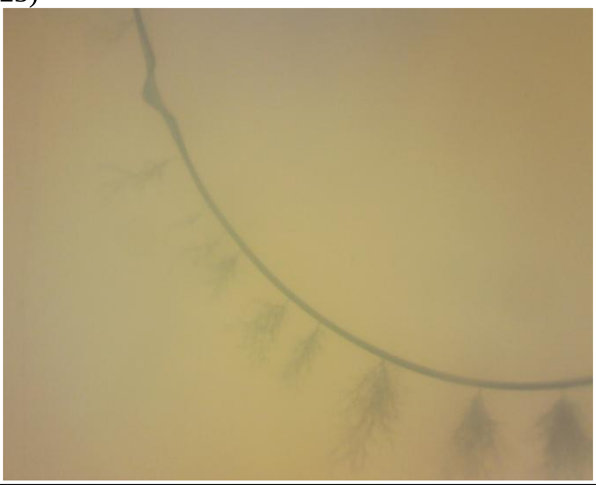	24) 

25) 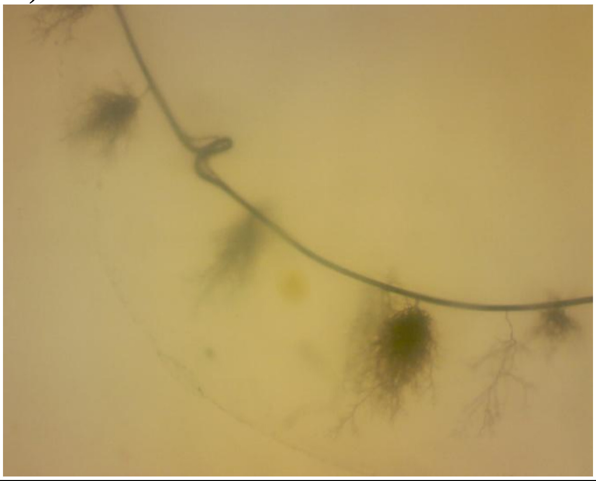	26) 
27) 	28) 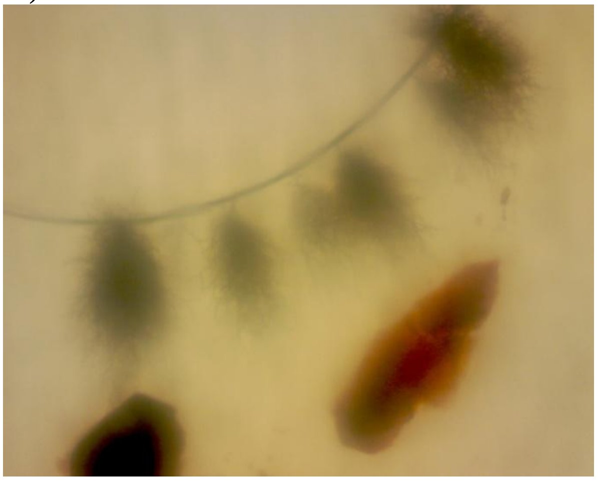
29) 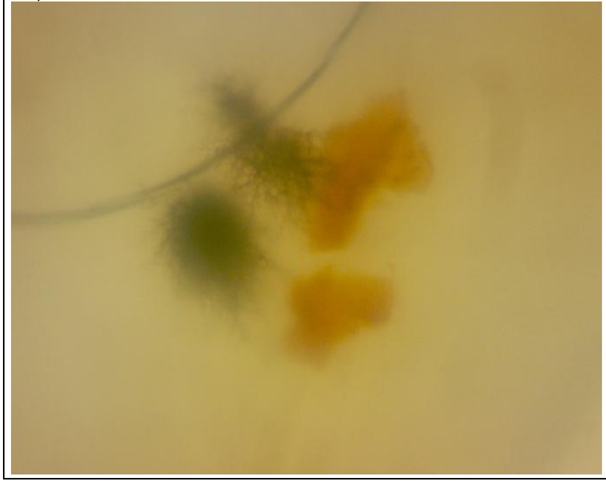	30) 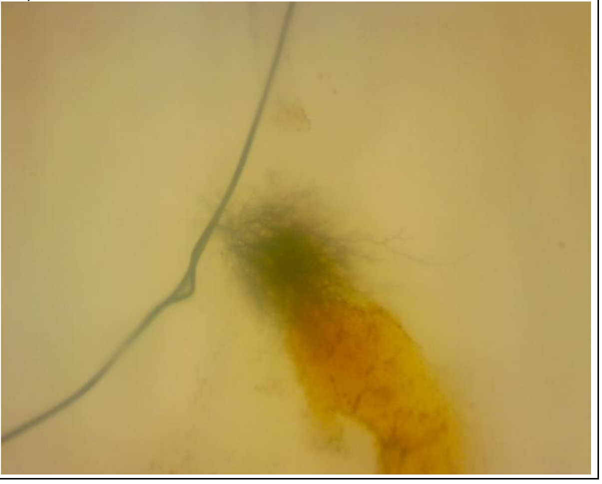

31)

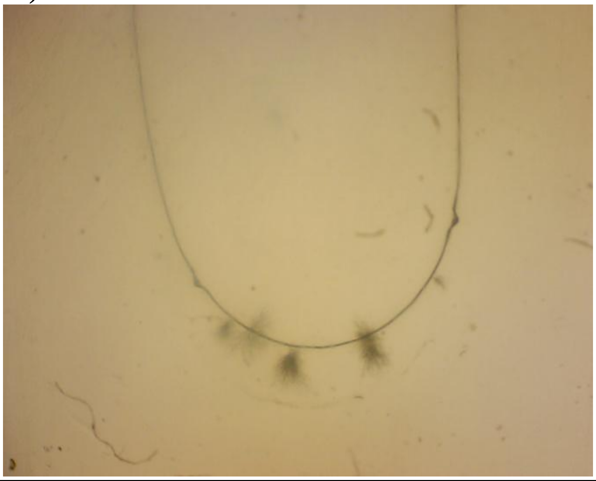

32)

33)

34)

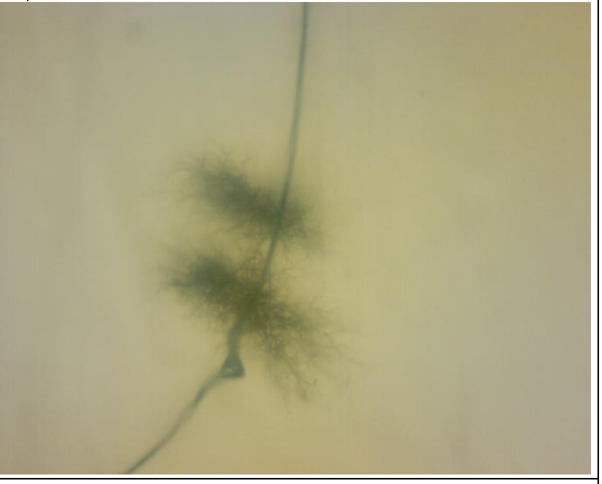

35)

36)

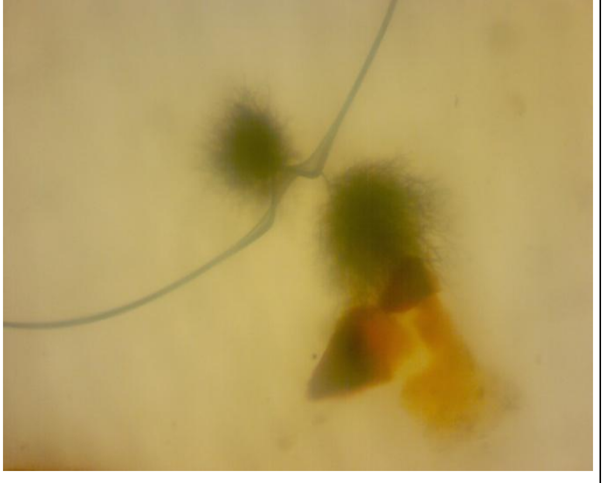

37)

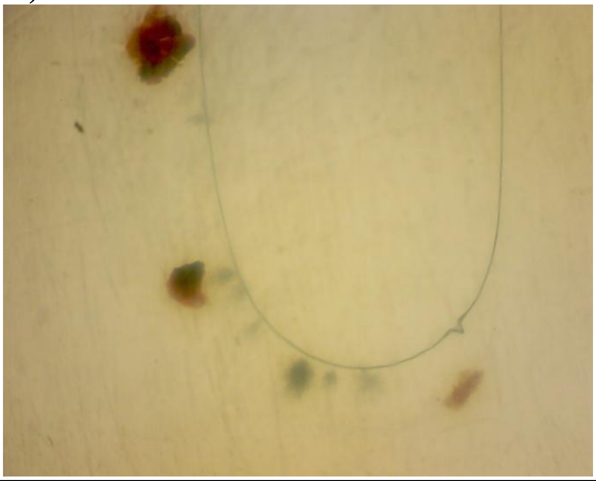

38)

39)

40)

41)

42)

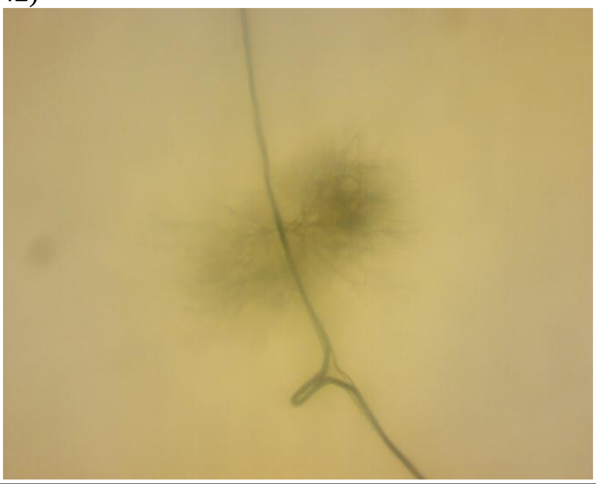

43)

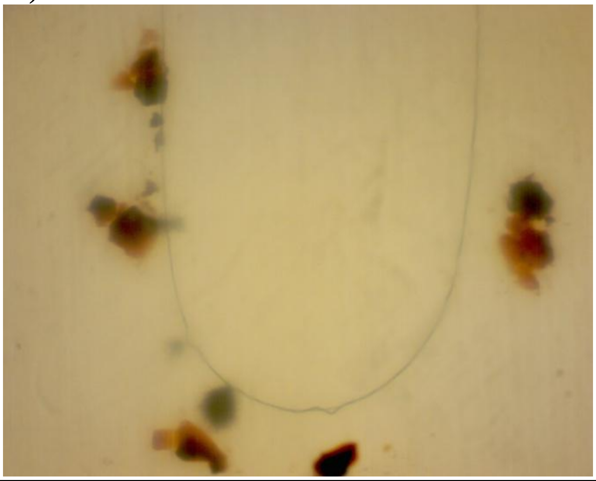

44)

45)

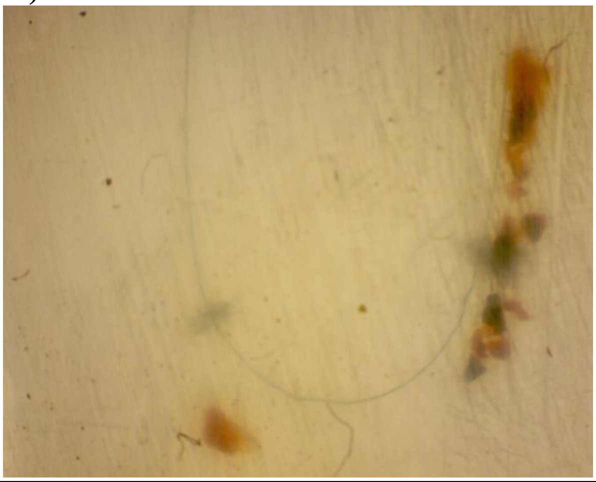

46)

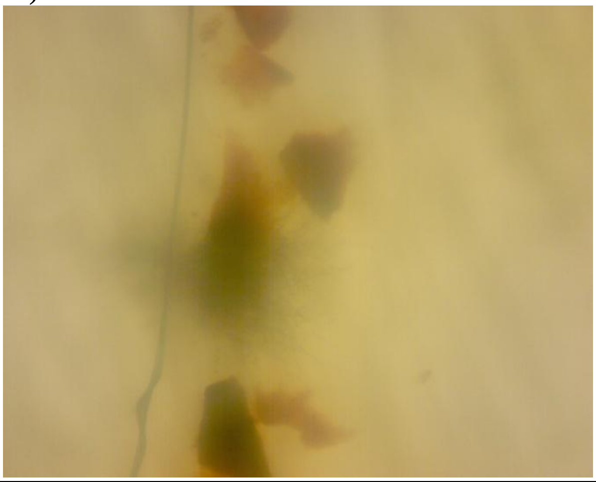

47)

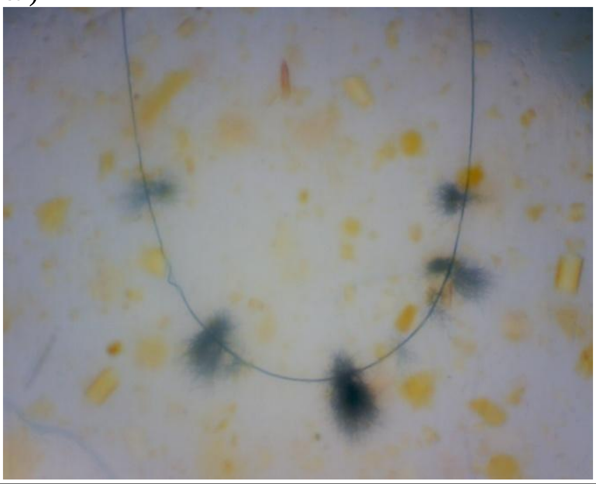

48)

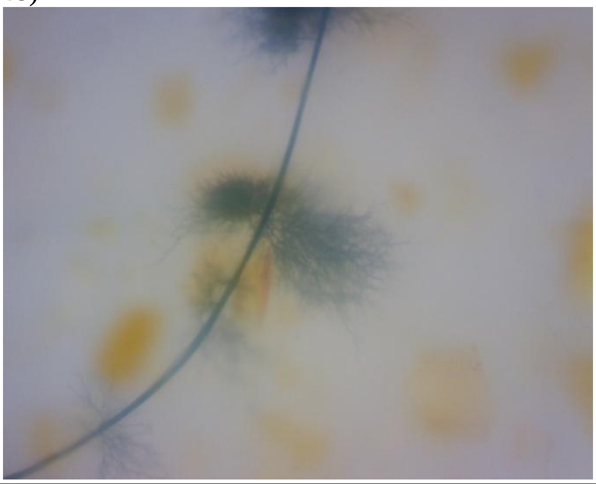

49) 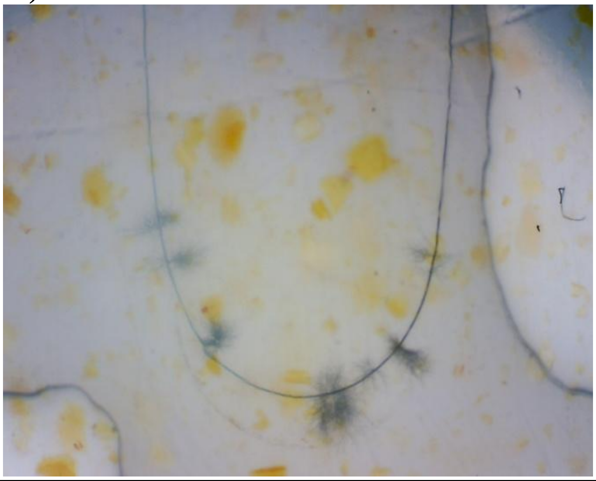	50) 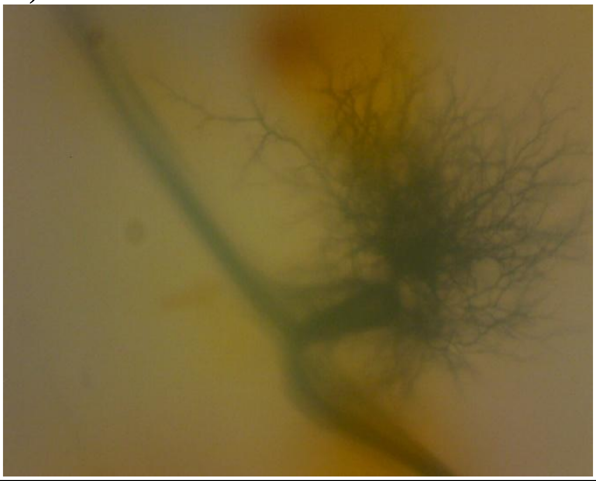
51) 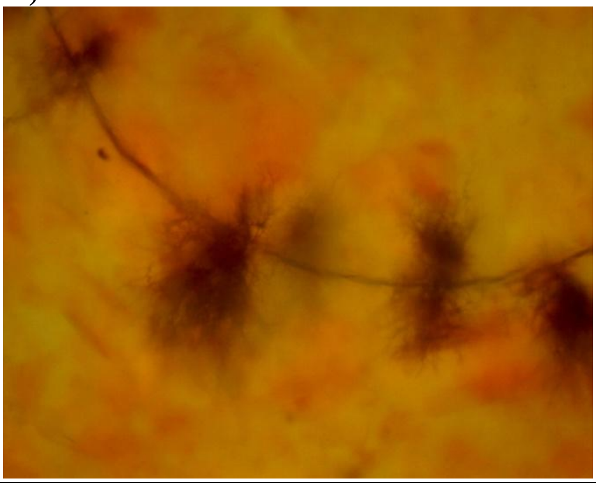	52) 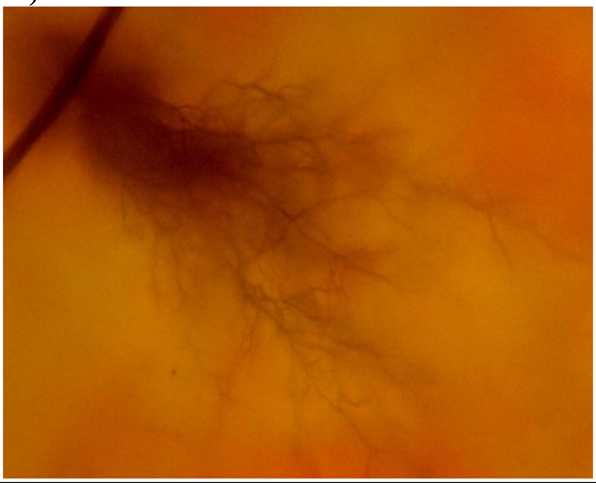
53) 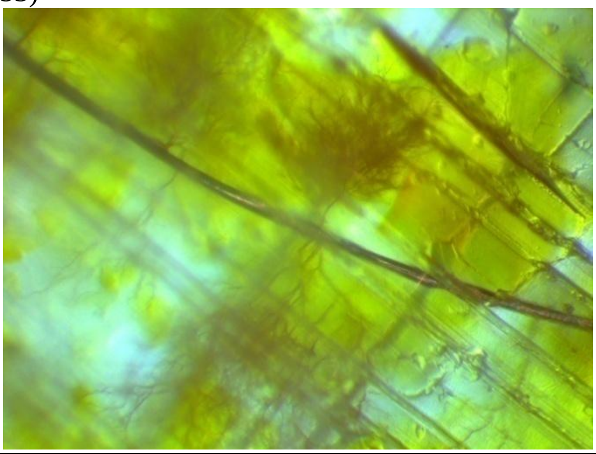	54) 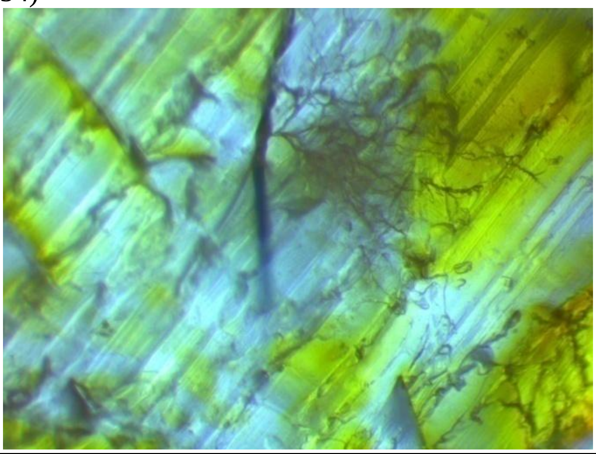

55)
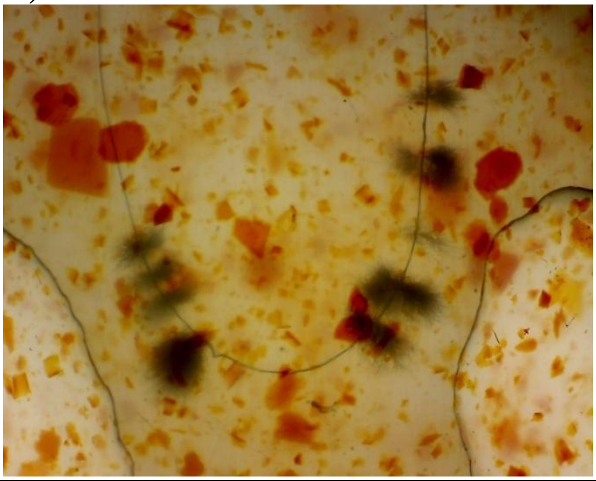

56)
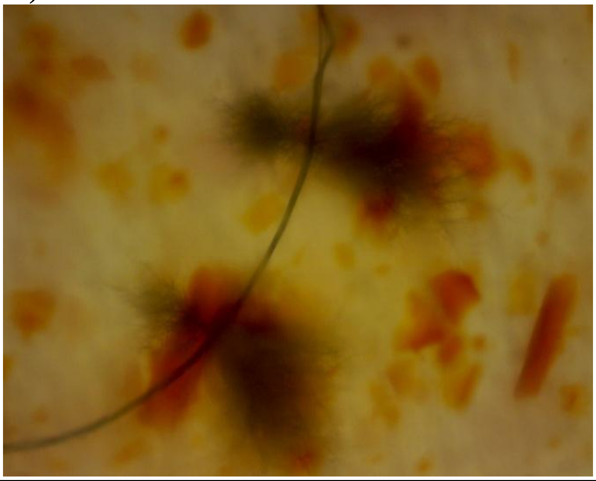

57)
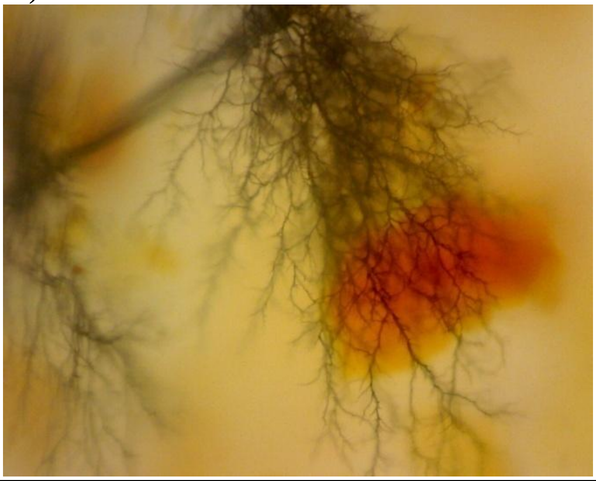

58)
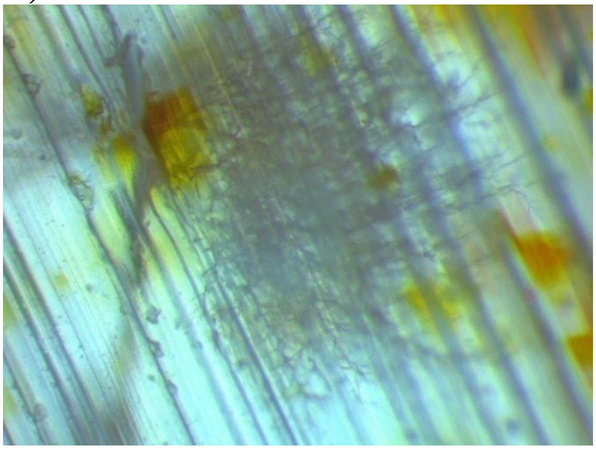

59)


60)


61)

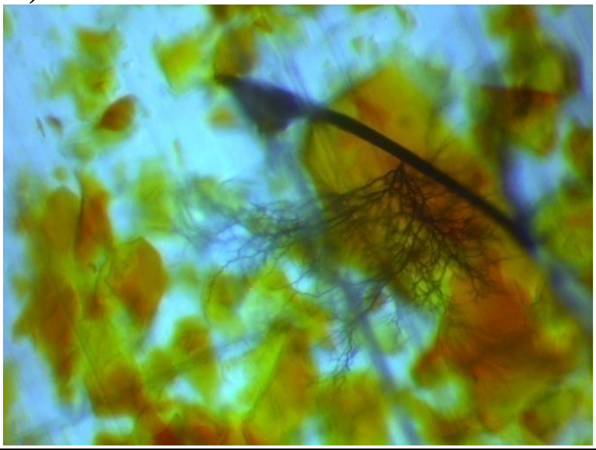

62)

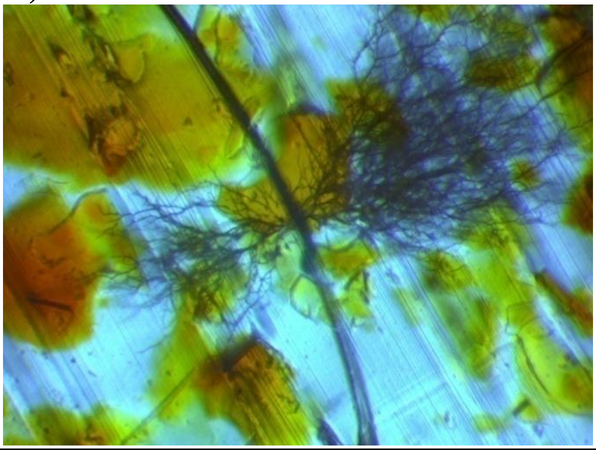

63)

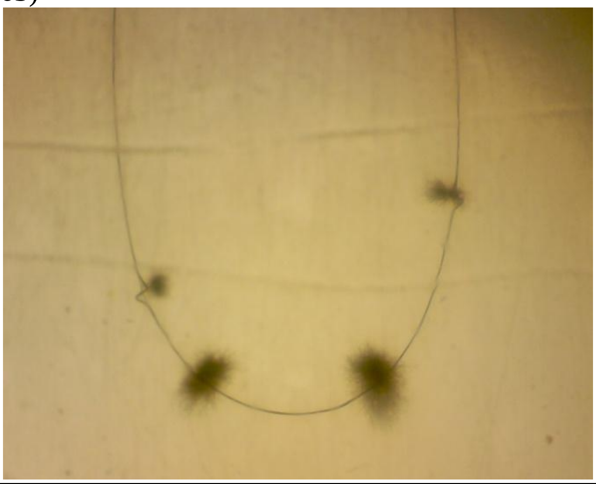

64)

65)

66)

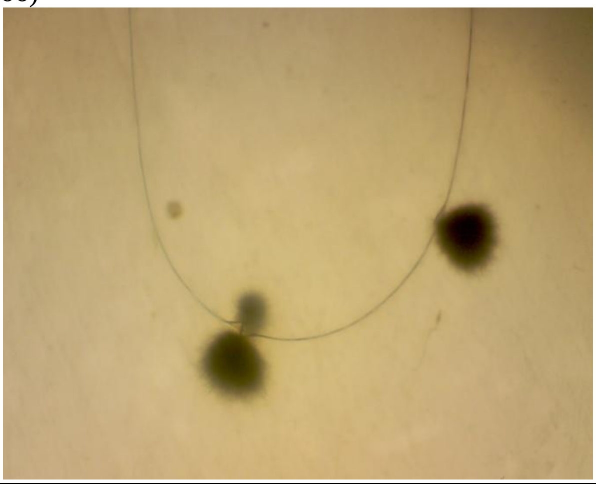

67)

68)

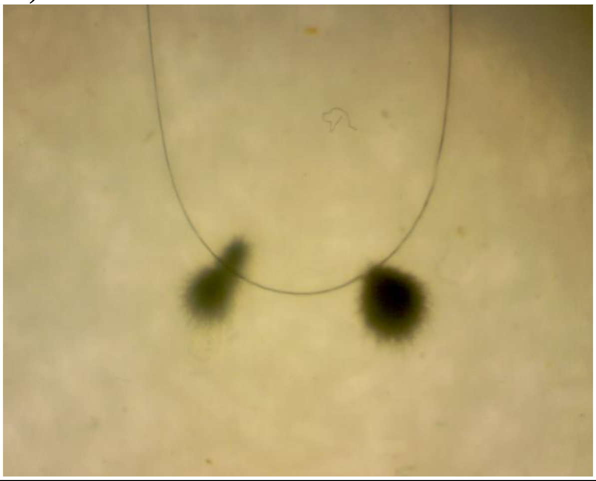

69)

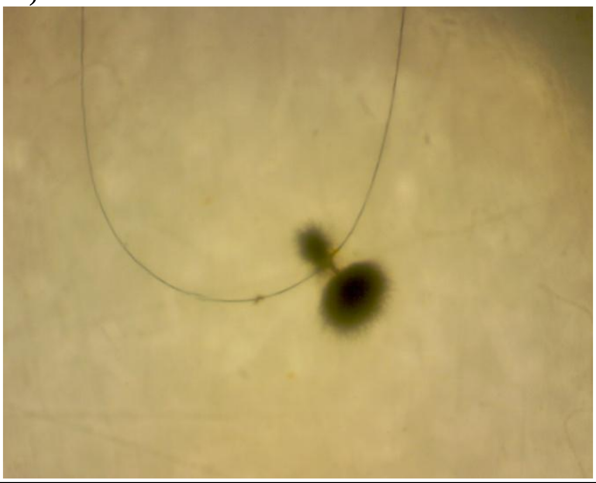

70)

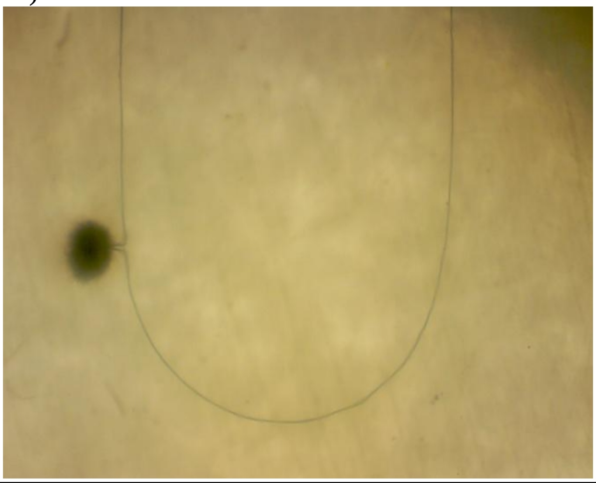

71)

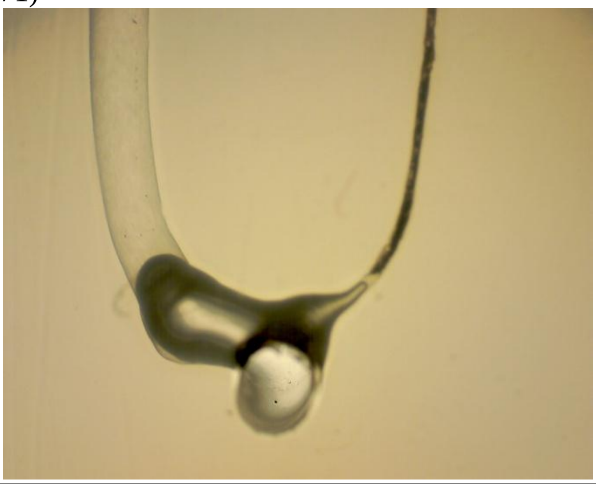

72)

73)

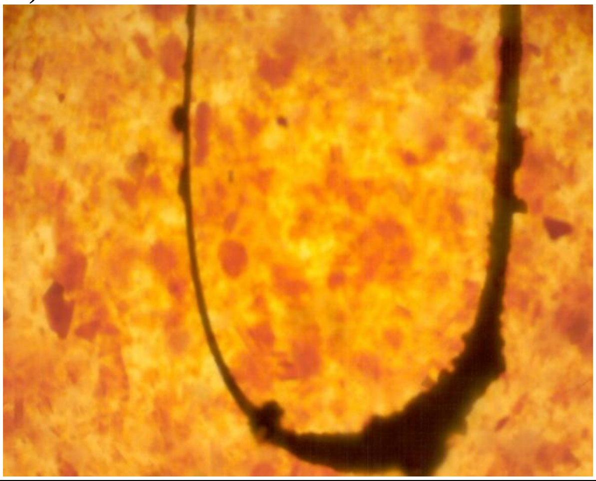

74)

75)

76)

77)

78)

79) 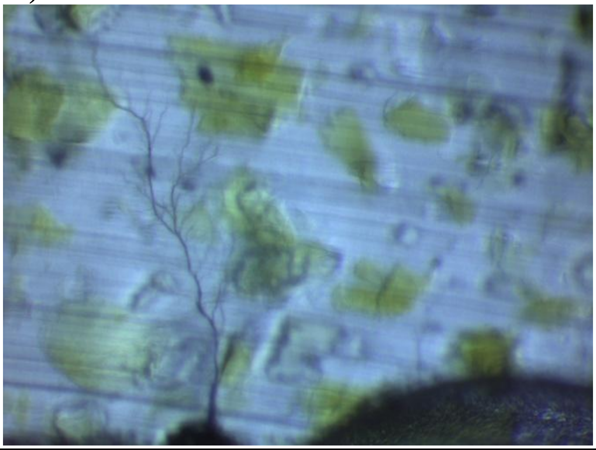	80) 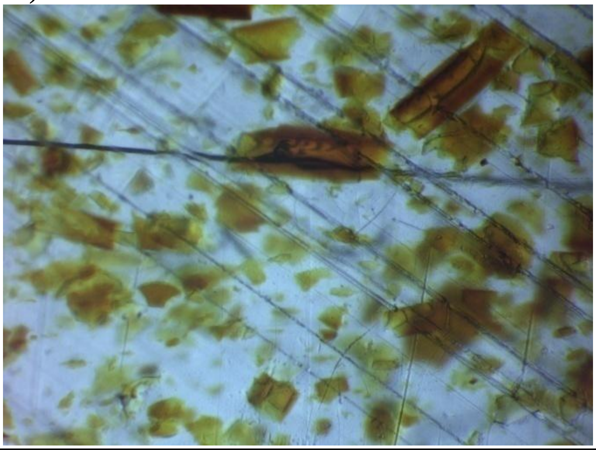
81) 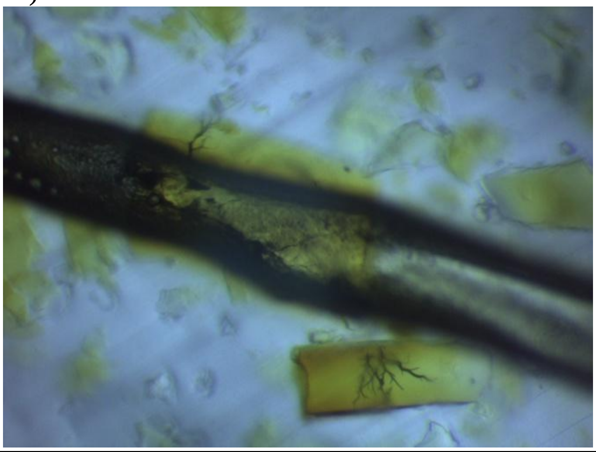	82) 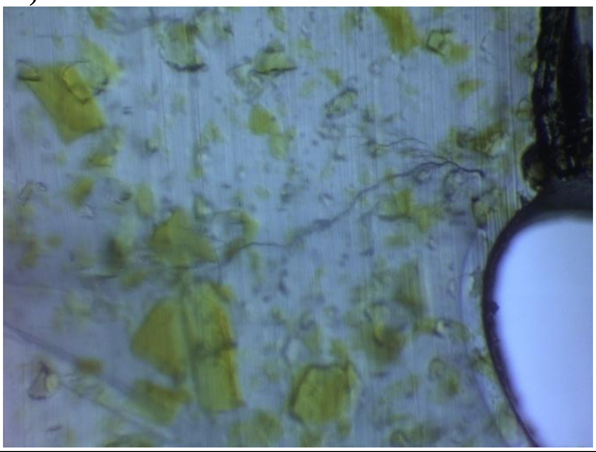

Picture descriptions:

1) Reference sample, Ramped AC 250 V/s, 7 trees initiated, 2 at kinks and 5 at the wire.
2) Reference sample, Ramped AC 250 V/s, closeup of (1).
3) Reference sample, Ramped AC 250 V/s, 2 trees initiated, 1 at a kink and 1 at the wire.
4) Reference sample, Ramped AC 250 V/s, closeup of (3).
5) Reference sample, Constant AC 22.5 kV rms, 5 trees initiated, 1 at kink and 4 at the wire.
6) Reference sample, Constant AC 22.5 kV rms, closeup of (5).
7) Reference sample, Constant AC 22.5 kV rms, 5 trees initiated, 5 at the wire.
8) Reference sample, Constant AC 22.5 kV rms, closeup of (7).
9) Reference sample Constant AC 20 kV rms, 5 trees initiated, 5 at the wire.
10) Reference sample Constant AC 20 kV rms, closeup of (9).
11) Reference sample Constant AC 20 kV rms, 3 trees initiated, 2 at kink and 1 at the wire.
12) Reference sample Constant AC 20 kV rms, closeup of (11).
13) Reference sample, constant AC 10kV rms, 18 hours of aging, 1 long branch tree initiated at kink
14) Reference sample, constant AC 10kV rms, 18 hours of aging, closeup of (13).
15) Dry aged sample (1 week 6 kV rms AC), 20 kV rms tested, without contaminants, 7 trees initiated, 2 at kink and 5 at the wire.
16) Dry aged sample (1 week 6 kV rms AC), 20 kV rms tested, without contaminants, closeup of (15).
17) Dry aged sample (1 week 6 kV rms AC), 20 kV rms tested, without contaminants, 3 trees initiated, 1 at kink and 2 at the wire.
18) Dry aged sample (1 week 6 kV rms AC), 20 kV rms tested, without contaminants, closeup of (17).

19) Dry aged sample (1 week 6 kV rms AC), 20 kV rms tested, with contaminants, 6 trees initiated, 3 at kinks and 3 at wire.
20) Dry aged sample (1 week 6 kV rms AC), 20 kV rms tested, with contaminants, closeup of (19), tree propagated into contaminant.
21) Dry aged sample (1 week 6 kV rms AC), 20 kV rms tested, with contaminants, 10 trees initiated, 1 at kink and 9 at the wire.
22) Dry aged sample (1 week 6 kV rms AC), 20 kV rms tested, with contaminants, closeup of (22).
23) Wet aged sample (1 week 6 kV rms AC), rewetted and 20 kV rms tested, without contaminants,10 trees initiated from the wire.
24) Wet aged sample (1 week 6 kV rms AC), rewetted and 20 kV rms tested, without contaminants, 9 trees initiated from the wire.
25) Wet aged sample (1 week 6 kV rms AC), rewetted and 20 kV rms tested, without contaminants,7 trees initiated from the wire.
26) Wet aged sample (1 week 6 kV rms AC), rewetted and 20 kV rms tested, without contaminants,5 trees initiated from the wire.
27) Wet aged sample (1 week 6 kV rms AC), rewetted and 20 kV rms tested, with contaminants, 3 trees initiated from the wire, contaminants further away from wire.
28) Wet aged sample (1 week 6 kV rms AC), rewetted and 20 kV rms tested, with contaminants,6 trees initiated from the wire, contaminants further away from wire.
29) Wet aged sample (1 week 6 kV rms AC), rewetted and 20 kV rms tested, with contaminants,2 trees initiated from the wire, contaminants closer to wire.
30) Wet aged sample (1 week 6 kV rms AC), rewetted and 20 kV rms tested, with contaminants,1 trees initiated from the wire, possibly affected by contaminant.
31) Wet aged sample (1 week 6 kV rms AC), dried and 20 kV rms tested, without contaminants, 5 trees initiated from the wire.
32) Wet aged sample (1 week 6 kV rms AC), dried and 20 kV rms tested, without contaminants, closeup of (31).
33) Wet aged sample (1 week 6 kV rms AC), dried and 20 kV rms tested, without contaminants, 2 trees initiated at the wire and 1 at kink.
34) Wet aged sample (1 week 6 kV rms AC), dried and 20 kV rms tested, without contaminants, closeup of the two wire trees from (33).
35) Wet aged sample (1 week 6 kV rms AC), dried and 20 kV rms tested, with contaminants, 2 trees initiated at kink and 1 at the wire.
36) Wet aged sample (1 week 6 kV rms AC), dried and 20 kV rms tested, with contaminants, closeup of (35).
37) Wet aged sample (1 week 6 kV rms AC), dried and 20 kV rms tested, with contaminants, 7 trees initiated from the wire.
38) Wet aged sample (1 week 6 kV rms AC), dried and 20 kV rms tested, with contaminants, closeup of (37).
39) Dry aged sample (1 week 6 kV rms AC), 20 kV rms tested, without contaminants, 3 trees initiated from the wire.
40) Dry aged sample (1 week 6 kV rms AC), 20 kV rms tested, without contaminants, closeup of (39), 2 branch trees.
41) Dry aged sample (1 week 6 kV rms AC), 20 kV rms tested, without contaminants, 1 tree initiated at the wire next to a kink.
42) Dry aged sample (1 week 6 kV rms AC), 20 kV rms tested, without contaminants, closeup of (41).
43) Dry aged sample (1 week 6 kV rms AC), 20 kV rms tested, with contaminants, 2 trees initiated from the wire and 1 at a kink.
44) Dry aged sample (1 week 6 kV rms AC), 20 kV rms tested, with contaminants, closeup of (43), wire tree possibly affected by a contaminant.
45) Dry aged sample (1 week 6 kV rms AC), 20 kV rms tested, with contaminants, 2 trees initiated from the wire.

46) Dry aged sample (1 week 6 kV rms AC), 20 kV rms tested, with contaminants, closeup of (45), wire tree possibly affected by a contaminant.
47) Sample with 2% wt addition of contaminant 1, 20 kV rms tested, 8 trees initiated at the wire.
48) Sample with 2% wt addition of contaminant 1, 20 kV rms tested, closeup of (47), trees affected by contaminants.
49) Sample with 2% wt addition of contaminant 1, 20 kV rms tested, 8 trees initiated, 1 at kink and 7 at the wire.
50) Sample with 2% wt addition of contaminant 1, 20 kV rms tested, closeup of (49), kink tree with unsymmetrical growth possibly due to contaminant.
51) Sample with 20% wt addition of contaminant 1, 20 kV rms tested, 5 trees initiated at the wire.
52) Sample with 20% wt addition of contaminant 1, 20 kV rms tested, 1 tree initiated at the wire.
53) Sample with 20% wt addition of contaminant 1, 20 kV rms tested, microtomed sample, 5 trees initiated at the wire.
54) Sample with 20% wt addition of contaminant 1, 20 kV rms tested, microtomed sample, tree propagated into contaminant.
55) Sample with 2% wt addition of contaminant 3, 20 kV rms tested, 10 trees initiated 1 at kink, 9 at the wire.
56) Sample with 2% wt addition of contaminant 3, 20 kV rms tested, 2 trees initiated at the wire.
57) Sample with 2% wt addition of contaminant 3, 20 kV rms tested, 2 trees initiated at the wire.
58) Sample with 2% wt addition of contaminant 3, 20 kV rms tested, microtomed sample, 1 tree initiated at wire, propagated through contaminant and bushed out in the XLPE.
59) Sample with 20% wt addition of contaminant 3, 20 kV rms tested, 1 tree initiated at kink and breakdown channel lower in the sample.
60) Sample with 20% wt addition of contaminant 3, 20 kV rms tested, 3 trees initiated, 2 at kink and 1 at the wire.
61) Sample with 20% wt addition of contaminant 3, 20 kV rms tested, microtomed sample, unsymmetrical electric tree affected by contaminant
62) Sample with 20% wt addition of contaminant 3, 20 kV rms tested, microtomed sample, electric tree propagated through contaminants.
63) Sample with 2% wt addition of pre-crosslinked XLPE, 20 kV rms tested, 4 trees initiated, 2 at kinks and 2 at the wire.
64) Sample with 2% wt addition of pre-crosslinked XLPE, 20 kV rms tested,3 trees initiated, 2 at kinks and 1 at the wire.
65) Sample with 2% wt addition of pre-crosslinked XLPE, 20 kV rms tested, 3 trees initiated at kinks
66) Sample with 2% wt addition of pre-crosslinked XLPE, 20 kV rms tested, 3 trees initiated at kinks.
67) Sample with 20% wt addition of pre-crosslinked XLPE, 20 kV rms tested, 4 trees initiated, 2 at kinks and 2 at the wire.
68) Sample with 20% wt addition of pre-crosslinked XLPE, 20 kV rms tested, 2 trees initiated, 1 at kink and 1 at the wire.
69) Sample with 20% wt addition of pre-crosslinked XLPE, 20 kV rms tested, 2 trees initiated at kinks
70) Sample with 20% wt addition of pre-crosslinked XLPE, 20 kV rms tested, only 1 tree initiated from a severe kink.
71) Reference sample subjected to DC breakdown test, a wide breakdown channel created.
72) Sample with 10% wt addition of contaminant 3 subjected to DC breakdown test, breakdown channel created, 1 contaminant fully included in the breakdown channel.
73) Sample with 10% wt addition of contaminant 3 subjected to DC breakdown test, breakdown channel created, contaminants fully included in the breakdown channel.
74) Sample with 10% wt addition of contaminant 2 subjected to DC breakdown test, breakdown channel created, 1 contaminant fully included in the breakdown channel.
75) Sample with 10% wt addition of contaminant 2 subjected to a DC treeing test, breakdown channel created due to a self sustained discharge in the oil.

76) Sample with 10% wt addition of contaminant 2 subjected to a DC treeing test, closeup of (75), DC bush tree initiated.
77) Sample with 10% wt addition of contaminant 2 subjected to a DC treeing test, closeup of (75), DC branch tree initiated.
78) Sample with 10% wt addition of contaminant 3 subjected to a DC treeing test, branch tree initiated.
79) Sample with 10% wt addition of contaminant 2 subjected to a DC treeing test and microtomed, branch tree
80) Sample with 10% wt addition of contaminant 3 subjected to a DC treeing test and microtomed, 1 small branch tree in sample, not visible due to loss of resolution.
81) Sample with 10% wt addition of contaminant 2 subjected to a DC treeing test and microtomed, 2 small branch trees at short circuit channel.
82) Sample with 10% wt addition of contaminant 2 subjected to a DC treeing test and microtomed, branch tree